國立交通大學

光電工程研究所

碩 士 論 文

直接偵測正交分頻多工多級格式I/Q全光升頻系統

Optical I/Q Up-Conversion for Direct Detection Multi-Level Format OFDM Systems

研 究 生：翁而咨

指導教授：陳智弘　教授

中 華 民 國 九 十 八 年 七 月

直接偵測正交分頻多工多級格式 I/Q 全光升頻系統

Optical I/Q Up-Conversion for Direct Detection Multi-Level Format OFDM Systems

研 究 生：翁而咨　　Student：Er-Zih Wong

指導教授：陳智弘　　Advisor：Jyehong Chen

國 立 交 通 大 學

光電工程研究所

碩 士 論 文

A Thesis Submitted to Department of Phptonics

College of Electrical Engineering and Computer Science

National Chiao Tung University

in partial Fulfillment of the Requirements

for the Degree of

Master

in

Photonics

July 2009

Hsinchu, Taiwan, Republic of China

中華民國九十八年七月

直接偵測多級格式正交多頻分工全光升頻系統

研 究 生: 翁而咨　　指導教授: 陳智弘 博士

國立交通大學　電機資訊學院
光電工程研究所

摘要

我們提出了一個新穎的全光升頻直接偵測多級格式正交多頻分工系統。藉由外接調變器產生單邊帶載子壓制調變來產生全光升頻向量訊號,此架構不需要電的混波器及能升頻。為了產生60GHz的訊號，我們引進四倍頻的調變技術，並成功地在 60GHz 的免授權 7GHz 頻段產生 28Gb/s 16-QAM OFDM 訊號。在沒有任何色散補償的狀況下，經過一百公里的單模光纖傳輸，此訊號幾乎沒有損耗。

除此之外，我們還討論這個架構的不平衡效應，並針對這些問題提出補償方法來提升訊號品質。造成不平衡的因素包括:振幅不相符、角度不為直角以及兩路訊號不同步。用 GSOP 校正方法可以成功解決這些問題。

最後我們討論光的相位雜訊對訊號的影響。當我們的訊號傳輸量愈大時，光的相位雜訊會對訊號品質造成很大的影響。

Optical Up-Conversion for Direct Detection Multi-Level Format OFDM Systems

Student: Er-Zih Wong Advisor: Dr. Jyehong Chen

Department of Photonics,

National Chiao Tung University

ABSTRACT

We propose a novel all optical up-conversion direct detection OFDM multi-level system. Utilizing an external modulator, we can up-converse vector signals without electrical mixer based on single side band with carrier suppression. In order to generate 60GHz signals without expensive high-speed components, we using frequency quadrupling modulation technique. A record 28-Gb/s 16-QAM OFDM system within 7-GHz license-free band at 60 GHz employing all-optical up-conversion with frequency quintupling is experimentally demonstrated. Negligible penalty is observed following 100-km SMF transmission without any dispersion compensation.

Besides, we also discuss imbalance effects and do compensation to improve signal quality. The imbalance factors include amplitude mismatch, conjugate misalignment and un-synchronization. Utilizing Gram-Schmidt Orthogonal procedure can successfully solve these problems.

Finally, we also do some discussion on phase noise. It affects high data rate signals seriously.

Acknowledgements

在研究所的求學過程中, 首先感謝我的指導老師 陳智弘教授與祁甦教授, 提供良好的實驗環境以及無私的照顧與指導, 使我可以心無旁騖得完成學業並從中獲得許多收穫與成長。實驗方面特別感謝林俊廷學長教導我許多實驗方法, 並無私的指教以及修正了許多理論概念以及物理意義, 另外感謝施伯宗學長和江文智學長教導我許多實驗技巧以及引領我解決實驗問題, 還有林玉明學長在程式方面提供不少協助。

接下來要感謝實驗室的夥伴。非常感謝同在這個實驗室的同學們–陳星宇、葉士愷、黃漢昇以及陳昱宏同學, 不僅在實驗上給予協助, 並幫助我解決不少生活上的小問題; 在此也要特別感謝熱心幫我處理許多瑣事的學弟們, 彥霖以及立穎, 在我忙碌時給予不少協助。還要感謝平時給我許多鼓勵的好友們, 謝謝你們的關心和支持, 讓我在受到挫折時能繼續向上努力。

最後要感謝我的家人, 感謝你們的支持與鼓勵, 並時時給予溫暖的關心, 讓我無後顧之憂的完成學業。

帶著愉快回憶和滿載的收穫邁向人生的下個旅程, 再會了交大！

翁而咨 于 風城 交大 民國九十八年六月

CONTENTS

LIST OF FIGURES

Chapter 1 Introduction

1.1 Review of Radio-over-fiber system

There are many applications in microwave band, such as 3G, WiFi (IEEE 80211 b/g/a), and WiMAX are very important for wireless network. The increasing demand for communication has attracted more and more research interests of new transmission systems. Hence, to develop higher frequency microwave, even millimeter-wave is a important issue now. Either employing multilevel modulation schemes or extending the carrier frequency into millimeter-wave band can achieve higher data rate. Especially, the 7-GHz license-free spectrum at 60 GHz is the most promising solution to wireless gigabit service [1-3]. However, 60-GHz millimeter-wave has very high atmospheric loss and the access coverage is limited to relatively short range.

Because the higher frequency millimeter-wave signals have smaller coverage area, we have to set a lot of base stations to deliver millimeter-wave signals as shown in Fig. 1-1. In order to reduce the system costs and base stations (BSs) we utilize a highly dense central station (CS) equipped with optical and mm-wave components. Using fiber transmission medium is one of the best solutions because of unlimited bandwidth and low transmission loss of optical fiber, radio-over-fiber (RoF) technology is a promising solution to provide broadband service, wide coverage, and mobility.

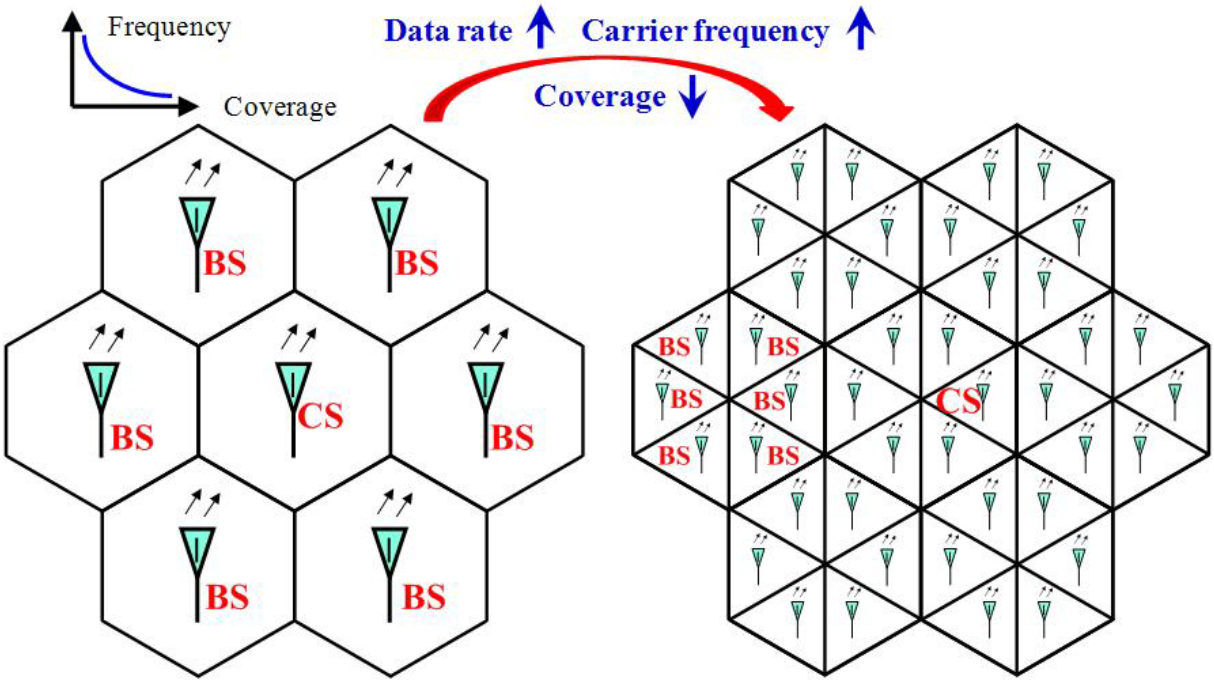

Figure 1-1 Basic structure of microwave/millimeter-wave wireless system.

Broadband wireless communications are shown in Fig. 1-2. ROF technology is a promising solution to provide multi-gigabits/sec service because of using millimeter wave band, and it has wide converge and mobility. On the other hand, due to high tolerance against fiber dispersion and polarization-mode dispersion, orthogonal frequency division multiplexing (OFDM) systems, which have been widely utilized in the current wireless communication, have attracted a lot of attention for optical high-capacity long-haul communication, multimode fiber links, and plastic optical fiber link. Besides, highly spectral efficiency and flexibility of OFDM makes it attractive for narrowband applications beyond the 10-Gb/s regime. Due to orthogonal characteristic of each subcarrier of OFDM signals, compared with single-carrier systems, an OFDM system has better spectral efficiency and can provide higher data rate within the 7-GHz license-free spectrum at 60 GHz.

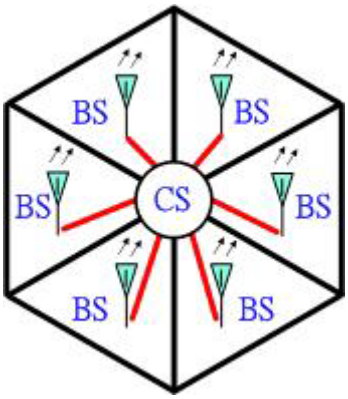

Figure 1-2 The Radio-over fiber system.

1.2 Basic modulation schemes

There are several kind of modulation schemes using an external modulator, such as double-sideband (DSB), single-sideband (SSB), and double-sideband with optical carrier suppression (DSBCS) modulation, and these schemes have already been demonstrated on many publications[1,2,4-8]. Each modulation scheme has its own advantage and disadvantage, respectively. DSB is the most compact system, but it suffers inferior sensitivities due to limited optical modulation index (OMI) [4-6,8], and fading issue because of fiber dispersion [6]. SSB can overcome fading, but it suffers inferior sensitivities as well. Among these modulation schemes, DSBCS modulation has been demonstrated to be effective in the millimeter-wave range with excellent spectral efficiency, a low bandwidth requirement for electrical components, and superior receiver sensitivity following transmission over a long distance [6]. Despite all these advantages, DSBCS schemes can only support on-off keying (OOK) format, but cannot transmit vector modulation formats, such as phase shift keying (PSK), quadrature amplitude modulation (QAM), or OFDM signals, which are of utmost importance for wireless applications.

This study proposes a modified single sideband (SSB) modulation scheme with carrier suppression using one MZM. A all optical up-conversion scheme is employed to reduce the requirement of bandwidth of electronic components and use no electrical mixer with noise figure 8 dB, which is an important issue at millimeter-wave RoF systems. Benchmarked against the OOK format, the 14.0625-Gb/s QPSK-OFDM and 28.125-Gb/s 16-QAM-OFDM format has the higher spectral efficiency.

1.3 Motivation

Recently , there several countries has already released the unlicensed spectrum about 7GHz near the 60GHz band . However, the coverage of the 60-GHz wireless signals is limited by the high path and atmospheric losses. To extend the signal coverage, radio-over-fiber (RoF) techniques become a promising solution for broad band wireless access networks. So in this work, we want to propose a new RoF system which has high spectral efficiency and satisfy the 60GHz applications.

Besides, traditional ways to generating SSB signals are shown as inset (i) and (ii) of figure 1-3. However, conventional SSB modulation approaches suffer from inferior sensitivities because the optical modulation index (OMI) is limited. Furthermore, to avoid beat noise after photo detection, an electrical I/Q mixer with a typical noise figure (NF) of more than 8 dB is needed to up-convert OFDM signal to intermedium frequency, which severely hinders implementation of highly spectral efficiency QAM OFDM signal for narrowband applications in the 10-Gb/s regime.

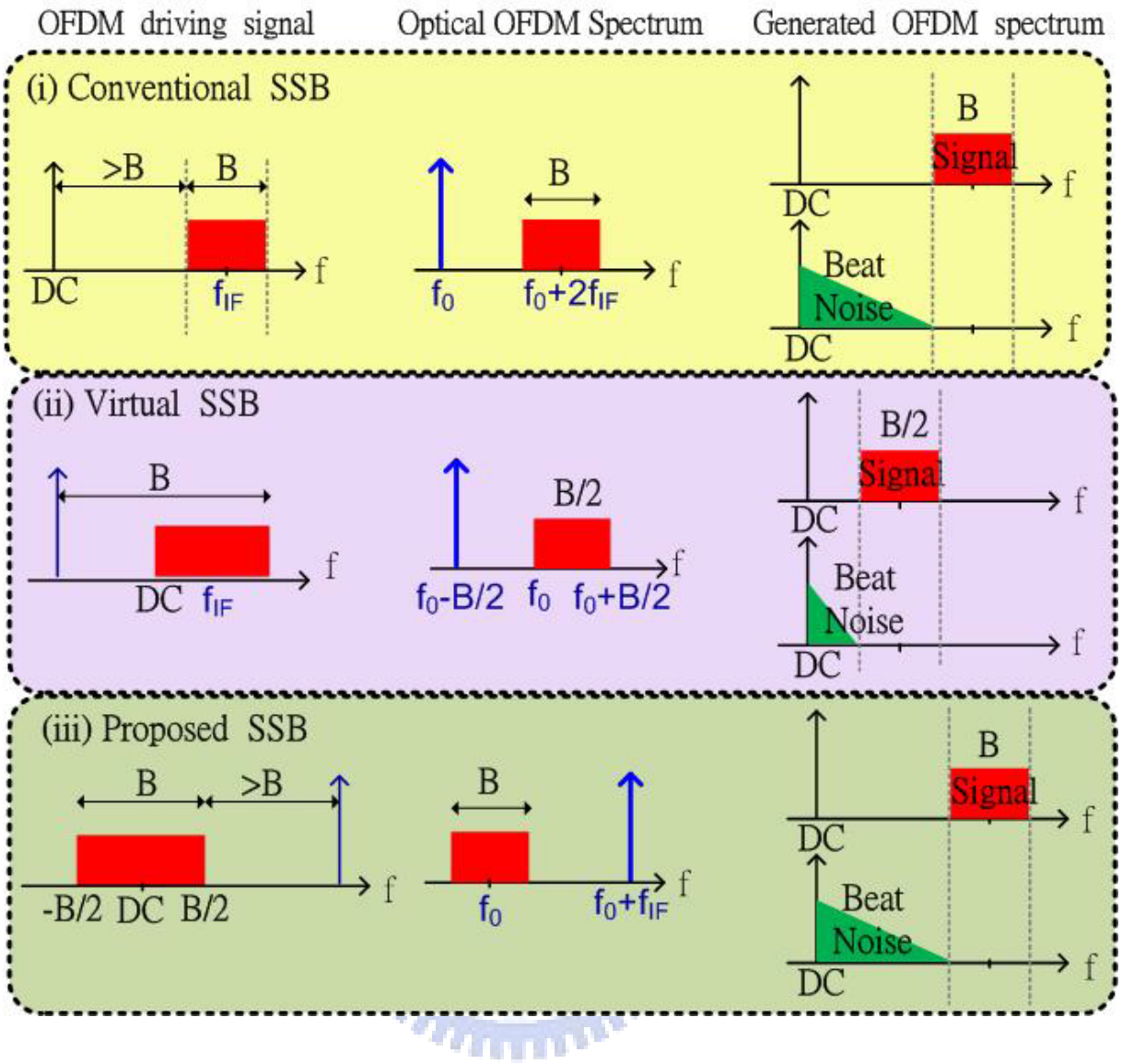

Figure1-3 Comparison of different DD-OFDM modulation shceme. (B: bandwidth of DAC, f_0: optical carrier frequency, f_0: intermedium frequency)

Virtual SSB modulation scheme without electrical I/Q mixer is proposed as shown in inset (ii) of Figure 1-3. The drawback is that half bandwidth of the DAC is wasted to avoid the beat noise interference. In order to improve these problems, we propose a modified SSB modulation.

Chapter 2 The concept of new optical modulation system

2.1 Preface

There are three parts in optical communication systems : optical transmitter, communication channel and optical receiver. In this chapter, we will briefly introduce about how these three parts work, and what is the external Mach-Zehnder Modulator (MZM), and how MZM construct a Radio-over-Fiber (RoF) system. In the end, we will propose a new model of the RoF system.

2.2 Mach-Zehnder Modulator (MZM)

Direct modulation and external modulation are two modulations of generated optical signal. When the bit rate of direct modulation signal is above 10 Gb/s, the frequency chirp imposed on signal becomes large enough. Hence, it is difficult to apply direct modulation to generate microwave/mm-wave. However, the bandwidth of signal generated by external modulator can exceed 10 Gb/s. Presently, most RoF systems are using external modulation with Mach-Zehnder modulator (MZM) or Electro-Absorption Modulator (EAM). The most commonly used MZM are based on LiNbO3 (lithium niobate) technology. According to the applied electric field, there are two types of LiNbO3 device : x-cut and z-cut. According to number of electrode, there are two types of LiNbO3 device: dual-drive Mach-Zehnder modulator (DD-MZM) and single-drive Mach-Zehnder modulator (SD-MZM) [6].

2.3 Single-drive Mach-Zehnder modulator

The SD-MZM has two arms and an electrode. The optical phase in each arm can be controlled by changing the voltage applied on the electrode. When the lightwaves are in phase, the modulator is in “on” state. On the other hand, when the lightwaves

are in opposite phase, the modulator is in “off ” state, and the lightwave cannot propagate by waveguide for output.

2.4 The architecture of ROF system

2.4.1 Optical transmitter

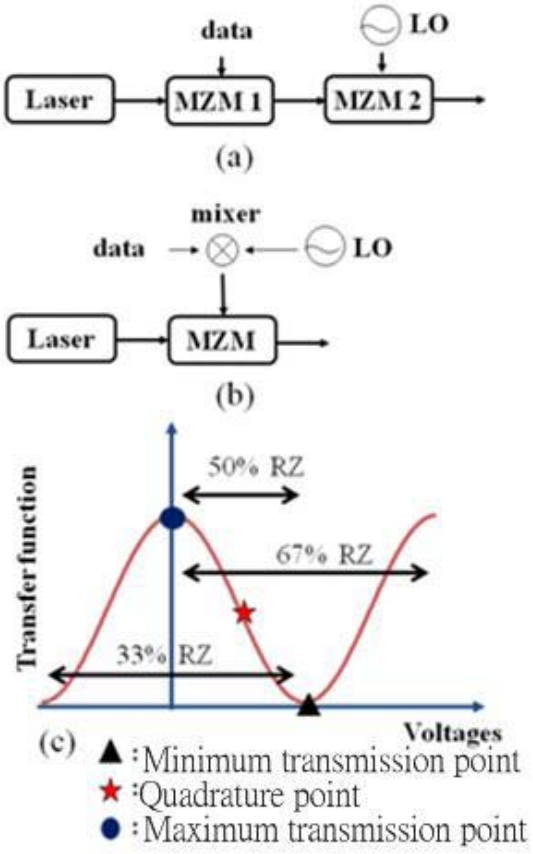

Figure 2-1(a) and (b) are two schemes of transmitter and (c) is duty cycle of subcarrier biased at different points in the transfer function. (LO: local oscillator)

Optical transmitter consists of optical source, optical modulator, RF signal, electrical mixer, electrical amplifier, etc.. Recently, most RoF systems are using laser as light source. The advantages of laser are compact size, high efficiency, good reliability small emissive area compatible with fiber core dimension, and possibility of direct modulation at relatively high frequency. The modulator is used for converting electrical signal into optical form. Because the external integrated modulator was

composed of MZMs, we select MZM as modulator to build the architecture of optical transmitter.

There are two schemes of optical transmitter generated optical signal. One scheme is used two MZM. First MZM generates optical carrier which carried the data. The output optical signal is BB signal. The other MZM generates optical subcarrier which carried the BB signal and then output the RF signal, as shown in Fig. 2-1 (a). The other scheme is used a mixer to get up-converted electrical signal and then send it into a MZM to generate the optical signal, as shown in Fig. 2-1 (b). Fig. 2-1 (c) shows the duty cycle of subcarrier biased at different points in the transfer function.

2.4.2 Optical signal generations based on $LiNbO_3$ MZM

The microwave and mm-wave generations are key techniques in RoF systems. The optical mm-waves using external MZM based on double-sideband (DSB), single-sideband (SSB), and double-sideband with optical carrier suppression (DSBCS) modulation schemes have been demonstrated, as shown in Fig. 2-2. Generated optical signal by setting the bias voltage of MZM at quadrature point, the DSB modulation experiences performance fading problems due to fiber dispersion, resulting in degradation of the receiver sensitivity. When an optical signal is modulated by an electrical RF signal, fiber chromatic dispersion causes the detected RF signal power to have a periodic fading characteristic. The DSB signals can be transmitted over

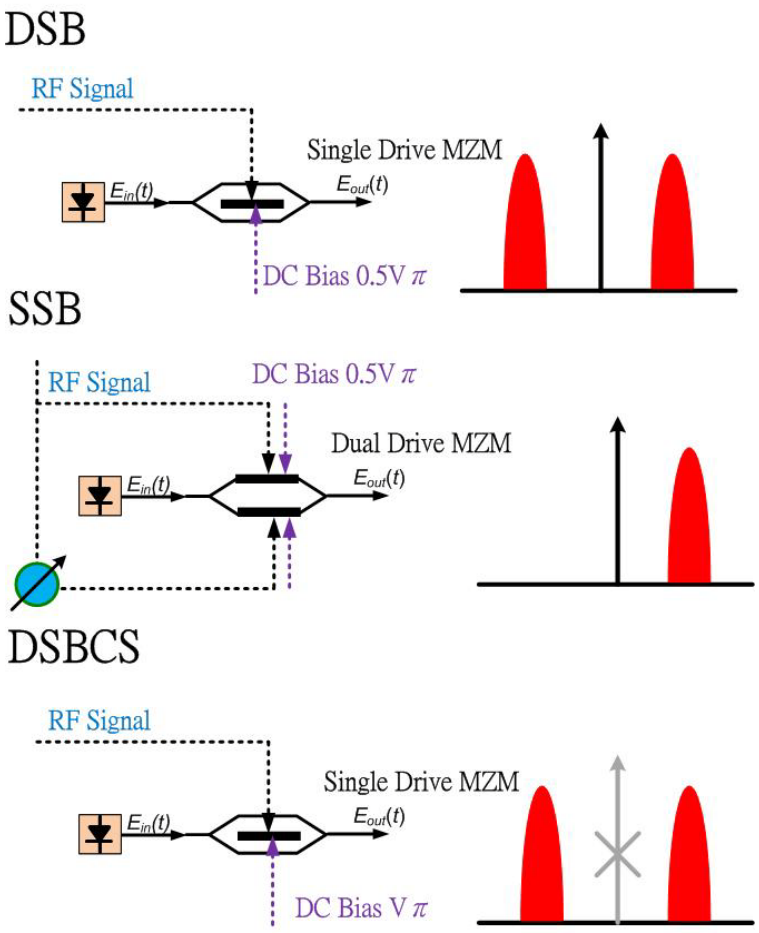

Figure2-2Optical microwave/mm-wave modulation scheme by using MZM.

several kilo-meters. Therefore, the SSB modulation scheme is proposed to overcome fiber dispersion effect. The SSB signal is generated when a phase difference of π/2 is applied between the two RF electrodes of the DD-MZM biased at quadrature point. Although the SSB modulation can reduce the impairment of fiber dispersion, it suffers worse receiver sensitivity due to limited optical modulation index (OMI). The DSBCS modulation is demonstrated optical mm-wave generation using DSBCS modulation. It has no performance fading problem and it also provides the best receiver sensitivity because the OMI is always equal to one. The other advantage is that the bandwidth requirement of the transmitter components is less than DSB and SSB modulation. However, the drawback of the DSBCS modulation is that it can't support vector

signals, such as phase shift keying (PSK), quadrature amplitude modulation (QAM), or OFDM signals, which are of utmost importance in wireless applications.

2.4.3 Communication channel

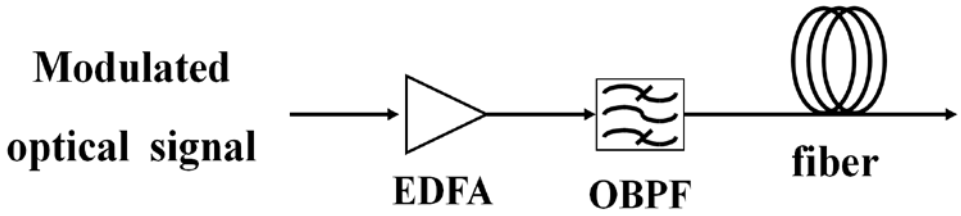

Figure2-3 The model of communication channel in a RoF system.

Communication channel concludes fiber, optical amplifier, etc.. Presently, most RoF systems are using single-mode fiber (SMF) or dispersion compensated fiber (DCF) as the transmission medium. When the optical signal transmits in optical fiber, dispersion will be happened. DCF is use to compensate dispersion. The transmission distance of any fiber-optic communication system is eventually limited by fiber losses. For long-haul systems, the loss limitation has traditionally been overcome using regenerator witch the optical signal is first converted into an electric current and then regenerated using a transmitter. Such regenerators become quite complex and expensive for WDM lightwave systems. An alternative approach to loss management makes use of optical amplifiers, which amplify the optical signal directly without requiring its conversion to the electric domain [14]. Presently, most RoF systems are using erbium-doped fiber amplifier (EDFA). An optical band-pass filter (OBPF) is necessary to filter out the ASE noise. The model of communication channel is shown in Fig. 2-3.

2.4.4 Demodulation of optical millimeter-wave signal

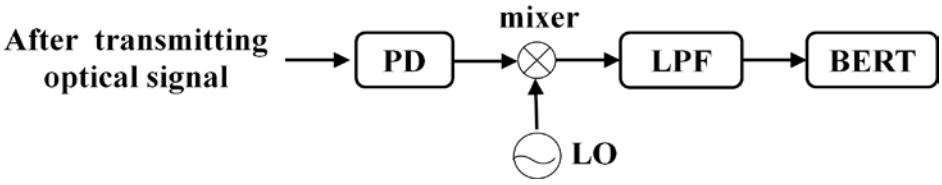

Figure 2-4 The model of receiver in a ROF system.

Optical receiver concludes photo-detector (PD), demodulator, etc.. PD usually consists of the photo diode and the trans-impedance amplifier (TIA). In the microwave or the mm-wave system, the PIN diode is usually used because it has lower transit time. The function of TIA is to convert photo-current to output voltage.

The BB and RF signals are identical after square-law photo detection. We can get RF signal by using a mixer to drop down RF signal to baseband then filtered by low-pass filter (LPF).

After getting down-converted signal, it will be sent into a signal tester to test the quality, just like bit-error-rate (BER) tester or oscilloscope, as shown in Fig. 2-4.

Combining the transmitter with communication channel and receiver, that is the model of ROF system, as shown in Fig. 2-5. We select the scheme of Fig. 2-3 (b) to become the transmitter in the model of ROF system.

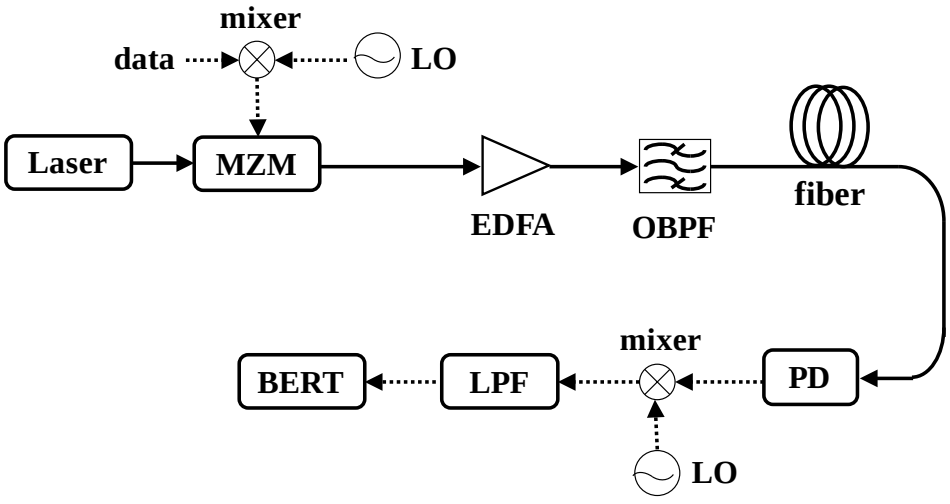

Figure 2-5 The model of ROF system.

2.5 The new proposed model of optical modulation system

Figure 2-6 schematically depicts the principle of the proposed optical I/Q up-conversion for direct-detection OFDM signal generation. Data I and Q of OFDM signals are sent to MZ-a and MZ-b of the optical I/Q modulator, respectively. To achieve high optical modulation depth and to operate in E-field linear region of the MZM, both MZ-a and MZ-b are biased at the null point. Therefore, optical OFDM signal at the center frequency of optical carrier with carrier suppression is generated as shown in inset (D) of Fig. 2-6.

To realize direct-detection OFDM signals, we insert an optical subcarrier to induce remote beating by using SSB modulation with carrier suppression. Except with a phase difference of 90°, the RF signals sent into the MZ-a and MZ-b are exactly the same. Since both MZ-a and MZ-b are biased at the null point, the generated optical spectrum consists of an upper sideband (USB) and a lower sideband (LSB) with optical carrier suppression as shown in insets (I) and (II) of Fig. 2-6. When MZ-c is biased at the quadrature point, the polarity of LSB in inset (Ⅰ) opposes that in inset (Ⅲ). The LSB will be eliminated whereas the USB is obtained. Therefore, as both RF and OFDM signals are simultaneously sent to I/Q modulator, the generated optical DD-OFDM signal consisting of an un-modulated subcarrier and an OFDM-modulated carrier.

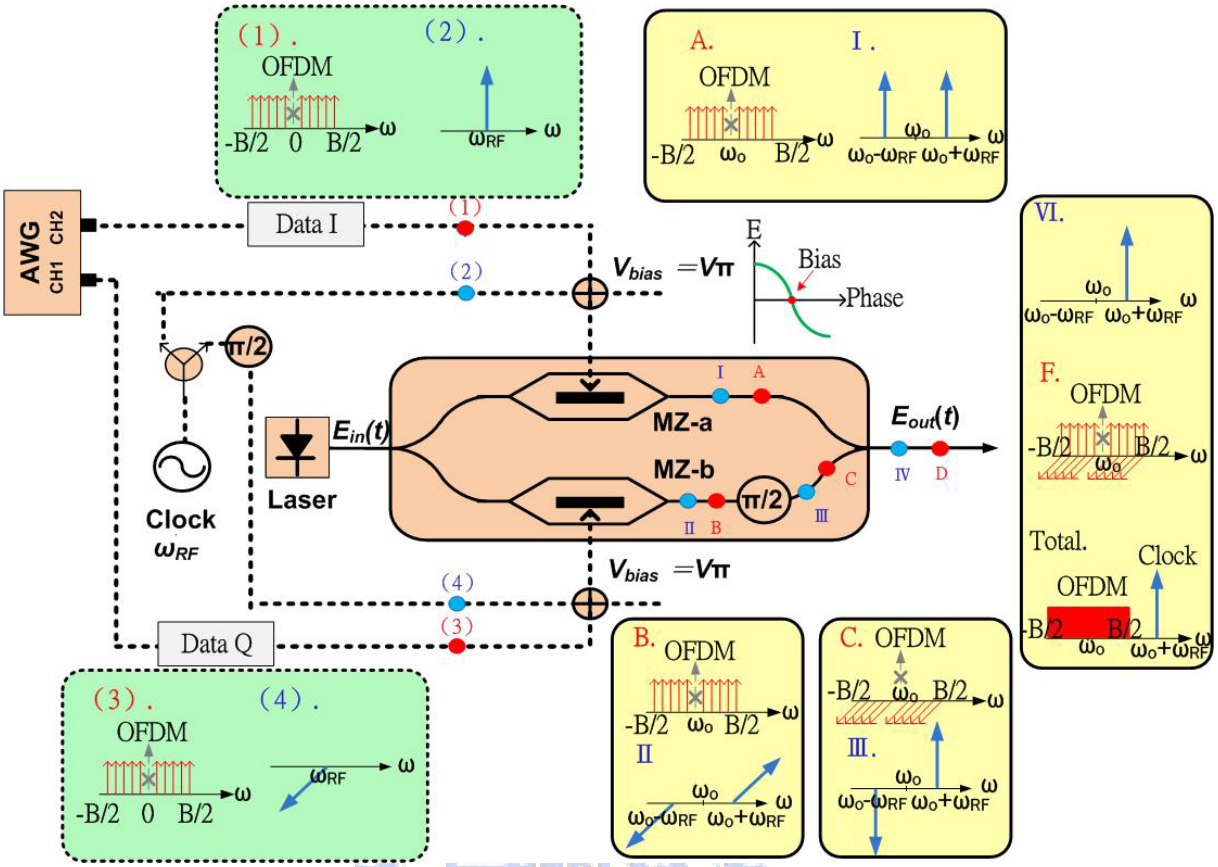

Figure 2-6 Conceptual diagram of optical I/Q up-conversion for direct-detection OFDM signals.

After square-law photo-diode (PD) detection, electrical RF-OFDM signals are obtained. Note that the proposed OFDM transmitter does not need an electrical mixer with a typical NF of more than 8 dB to avoid the beating noise interference, which is very important for highly spectral efficiency OFDM signals (i.e. 16-QAM or 64-QAM OFDM signal). Additionally, the relative intensity between the un-modulated and OFDM-modulated subcarriers can be easily tuned by adjusting the individual power of the electrical sinusoidal and OFDM signals to optimize the performance of the optical RF signals.

Chapter 3 The theoretical calculations of Proposed system

3.1 Introduce MZM

For MZM with configuration as Fig. 3-1, the output E-filed for upper arm is

$$E_U = E_0 \cdot a \cdot e^{j\Delta\varphi_1} \quad (1)$$

$$\Delta\varphi_1 \triangleq \frac{v_1}{v_\pi} \cdot \pi \quad (2)$$

$\Delta\varphi_1$ is the optical carrier phase difference that is induced by v_1, where a is the power splitting ratio.

The output E-filed for upper arm is

$$E_L = E_0 \cdot \sqrt{1-a^2} \cdot e^{j\Delta\varphi_2} \quad (3)$$

$\Delta\varphi_2$ is the optical carrier phase difference that is induced by v_2

$$\Delta\varphi_2 \triangleq \frac{v_2}{v_\pi} \cdot \pi \quad (4)$$

The output E-filed for MZM is

$$E_T = E_0 \cdot \left\{a \cdot b \cdot e^{j\Delta\varphi_1} + \sqrt{1-a^2} \cdot \sqrt{1-b^2} \cdot e^{j\Delta\varphi_2}\right\} \quad (5)$$

where a and b are the power splitting ratios of the first and second Y-splitters in MZM, respectively. The power splitting ratio of two arms of a balanced MZM is 0.5. The electrical field at the output of the MZM is given by

$$E_T = \frac{1}{2} \cdot E_0 \cdot \{e^{j\Delta\varphi_1} + e^{j\Delta\varphi_2}\} \quad (6)$$

$$E_T = E_0 \cdot \cos\left(\frac{\Delta\varphi_1 - \Delta\varphi_2}{2}\right) \cdot \exp\left(j\frac{\Delta\varphi_1 + \Delta\varphi_2}{2}\right) \quad (7)$$

For single electro x-cut MZM. The electrical field at the output is given by

$$E_{OUT} = E_0 \cdot \cos\left(\frac{\Delta\varphi - (-\Delta\varphi)}{2}\right) \cdot \exp\left(j\frac{\Delta\varphi + (-\Delta\varphi)}{2}\right) \quad (8)$$

Add time component, the electrical field is

$$E_{OUT} = E_0 \cdot \cos(\Delta\varphi) \cdot \cos(\omega_0 t) \quad (9)$$

where E_0 and ω_c denote the amplitude and angular frequency of the input optical

carrier, respectively; $V(t)$ is the applied driving voltage, and $\Delta\varphi$ is the optical carrier phase difference that is induced by $V(t)$ between the two arms of the MZM. The loss of MZM is neglected. $V(t)$ consisting of an electrical sinusoidal signal and a dc biased voltage can be written as,

$$V(t) = V_{bias} + V_m \cos(\omega t) \tag{10}$$

where V_{bias} is the dc biased voltage, V_m and ω_{RF} are the amplitude and the angular frequency of the electrical driving signal, respectively. The optical carrier phase difference induced by $V(t)$ is given by

$$\Delta\varphi = \frac{V(t)}{2V_\pi} = \frac{V_{bias} + V_m \cos(\omega t)}{V_\pi} \cdot \frac{\pi}{2} \tag{11}$$

Eq. (10) can be written as:

$$\begin{aligned} E_{OUT} &= E_0 \cdot \cos\left[\frac{V_{bias} + V_m \cos(\omega t)}{V_\pi} \cdot \frac{\pi}{2}\right] \cdot \cos(\omega_0 t) \\ &= E_0 \cdot \cos[b + m \cdot \cos(\omega_{RF} t)] \cdot \cos(\omega_0 t) \\ &= E_0 \cdot \cos(\omega_0 t) \cdot \{\cos(b) \cdot \cos[m \cdot \cos(\omega_{RF} t)] \\ &\qquad -\sin(b) \cdot \sin[m \cdot \cos(\omega_{RF} t)]\} \end{aligned} \tag{12}$$

where $b \triangleq \frac{V_{bias}}{2V_\pi}\pi$ is a constant phase shift that is induced by the dc biased voltage, and $m \triangleq \frac{V_m}{2V_\pi}\pi$ is the phase modulation index.

$$\begin{cases} \cos(x \sin\theta) = J_0(x) + 2\sum_{n=1}^{\infty} J_{2n}(x)\cos(2n\theta) \\ \sin(x \sin\theta) = 2\sum_{n=1}^{\infty} J_{2n-1}(x)\sin[(2n-1)\theta] \end{cases}$$

$$\begin{cases} \cos(x \cos\theta) = J_0(x) + 2\sum_{n=1}^{\infty} (-1)^n J_{2n}(x)\cos(2n\theta) \\ \sin(x \cos\theta) = 2\sum_{n=1}^{\infty} (-1)^n J_{2n-1}(x)\cos[(2n-1)\theta] \end{cases}$$

(13)

Expanding Eq. (12) using Bessel functions, as detailed in Eq. (13). The electrical field at the output of the MZM can be written as:

$$\mathrm{E_{OUT}} = \mathrm{E_0} \cdot \cos(\omega_0 t) \cdot \{\cos(b) \cdot [J_0(m) + 2 \cdot \sum_{\mathrm{i}=1}^{\infty} (-1)^n \cdot J_{2n}(\mathrm{m}) \cdot \cos(2n\omega_{RF} t)] - \sin(b) \cdot [2 \cdot \sum_{\mathrm{i}=1}^{\infty} (-1)^n \cdot J_{2n-1}(m) \cdot \cos[(2n-1)\omega_{RF} t]]\} \quad (14)$$

where J_n is the Bessel function of the first kind of order n. the electrical field of the mm-wave signal can be written as

$$\begin{aligned}\mathrm{E_{OUT}} &= \mathrm{E_0} \cdot \cos(b) \cdot \mathrm{J_0(m)} \cdot \cos(\omega_0 \mathrm{t}) \\ &+ \mathrm{E_0} \cdot \cos(b) \cdot \sum_{\mathrm{i}=1}^{\infty} J_{2n}(m) \cdot \cos[\,(\omega_0 - 2n\omega_{RF})t + n\pi] \\ &+ \mathrm{E_0} \cdot \cos(b) \cdot \sum_{\mathrm{i}=1}^{\infty} J_{2n}(m) \cdot \cos[(\omega_0 + 2n\omega_{RF})t + n\pi] \\ &- \mathrm{E_0} \cdot \sin(b) \cdot \sum_{\mathrm{i}=1}^{\infty} J_{2n-1}(m) \cdot \cos[\,\omega_0 - (2n-1)\omega_{RF})t + n\pi] \\ &- \mathrm{E_0} \cdot \sin(b) \cdot \sum_{\mathrm{i}=1}^{\infty} J_{2n-1}(m) \cdot \cos[\,\omega_0 + (2n-1)\omega_{RF})t + n\pi]\end{aligned} \quad (15)$$

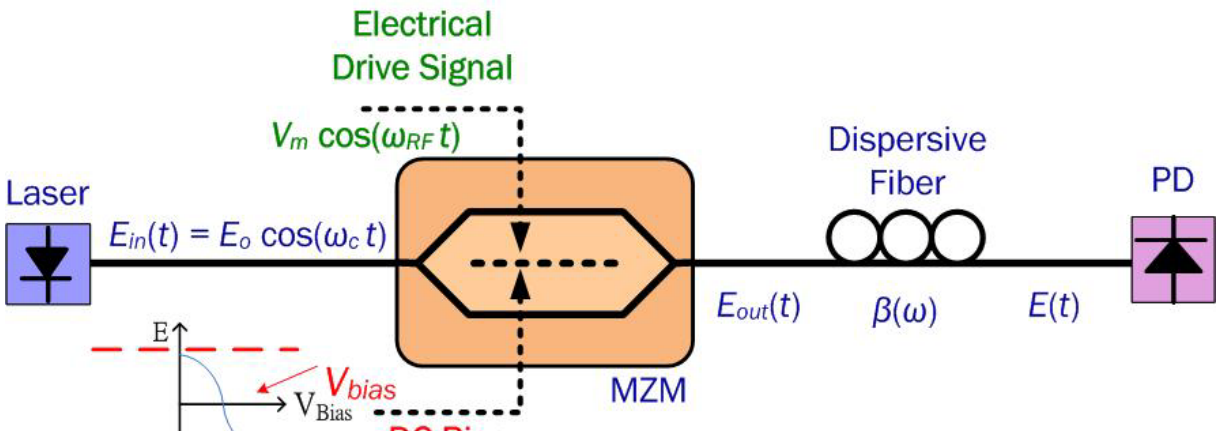

Figure 3-3 The principle diagram of the optical mm-wave generation using balanced MZM.

3.2 Theoretical calculation of single drive MZM

3.2.1 Bias at maximum transmission point

When the MZM is biased at the maximum transmission point, the bias voltage is set at $V_{bias} = 0$, and $\cos b = 1$ and $\sin b = 0$. Consequently, the electrical field of the mm-wave signal can be written as

$$E_{OUT}(t) = E_0 \cdot J_0(m) \cdot \cos(\omega_0 t)$$
$$+E_0 \cdot \sum_{n=1}^{\infty} J_{2n}(m) \cdot \cos[\,(\omega_0 - 2n\omega_{RF})t + n\pi]$$
$$+E_0 \cdot \sum_{n=1}^{\infty} J_{2n}(m) \cdot \cos[(\omega_0 + 2n\omega_{RF})t + n\pi] \quad (16)$$

The amplitudes of the generated optical sidebands are proportional to those of the corresponding Bessel functions associated with the phase modulation index m. With the amplitude of the electrical driving signal V_m equal to V_π, the maximum m is $\frac{\pi}{2}$.

As $0 < m < \frac{\pi}{2}$, the Bessel function J_n for $n \geq 1$ decreases and increases with the order of Bessel function and m, respectively, as shown in Figure 3-2. $J_1\left(\frac{\pi}{2}\right)$, $J_2\left(\frac{\pi}{2}\right)$, $J_3\left(\frac{\pi}{2}\right)$, and $J_4\left(\frac{\pi}{2}\right)$ are 0.5668, 0.2497, 0.069, and 0.014, respectively. Therefore, the optical sidebands with the Bessel function higher than $J_3(m)$ can be ignored, and Eq. (14) can be further simplified to

$$\begin{aligned} E_{OUT} &= E_0 \cdot J_0(m) \cdot \cos(\omega_0 t) \\ &+ E_0 \cdot J_2(m) \cdot \cos[(\omega_0 - 2\omega_{RF})t + \pi] \\ &+ E_0 \cdot J_2(m) \cdot \cos[(\omega_0 + 2\omega_{RF})t + \pi] \\ &+ E_0 \cdot J_4(m) \cdot \cos[(\omega_0 - 4\omega_{RF})t] \\ &+ E_0 \cdot J_4(m) \cdot \cos[(\omega_0 + 4\omega_{RF})t] \end{aligned} \quad (17)$$

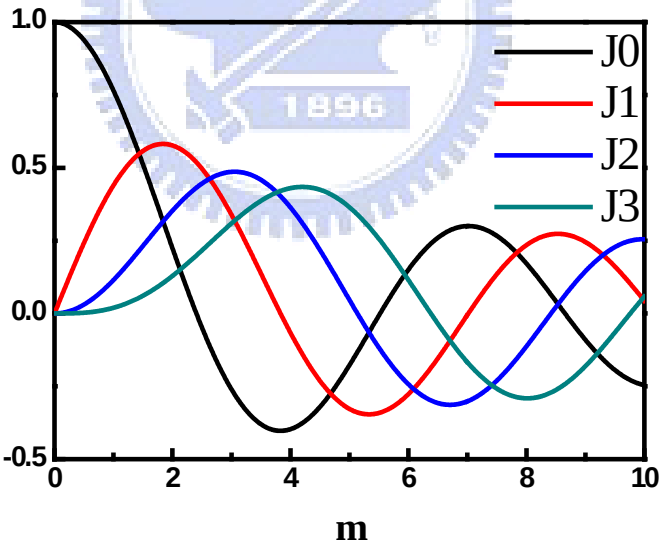

Figure 3-4 The different order of Bessel functions vs. m.

3.2.2 Bias at quadrature point

When the MZM is biased at the quadrature point, the bias voltage is set at $V_{bias} = \frac{V_\pi}{2}$, and $\cos b = \frac{\sqrt{2}}{2}$ and $\sin b = \frac{\sqrt{2}}{2}$. Consequently, the electrical field of the mm-wave signal can be written as

$$\begin{aligned} E_{OUT} = & \frac{1}{\sqrt{2}} \cdot E_0 \cdot J_0(m) \cdot \cos(\omega_0 t) \\ & + \frac{1}{\sqrt{2}} \cdot E_0 \cdot J_1(m) \cdot \cos[(\omega_0 - \omega_{RF})t] \\ & + \frac{1}{\sqrt{2}} \cdot E_0 \cdot J_1(m) \cdot \cos[(\omega_0 + \omega_{RF})t] \\ & + \frac{1}{\sqrt{2}} \cdot E_0 \cdot J_2(m) \cdot \cos[(\omega_0 - 2\omega_{RF})t + \pi] \\ & + \frac{1}{\sqrt{2}} \cdot E_0 \cdot J_2(m) \cdot \cos[(\omega_0 + 2\omega_{RF})t + \pi] \\ & + \frac{1}{\sqrt{2}} \cdot E_0 \cdot J_3(m) \cdot \cos[(\omega_0 - 3\omega_{RF})t + \pi] \\ & + \frac{1}{\sqrt{2}} \cdot E_0 \cdot J_3(m) \cdot \cos[(\omega_0 + 3\omega_{RF})t + \pi] \end{aligned} \quad (18)$$

3.2.3 Bias at null point

When the MZM is biased at the null point, the bias voltage is set at $V_{bias} = V_\pi$, and $\cos b = 0$ and $\sin b = 1$. Consequently, the electrical field of the mm-wave signal using DSBCS modulation can be written as

$$\begin{aligned} E_{OUT} = & E_0 \cdot J_1(m) \cdot \cos[(\omega_0 - \omega_{RF})t] \\ & + E_0 \cdot J_1(m) \cdot \cos[(\omega_0 + \omega_{RF})t] \\ & + E_0 \cdot J_3(m) \cdot \cos[(\omega_0 - 3\omega_{RF})t + \pi] \\ & + E_0 \cdot J_3(m) \cdot \cos[(\omega_0 + 3\omega_{RF})t + \pi] \\ & + E_0 \cdot J_5(m) \cdot \cos[(\omega_0 - 5\omega_{RF})t] \\ & + E_0 \cdot J_5(m) \cdot \cos[(\omega_0 + 5\omega_{RF})t] \end{aligned}$$

3.3 Theoretical calculations

3.3.1 The generated optical signal

The theoretical calculations of proposed system, the driving RF signal $V(t)_{up}$ and $V(t)_{down}$ consisting of an electrical sinusoidal signal and a dc biased voltage can be written as

$$V(t)_{up} = V_{bias} + V_1\cos\omega_1 t + V_2\cos\omega_2 t$$
$$V(t)_{down} = V_{bias} + V_1\cos\omega_1 t + V_2\cos\omega_2 t \quad (20)$$

where V_{bias} is the dc biased voltage, V_1, V_2 and ω_1, ω_2 are the amplitude and the angular frequency of the electrical driving signals, respectively. The optical carrier phase difference induced by $V(t)$ is given by

$$E_{OUT\_up} = E_0 \cdot \cos[\frac{\pi}{2V_\pi}(V_{bias} + V_1\cos\omega_1 t + V_2\cos\omega_2 t)]$$
$$E_{OUT\_down} = E_0 \cdot \cos[\frac{\pi}{2V_\pi}(V_{bias} + V_1\cos\omega_1 t + V_2\cos\omega_2 t)]$$
$$E_{OUT\_up} = E_0 \cdot \cos[b + m_1\cos\omega_1 t + m_2\cos\omega_2 t]$$
$$E_{OUT\_down} = E_0 \cdot \cos[b + m_1\cos(\omega_1 t + \frac{\pi}{2}) + m_2\cos\omega_2 t] \quad (21)$$

where $b \triangleq \frac{V_{bias}\,\pi}{2\pi}$ is a constant phase shift that is induced by the dc biased voltage, and $m_1 = \frac{V_1\pi}{2V_\pi}, m_2 = \frac{V_2\pi}{2V_\pi}$ is the phase modulation index.

$$E_{OUT\_up} = E_0 \cdot \cos b \cdot \cos(m_1\cos\omega_1 t + m_2\cos\omega_2 t)$$
$$-E_0 \cdot \sin b \cdot \sin(m_1\cos\omega_1 t + m_2\cos\omega_2 t)$$
$$E_{OUT\_down} = E_0 \cdot \cos b \cdot \cos(m_1\cos(\omega_1 t + \pi/2) + m_2\cos\omega_2 t)$$
$$-E_0 \cdot \sin b \cdot \sin(m_1\cos(\omega_1 t + \pi/2) + m_2\cos\omega_2 t)$$

$$E_{OUT\_up} = E_0 \cdot \cos b\{\cos(\mathrm{m}_1\cos\omega_1 t)\cos(m_2\cos\omega_2 t)$$
$$-\sin(m_1\cos\omega_1 t)\sin(m_2\cos\omega_2 t)\}$$
$$-E_0 \cdot \sin b\{\sin(m_1\cos\omega_1 \mathrm{t})\cos(m_2\cos\omega_2 \mathrm{t})$$
$$+\cos(m_1\cos\omega_1 \mathrm{t})\sin(m_2\cos\omega_2 \mathrm{t})\}$$
$$E_{OUT\_down} = E_0 \cdot \cos b\{\cos(\mathrm{m}_1\cos(\omega_1 \mathrm{t}+\pi/2))\cos(m_2\cos\omega_2 t)$$
$$-\sin(m_1\cos(\omega_1 \mathrm{t}+\pi/2))\sin(m_2\cos\omega_2 t)\}$$
$$-E_0 \cdot \sin b\{\sin(m_1\cos(\omega_1 \mathrm{t}+\pi/2))\cos(m_2\cos\omega_2 \mathrm{t})$$
$$+\cos(m_1\cos(\omega_1 \mathrm{t}+\pi/2))\sin(m_2\cos\omega_2 \mathrm{t})\} \quad (22)$$

When the MZM is biased at the null point, the bias voltage is set at $V_{bias} = \mathrm{V}_\pi$, and $\cos b = 0$ and $\sin b = 1$. Consequently, the electrical field of the mm-wave signal using SSBCS modulation can be written as

$$E_{OUT\_up} = -E_0\{\sin(m_1\cos\omega_1 \mathrm{t})\cos(m_2\cos\omega_2 \mathrm{t})$$
$$+\cos(m_1\cos\omega_1 \mathrm{t})\sin(m_2\cos\omega_2 \mathrm{t})\}$$
$$E_{OUT\_down} = -E_0\{\sin(m_1\cos(\omega_1 \mathrm{t}+\pi/2))\cos(m_2\cos\omega_2 \mathrm{t})$$
$$+\cos(m_1\cos(\omega_1 \mathrm{t}+\pi/2))\sin(m_2\cos\omega_2 \mathrm{t})\} \quad (23)$$

First, to expand equation $\sin(m_1\cos\omega_1 \mathrm{t})\cos(m_2\cos\omega_2 \mathrm{t})$

$\sin(m_1\cos\omega_1 \mathrm{t})\cos(m_2\cos\omega_2 \mathrm{t})$

$$= \left\{2\sum_{\mathrm{n}=1}^{\infty}(-1)^{\mathrm{n}}\mathrm{J}_{2\mathrm{n}-1}(m_1)\cos[(2\mathrm{n}-1)\omega_1 \mathrm{t}]\right\}$$
$$\cdot\left\{\mathrm{J}_0(m_2) + 2\sum_{\mathrm{n}=1}^{\infty}(-1)^{\mathrm{n}}\mathrm{J}_{2\mathrm{n}}(m_2)\cos(2\mathrm{n}\omega_2 \mathrm{t})\right\}$$
$$= \{-2\mathrm{J}_1(m_1)\cos(\omega_1 \mathrm{t}) + 2\mathrm{J}_3(m_1)\cos(3\omega_1 \mathrm{t}) - \cdots\}$$
$$\cdot\{\mathrm{J}_0(m_2) - 2\mathrm{J}_2(m_2)\cos(2\omega_2 \mathrm{t}) + 2\mathrm{J}_4(m_2)\cos(4\omega_2 \mathrm{t}) - \cdots\}$$

$\sin(m_1\cos(\omega_1 \mathrm{t}+\pi/2))\cos(m_2\cos\omega_2 \mathrm{t})$

$$= \left\{ 2\sum_{n=1}^{\infty} (-1)^n J_{2n-1}(m_1)\cos[(2n-1)\omega_1 t + (2n-1)\pi/2] \right\}$$

$$\cdot \left\{ J_0(m_2) + 2\sum_{n=1}^{\infty} (-1)^n J_{2n}(m_2)\cos(2n\omega_2 t) \right\}$$

$$= \{-2J_1(m_1)\cos(\omega_1 t + \pi/2) + 2J_3(m_1)\cos(3\omega_1 t + 3\pi/2) - \cdots\}$$

$$\cdot \{J_0(m_2) - 2J_2(m_2)\cos(2\omega_2 t) + 2J_4(m_2)\cos(4\omega_2 t) - \cdots\} \quad (24)$$

The optical sidebands with the Bessel function higher than $J_3(m)$ can be ignored. Consequently, the electrical field can be written as

$$\sin(m_1\cos\omega_1 t)\cos(m_2\cos\omega_2 t)$$

$$\approx -2J_0(m_2)J_1(m_1)\cos\omega_1 t$$

$$+2J_0(m_2)J_3(m_1)\cos(3\omega_1 t)$$

$$+4J_1(m_1)J_2(m_2)\cdot\frac{1}{2}[\cos(\omega_1 + 2\omega_2)t + \cos(\omega_1 - 2\omega_2)t]$$

$$-4J_2(m_2)J_3(m_1)\cdot\frac{1}{2}[\cos(3\omega_1 + 2\omega_2)t + \cos(3\omega_1 - 2\omega_2)t]$$

$$\sin(m_1\cos(\omega_1 t + \pi/2))\cos(m_2\cos\omega_2 t)$$

$$\approx -2J_0(m_2)J_1(m_1)\cos(\omega_1 t + \pi/2)$$

$$+2J_0(m_2)J_3(m_1)\cos(3\omega_1 t + 3\pi/2)$$

$$+4J_1(m_1)J_2(m_2)\cdot\frac{1}{2}[\cos((\omega_1 + 2\omega_2)t + \pi/2) + \cos((\omega_1 - 2\omega_2)t + \pi/2)]$$

$$-4J_2(m_2)J_3(m_1)\cdot\frac{1}{2}[\cos((3\omega_1 + 2\omega_2)t + 3\pi/2) + \cos((3\omega_1 - 2\omega_2)t + 3\pi/2)]$$

(25)

Add time component $\cos(\omega_c t)$

$$\sin(m_1\cos\omega_1 t)\cos(m_2\cos\omega_2 t)\cos(\omega_c t)$$
$$= -2J_0(m_2)J_1(m_1)\cos\omega_1 t\cos(\omega_c t)$$
$$+2J_0(m_2)J_3(m_1)\cos(3\omega_1 t)\cos(\omega_c t)$$
$$+4J_1(m_1)J_2(m_2)\cdot\frac{1}{2}[\cos(\omega_1+2\omega_2)t+\cos(\omega_1-2\omega_2)t]\cos(\omega_c t)$$
$$-4J_2(m_2)J_3(m_1)\cdot\frac{1}{2}[\cos(3\omega_1+2\omega_2)t+\cos(3\omega_1-2\omega_2)t]\cos(\omega_c t)$$

$$\sin(m_1\cos(\omega_1 t+\pi/2))\cos(m_2\cos\omega_2 t)\cos(\omega_c t+\pi/2)$$
$$= -2J_0(m_2)J_1(m_1)\cos(\omega_1 t+\pi/2)\cos(\omega_c t+\pi/2)$$
$$+2J_0(m_2)J_3(m_1)\cos(3\omega_1 t+3\pi/2)\cos(\omega_c t+\pi/2)$$
$$+4J_1(m_1)J_2(m_2)\cdot\frac{1}{2}[\cos(\omega_1+\pi/2+2\omega_2)t+\cos(\omega_1+\pi/2-2\omega_2)t]\cos(\omega_c t+\pi/2)$$
$$-4J_2(m_2)J_3(m_1)\cdot\frac{1}{2}[\cos(3\omega_1+3\pi/2+2\omega_2)t+\cos(3\omega_1+3\pi/2-2\omega_2)t]\cos(\omega_c t+\pi/2)$$

(26)

$J_0(m_2)J_1(m_1)$, $2J_0(m_2)J_3(m_1)$, $4J_1(m_1)J_2(m_2)$, and $4J_2(m_2)J_3(m_1)$ are shown in Figure 3-3. Therefore, the optical sidebands with the Bessel function $4J_2(m_2)J_3(m_1)$ can be ignored, and Eq. (14) can be further simplified to

$$\sin(m_1\cos\omega_1 t)\cos(m_2\cos\omega_2 t)\cos(\omega_c t)$$

$$= -J_0(m_2)J_1(m_1)[\cos(\omega_c+\omega_1)t+\cos(\omega_c-\omega_1)t]$$

$$+J_0(m_2)J_3(m_1)[\cos(\omega_c+3\omega_1)t+\cos(\omega_c-3\omega_1)t]$$

$$+J_1(m_1)J_2(m_2)[\cos(\omega_c+\omega_1+2\omega_2)\,t+\cos(\omega_c-\omega_1-2\omega_2)\,t]$$

$$+J_1(m_1)J_2(m_2)[\cos(\omega_c+\omega_1-2\omega_2)\,t+\cos(\omega_c-\omega_1+2\omega_2)\,t]$$

$$\sin(m_1\cos\omega_1 t+\pi/2)\cos(m_2\cos\omega_2 t)\cos(\omega_c t+\pi/2)$$

$$= -J_0(m_2)J_1(m_1)[\cos(\omega_c+\omega_1+\pi)t+\cos(\omega_c-\omega_1)t]$$

$$+J_0(m_2)J_3(m_1)[\cos(\omega_c+3\omega_1+2\pi)t+\cos(\omega_c-3\omega_1-\pi)t]$$

$$+J_1(m_1)J_2(m_2)[\cos(\omega_c+\omega_1+2\omega_2+\pi)\,t+\cos(\omega_c-\omega_1-2\omega_2)\,t]$$

$$+J_1(m_1)J_2(m_2)[\cos(\omega_c+\omega_1-2\omega_2+\pi)\,t+\cos(\omega_c-\omega_1+2\omega_2)\,t]$$

(27)

Second: To expand equation $\cos(m_1\cos\omega_1 t)\sin(m_2\cos\omega_2 t)$ and $\cos(m_1\cos(\omega_1 t+\frac{\pi}{2}))\sin(m_2\cos\omega_2 t)$

$$\cos(m_1\cos\omega_1 t)\sin(m_2\cos\omega_2 t)$$

$$= \left\{J_0(m_1)+2\sum_{n=1}^{\infty}(-1)^n J_{2n}(m_1)\cos(2n\omega_1 t)\right\}$$

$$\cdot\left\{2\sum_{n=1}^{\infty}(-1)^n J_{2n-1}(m_2)\cos[(2n-1)\omega_2 t]\right\}$$

$$= \{J_0(m_1)-2J_2(m_1)\cos(2\omega_1 t)+2J_4(m_1)\cos(4\omega_1 t)-\cdots\}$$

$$\cdot\{-2J_1(m_2)\cos(\omega_2 t)+2J_3(m_2)\cos(3\omega_2 t)-\cdots\}$$

$$\approx -2J_0(m_1)J_1(m_2)\cos\omega_2 t$$

$$+2J_0(m_1)J_3(m_2)\cos(3\omega_2 t)$$

$$+4J_1(m_2)J_2(m_1)\cdot\frac{1}{2}[\cos(\omega_2+2\omega_1)\,t+\cos(\omega_2-2\omega_1)\,t]$$

$$-4J_2(m_1)J_3(m_2)\cdot\frac{1}{2}[\cos(3\omega_2+2\omega_1)\,t+\cos(3\omega_2-2\omega_1)\,t]$$

$$\cos(m_1\cos(\omega_1 t+\frac{\pi}{2}))\sin(m_2\cos\omega_2 t)$$

$$\approx -2J_0(m_1)J_1(m_2)\cos\omega_2 t$$

$$+2J_0(m_1)J_3(m_2)\cos(3\omega_2 t)$$

$$+4J_1(m_2)J_2(m_1)\cdot\frac{1}{2}[\cos(\omega_2+2\omega_1+\pi)\,t+\cos(\omega_2-2\omega_1-\pi)\,t]$$

$$-4J_2(m_1)J_3(m_2)\cdot\frac{1}{2}[\cos(3\omega_2+2\omega_1+\pi)\,t+\cos(3\omega_2-2\omega_1-\pi)\,t]$$

(28)

Add time component $\cos(\omega_c t)$

$$\cos(m_1\cos\omega_1 t)\sin(m_2\cos\omega_2 t)\cos(\omega_c t)$$

$$=-2J_0(m_1)J_1(m_2)\cos\omega_2 t\cos(\omega_c t)$$

$$+2J_0(m_1)J_3(m_2)\cos(3\omega_2 t)\cos(\omega_c t)$$

$$+4J_1(m_2)J_2(m_1)\cdot\frac{1}{2}[\cos(\omega_2+2\omega_1)\,t+\cos(\omega_2-2\omega_1)\,t]\cos(\omega_c t)$$

$$-4J_2(m_1)J_3(m_2)\cdot\frac{1}{2}[\cos(3\omega_2+2\omega_1)\,t+\cos(3\omega_2-2\omega_1)\,t]\cos(\omega_c t)$$

$$=-J_0(m_1)J_1(m_2)[\cos(\omega_c+\omega_2)t+\cos(\omega_c-\omega_2)t]$$

$$+J_0(m_1)J_3(m_2)[\cos(\omega_c+3\omega_2)t+\cos(\omega_c-3\omega_2)t]$$

$$+J_1(m_2)J_2(m_1)[\cos(\omega_c+\omega_2+2\omega_1)\,t+\cos((\omega_c-\omega_2-2\omega_1)\,t]$$

$$+J_1(m_2)J_2(m_1)[\cos(\omega_c+\omega_2-2\omega_1)\,t+\cos(\omega_c-\omega_2+2\omega_1)\,t]$$

$$\cos(m_1\cos(\omega_1 t+\pi/2)\sin(m_2\cos\omega_2 t)\cos(\omega_c t+\pi/2)$$

$$=-J_0(m_1)J_1(m_2)[\cos((\omega_c+\omega_2)t+\pi/2)+\cos((\omega_c-\omega_2)t+\pi/2)]$$

$$+J_0(m_1)J_3(m_2)[\cos((\omega_c+3\omega_2)t+\frac{\pi}{2})+\cos((\omega_c-3\omega_2)t+\frac{\pi}{2})]$$

$$+J_1(m_2)J_2(m_1)[\cos((\omega_c+\omega_2+2\omega_1)\,t+3\pi/2)+\cos((\omega_c-\omega_2-2\omega_1)\,t-\pi/2)]$$

$$+J_1(m_2)J_2(m_1)[\cos((\omega_c+\omega_2-2\omega_1)\,t-\pi/2)+\cos((\omega_c-\omega_2+2\omega_1)\,t+3\pi/2) \quad (29)$$

The output electrical filed can be rewritten as

$$E_{OUT_{up}}(t)=E_0\cos(\omega_c t)\{\sin(m_1\cos\omega_1 t)\cos(m_2\cos\omega_2 t)+\cos(m_1\cos\omega_1 t)\sin(m_2\cos\omega_2 t)\}$$

$$E_{OUT\_down}=-E_0\cos(\omega_c t+\pi/2)\{\sin(m_1\cos(\omega_1 t+\pi/2))\cos(m_2\cos\omega_2 t)+\cos(m_1\cos(\omega_1 t+\pi/2))\sin(m_2\cos\omega_2 t)\}$$

$$E_{OUT\_up}(t)=E_0\cdot$$
$$\{J_0(m_2)J_1(m_1)[\cos(\omega_c+\omega_1)t+\cos(\omega_c-\omega_1)t]$$
$$-J_0(m_2)J_3(m_1)[\cos(\omega_c+3\omega_1)t+\cos(\omega_c-3\omega_1)t]$$
$$-J_1(m_1)J_2(m_2)[\cos(\omega_c+\omega_1+2\omega_2)\,t+\cos(\omega_c-\omega_1-2\omega_2)\,t]$$
$$-J_1(m_1)J_2(m_2)[\cos(\omega_c+\omega_1-2\omega_2)\,t+\cos(\omega_c-\omega_1+2\omega_2)\,t]$$
$$+J_0(m_1)J_1(m_2)[\cos(\omega_c+\omega_2)t+\cos(\omega_c-\omega_2)t]$$
$$-J_0(m_1)J_3(m_2)[\cos(\omega_c+3\omega_2)t+\cos(\omega_c-3\omega_2)t]$$
$$-J_1(m_2)J_2(m_1)[\cos(\omega_c+\omega_2+2\omega_1)\,t+\cos(\omega_c-\omega_2-2\omega_1)\,t]$$
$$-J_1(m_2)J_2(m_1)[\cos(\omega_c+\omega_2-2\omega_1)\,t+\cos(\omega_c-\omega_2+2\omega_1)\,t]\}$$

$$E_{OUT_{down}}(t)=E_0\cdot$$
$$\{J_0(m_2)J_1(m_1)[\cos((\omega_c+\omega_1)t+\pi)+\cos((\omega_c-\omega_1)t)]$$
$$-J_0(m_2)J_3(m_1)[\cos((\omega_c+3\omega_1)t+2\pi)+\cos((\omega_c-3\omega_1)t-2\pi)]$$
$$-J_1(m_1)J_2(m_2)[\cos((\omega_c+\omega_1+2\omega_2)\,t+\pi)+\cos((\omega_c-\omega_1-2\omega_2)\,t)]$$
$$-J_1(m_1)J_2(m_2)[\cos((\omega_c+\omega_1-2\omega_2)\,t+\pi)+\cos((\omega_c-\omega_1+2\omega_2)\,t)]$$

$$+J_0(m_1)J_1(m_2)[\cos((\omega_c+\omega_2)t+\frac{\pi}{2})+\cos((\omega_c-\omega_2)t+\frac{\pi}{2})]$$

$$-J_0(m_1)J_3(m_2)[\cos((\omega_c+3\omega_2)t+\frac{\pi}{2})+\cos((\omega_c-3\omega_2)t+\frac{\pi}{2})]$$

$$-J_1(m_2)J_2(m_1)\left[\cos((\omega_c+\omega_2+2\omega_1)\,t+\frac{3\pi}{2})+\cos((\omega_c-\omega_2-2\omega_1)\,t-\frac{\pi}{2})\right]$$

$$-J_1(m_2)J_2(m_1)\left[\cos((\omega_c+\omega_2-2\omega_1)\,t-\frac{\pi}{2})+\cos((\omega_c-\omega_2+2\omega_1)\,t+\frac{3\pi}{2})\right]\}$$

(30)

$$E_{OUT}(\mathrm{t})=E_{OUT_{up}}(\mathrm{t})+E_{OUT_{down}}(\mathrm{t})$$

$$=E_0\cdot 2\{J_0(m_2)J_1(m_1)\cos(\omega_c-\omega_1)t]$$

$$-2J_0(m_2)J_3(m_1)[\cos((\omega_c+3\omega_1)t+\cos((\omega_c-3\omega_1)t]$$

$$-2J_1(m_1)J_2(m_2)[\cos(\omega_c-\omega_1-2\omega_2)\,t]$$

$$-2J_1(m_1)J_2(m_2)[\cos(\omega_c-\omega_1+2\omega_2)\,t]$$

$$+J_0(m_1)J_1(m_2)\big[[\cos((\omega_c+\omega_2)t-\sin((\omega_c+\omega_2)t+\cos(\omega_c-\omega_2)t-\sin(\omega_c-\omega_2)t)]$$

$$-J_0(m_1)J_3(m_2)[\cos(\omega_c+3\omega_2)t-\sin(\omega_c+3\omega_2)t+\cos(\omega_c-3\omega_2)\,t-\sin((\omega_c-3\omega_2)t]$$

$$-J_1(m_2)J_2(m_1)[\cos(\omega_c+\omega_2+2\omega_1)\,t+\sin(\omega_c+\omega_2+2\omega_1)\,t+\cos(\omega_c-\omega_2-2\omega_1)\,t+\sin(\omega_c-\omega_2-2\omega_1)\,t]$$

$$-J_1(m_2)J_2(m_1)[\cos(\omega_c+\omega_2-2\omega_1)\,t+\sin(\omega_c+\omega_2-2\omega_1)\,t+\cos(\omega_c-\omega_2+2\omega_1)\,t+\sin(\omega_c-\omega_2+2\omega_1)\,t]\}$$

$$\approx E_0 \cdot$$
$$\{2J_0(m_2)J_1(m_1)\cos(\omega_c - \omega_1)t]$$
$$+J_0(m_1)J_1(m_2)\big[[\cos(\omega_c + \omega_2)t - \sin(\omega_c + \omega_2)t + \cos(\omega_c - \omega_2)t - \sin(\omega_c - \omega_2)t)]\}$$

(31)

First part is subcarrier and second part is our signals.

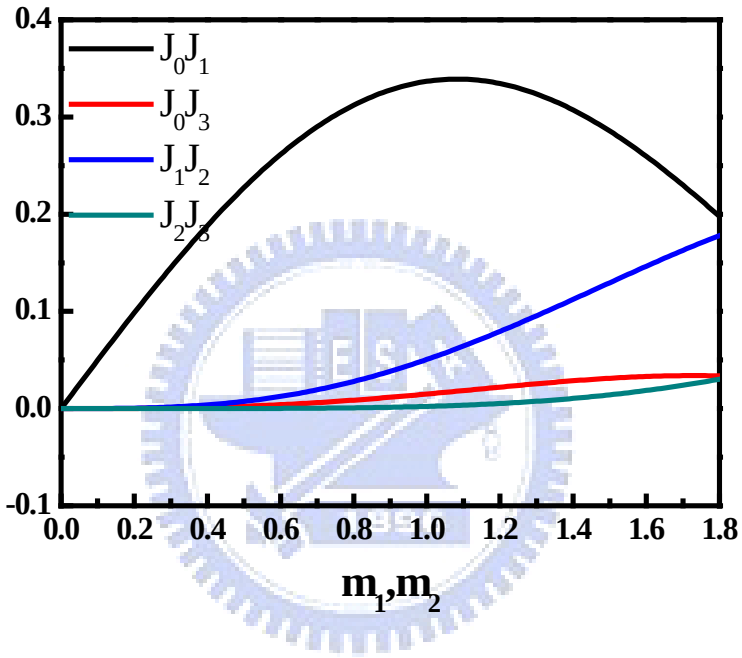

Figure 3-5 The different order of Bessel functions vs. m.

3.4 IQ Imbalance

3.4.1 Preface

In this chapter, a novel compensation scheme for I/Q imbalance is proposed and experimentally demonstrated. Both simulation and experiment results confirm a significant increase of the tolerance of both the amplitude mismatch and conjugate misalignment. At the bit-error-ratio of 10^{-9}, experimental results shows that the

amplitude mismatch can increase from 2 dB to 6 dB, and the conjugate misalignment from 5° to 13°. With the I/Q compensation, a 5-Gb/s QPSK signal at 7.5-GHz is generated and negligible penalty is observed after 100-km single mode fiber (SMF) transmission.

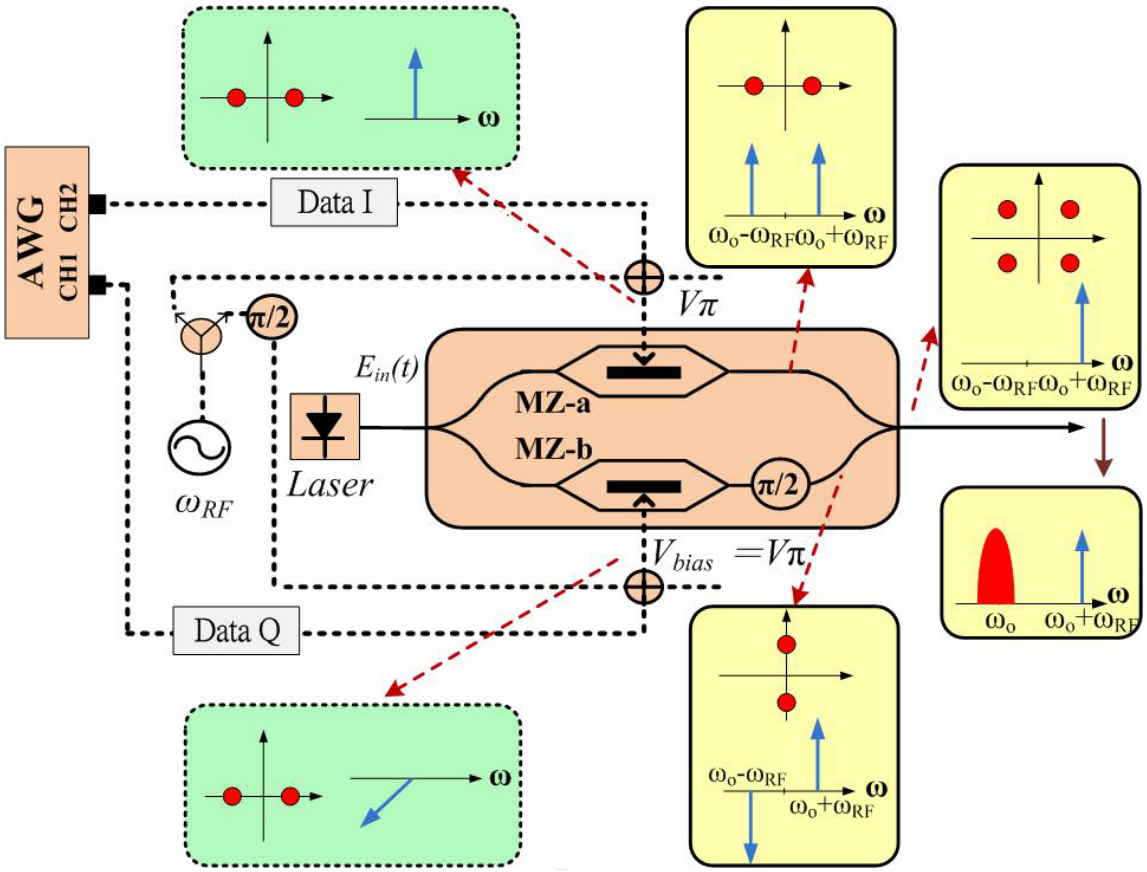

Figure 3-4 The concept of proposed system

3.4.2 Concept of Proposed System

Figure 3-4 schematically depicts the principle of the proposed optical I/Q up-conversion for direct-detection RoF signal generation. Data I and Q of RoF signals are sent to MZ-a and MZ-b of the optical I/Q modulator, respectively. To achieve high optical modulation depth and to operate in E-field linear region of the MZM, both MZ-a and MZ-b are biased at the null point.

To realize direct-detection RoF signals, we insert an optical subcarrier to induce remote beating by using SSB modulation with carrier suppression. Except with a phase difference of 90°, the RF signals sent into the MZ-a and MZ-b are exactly the same. Therefore, as both RF and vector signals are simultaneously sent to I/Q modulator, the generated optical signal consisting of an un-modulated subcarrier and a data-modulated carrier. After square-law photo-diode (PD) detection, electrical RF vector signals are obtained. Note that the proposed RoF transmitter does not need an electrical mixer with a typical NF of more than 8 dB to up-convert the electrical signal. Additionally, the relative intensity between the un-modulated and data-modulated subcarriers can be easily tuned by adjusting the individual power of the electrical sinusoidal and vector signals to optimize the performance of the optical RF signals.

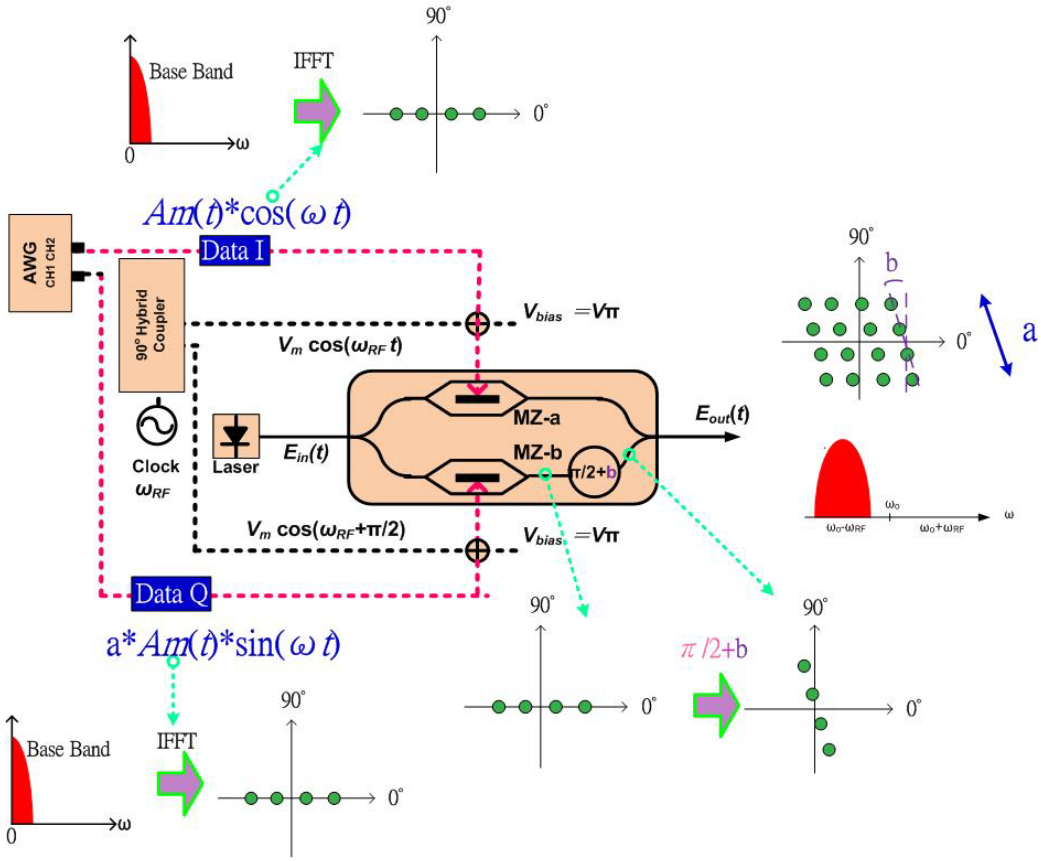

Figure 3-5 Imbalance factors of proposed system.

Due to the in-phase (I) and quadrature (Q) data go through different paths, without precisely controlled, small amplitude mismatch and conjugate misalignment

will destroy the orthogonality between the I/Q channels and the performance of the system will be substantial deteriorated. These imbalance factors are shown as Figure 3-5. In this figure, pink dash-line shows different paths. If the two paths are not the same, that will make the signals distortion or mistake. If data-I and data-Q's amplitude are Vm and a*Vm, the constellation will be a rectangular. If the phase modulator does not delay π /2, the constellation will become a parallelogram rather a square.

3.4.3 Amplitude mismatch- I/Q Ratio (dB)

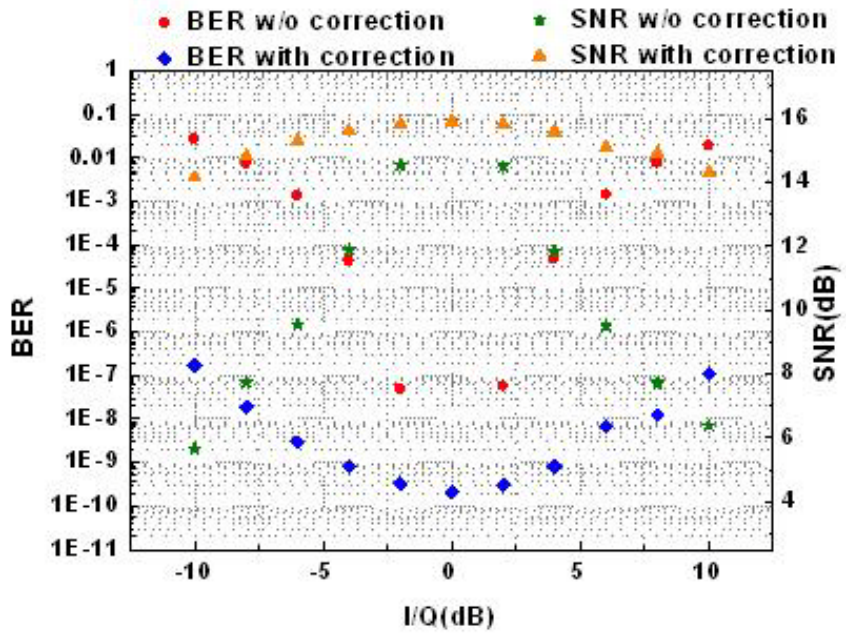

Figure 3-6 BER and SNR vs. I/Q ratio for simulation single carrier QPSK.

As shown in Figure 3-6, single carrier QPSK simulation results indicate that a 8dB amplitude mismatch corresponding to about 8 dB SNR degradation. However, after employing the Gram–Schmidt orthogonalization procedure (GSOP), substantial performance improvement is obtained. With a 8 dB amplitude mismatch, only about 1 dB SNR degradation is observed.

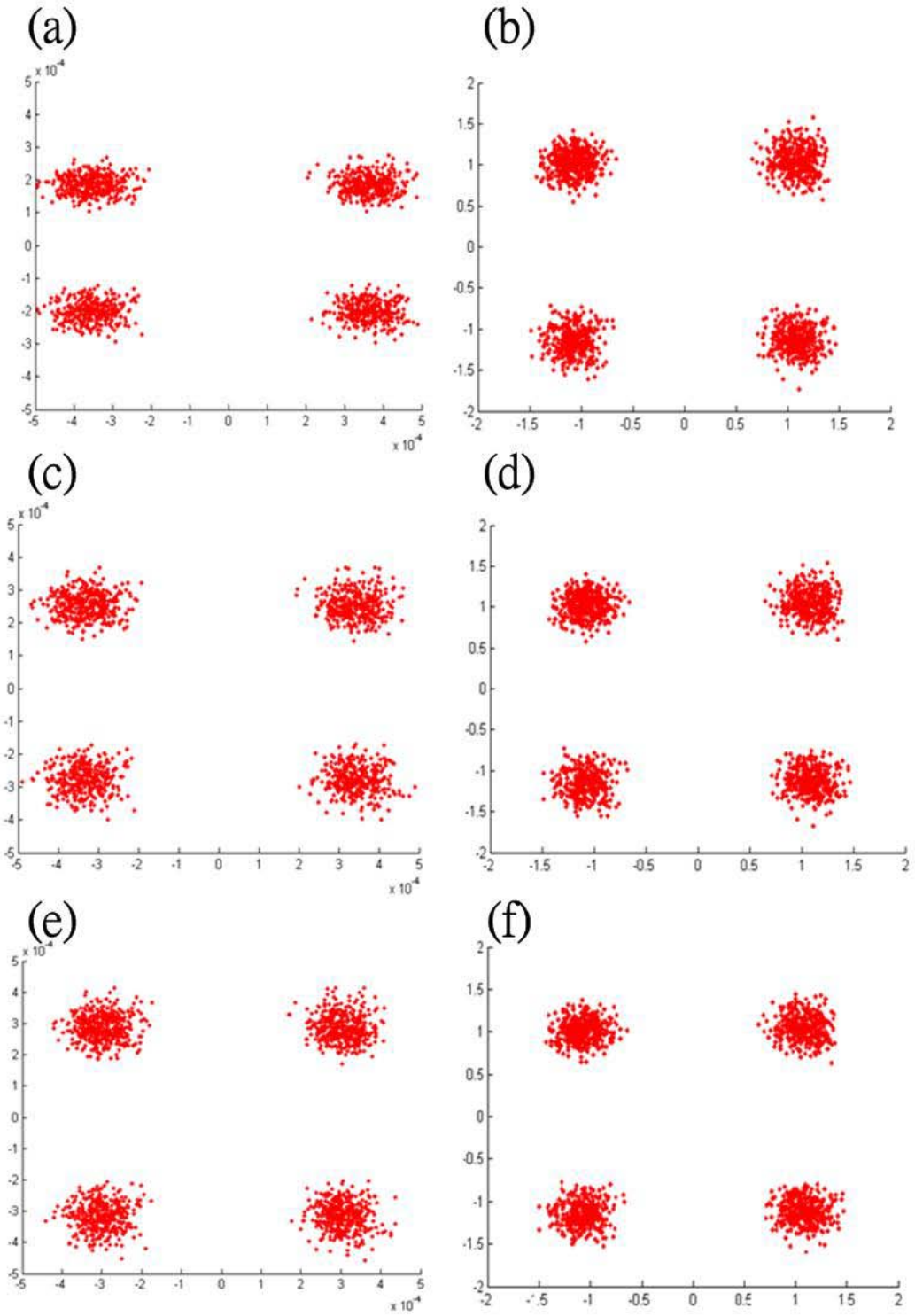

Figure 3-7 Constellations for simulation QPSK amplitude mismatch w/ and w/o correction.

(a) I/Q=8dB w/o correction (b) I/Q=8dB w/ correction (c) I/Q=4dB w/o correction

(d) I/Q=4dB w/ correction (e) I/Q=0dB w/o correction (f) I/Q=0dB w/ correction

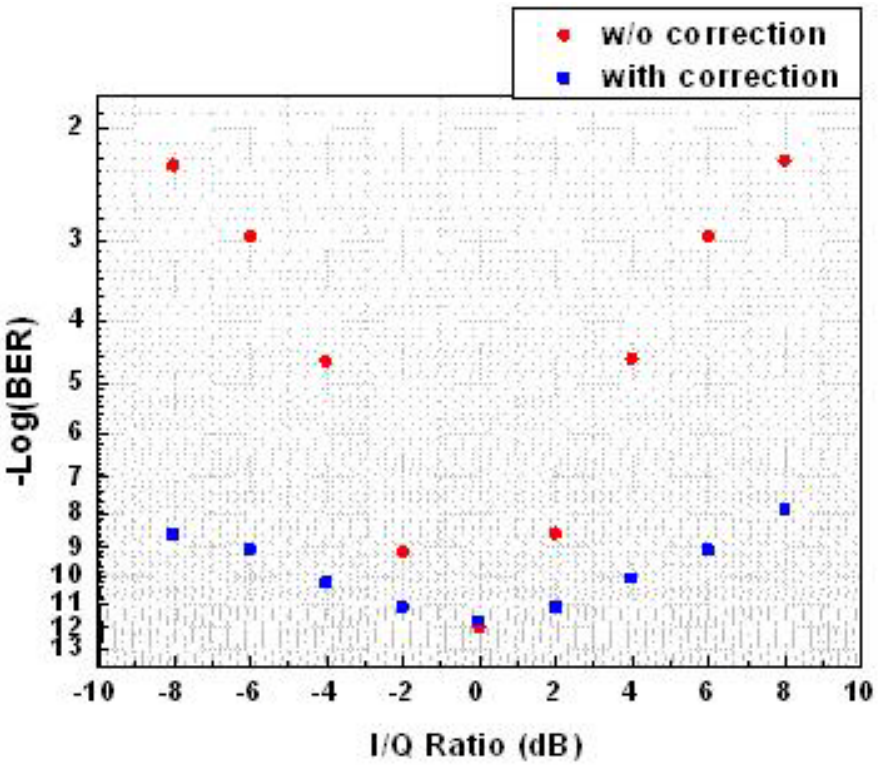

Figure 3-8 BER vs. I/Q ratio(Amplitude Mismatch) for experimental single carrier QPSK.

Figure 3-6 shows single carrier QPSK experimental results and indicates that a 8 dB amplitude mismatch corresponding to about 10 orders BER degradation. After employing the GSOP, substantial performance improvement is obtained. With a 8 dB amplitude mismatch, only about 4 orders BER degradation is observed. And we can see that the curve trend is like simulation result.

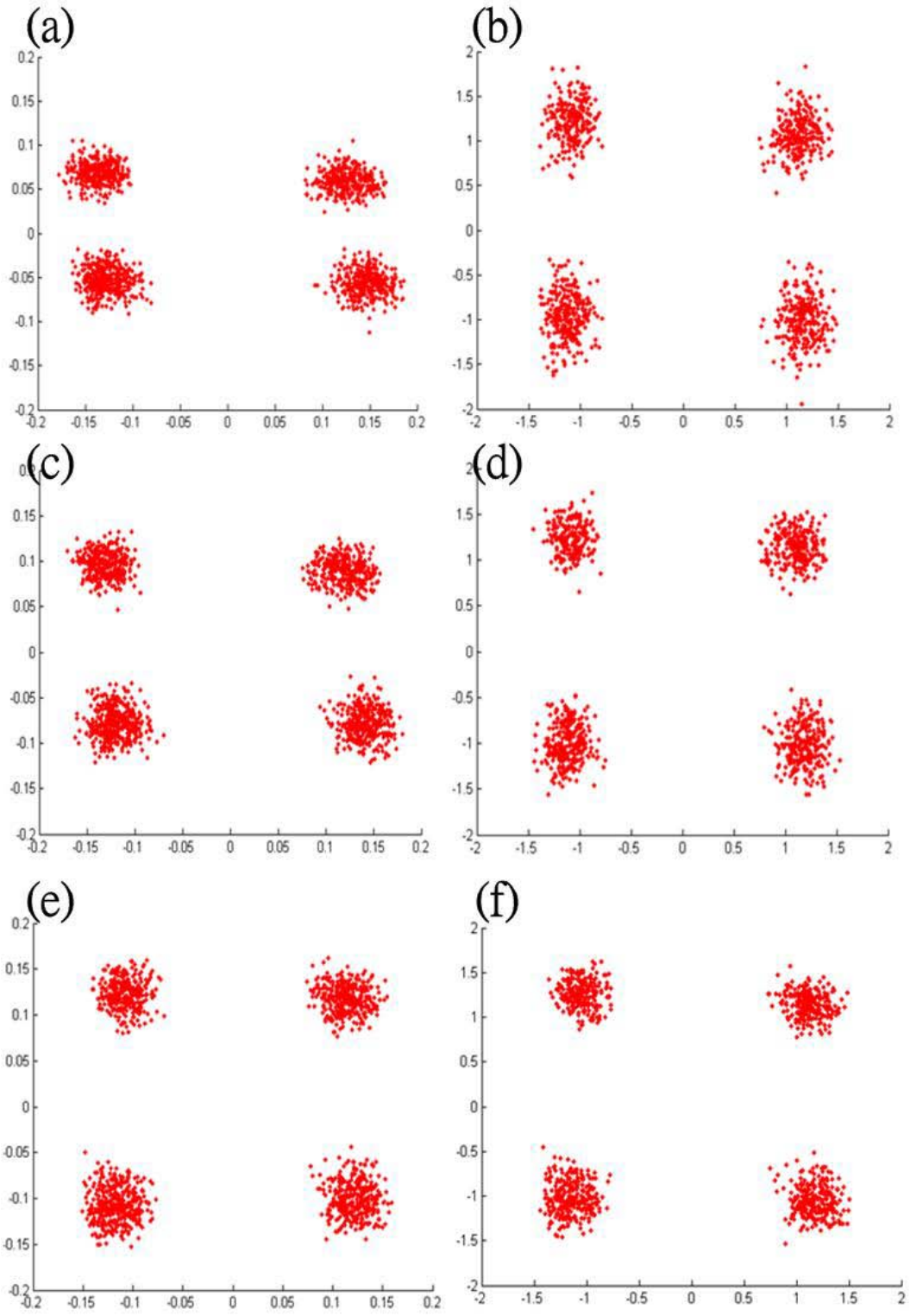

Figure 3-9 Constellations for experimental QPSK amplitude mismatch w/ and w/o correction.

(a) I/Q=8dB w/o correction (b) I/Q=8dB w/ correction (c) I/Q=4dB w/o correction

(d) I/Q=4dB w/ correction (e) I/Q=0dB w/o correction (f) I/Q=0dB w/ correction

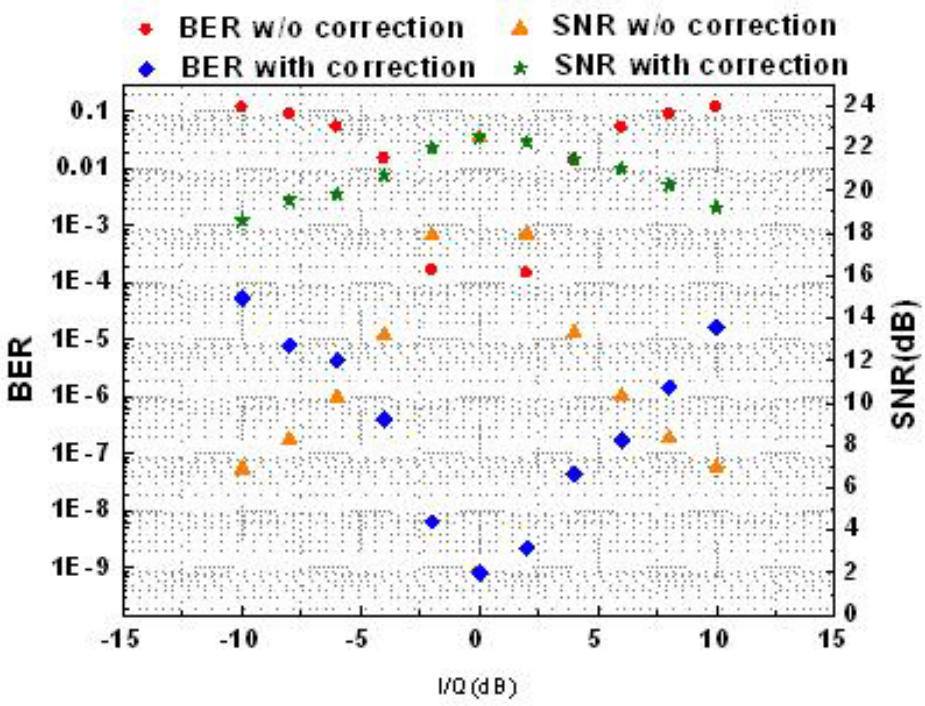

Figure 3-10 BER and SNR vs. I/Q ratio for simulation single carrier 16-QAM.

Figure 3-10 is single carrier 16-QAM simulation results and indicates that a 8 dB amplitude mismatch corresponding to about 14 dB SNR degradation. Employing the Gram–Schmidt orthogonalization procedure (GSOP), substantial performance improvement is obtained, only about 3 dB SNR degradation is observed.

Figure 3-11 is the constellations for simulation 16-QAM amplitude mismatch with and without GSOP, respectively. Inset (a), (b), (c), (d), (e) and (f) of Figure3-11 illustrate I/Q=8dB without GSOP, I/Q=8dB with GSOP, I/Q=4dB without GSOP, I/Q=4dB with GSOP, I/Q=0dB without GSOP and I/Q=0dB with GSOP.

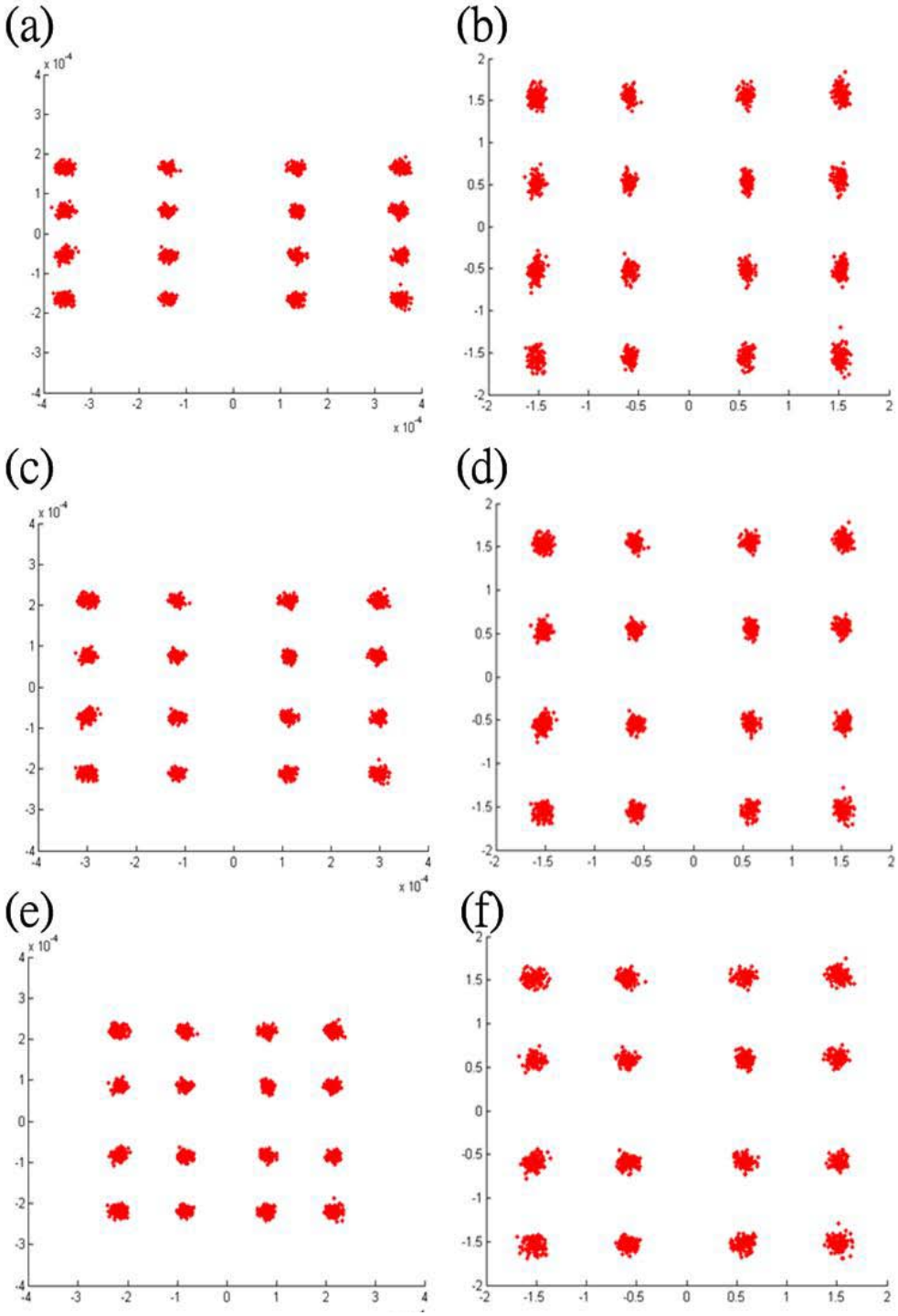

Figure 3-11 Constellations for simulation QPSK conjugate misalignment w/ and w/o GSOP. (a) I/Q=8dB w/o GSOP (b) I/Q=8dB w/ GSOP (c) I/Q=4dB w/o GSOP (d) I/Q=4dB w/ GSOP (e) I/Q=0dB w/o GSOP (f) I/Q=0dB w/ GSOP

3.4.4 Conjugate misalignment

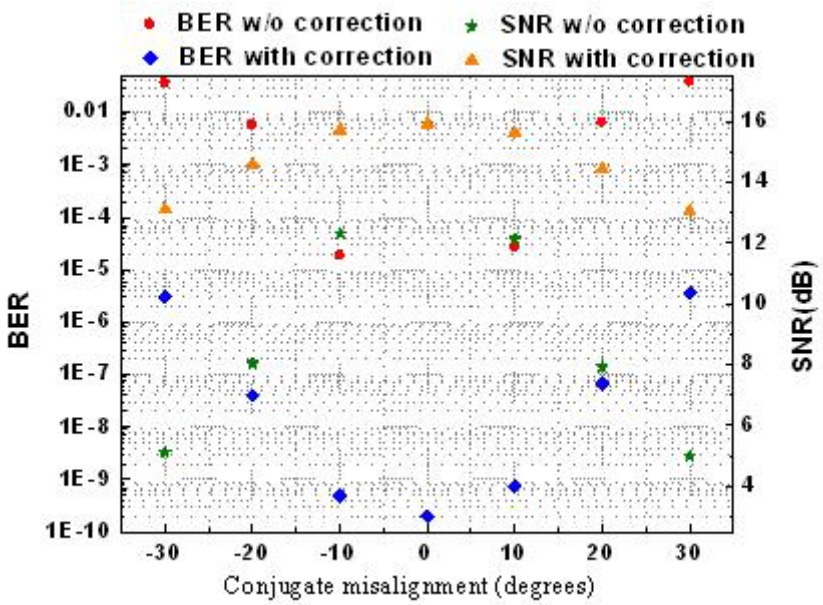

Figure 3-12 BER and SNR vs. conjugate misalignment for simulation single carrier QPSK.

Figure 3-12 and Figure 3-14 show simulation and experimental results and indicate that a 30° conjugate misalignment corresponding to about 11 dB SNR and about 13 orders BER degradation, respectively. After employing the GSOP, substantial performance improvement is obtained. With a 30° conjugate misalignment, only about 3 dB SNR and 8 orders BER degradation are observed for simulation and experimental results, respectively.

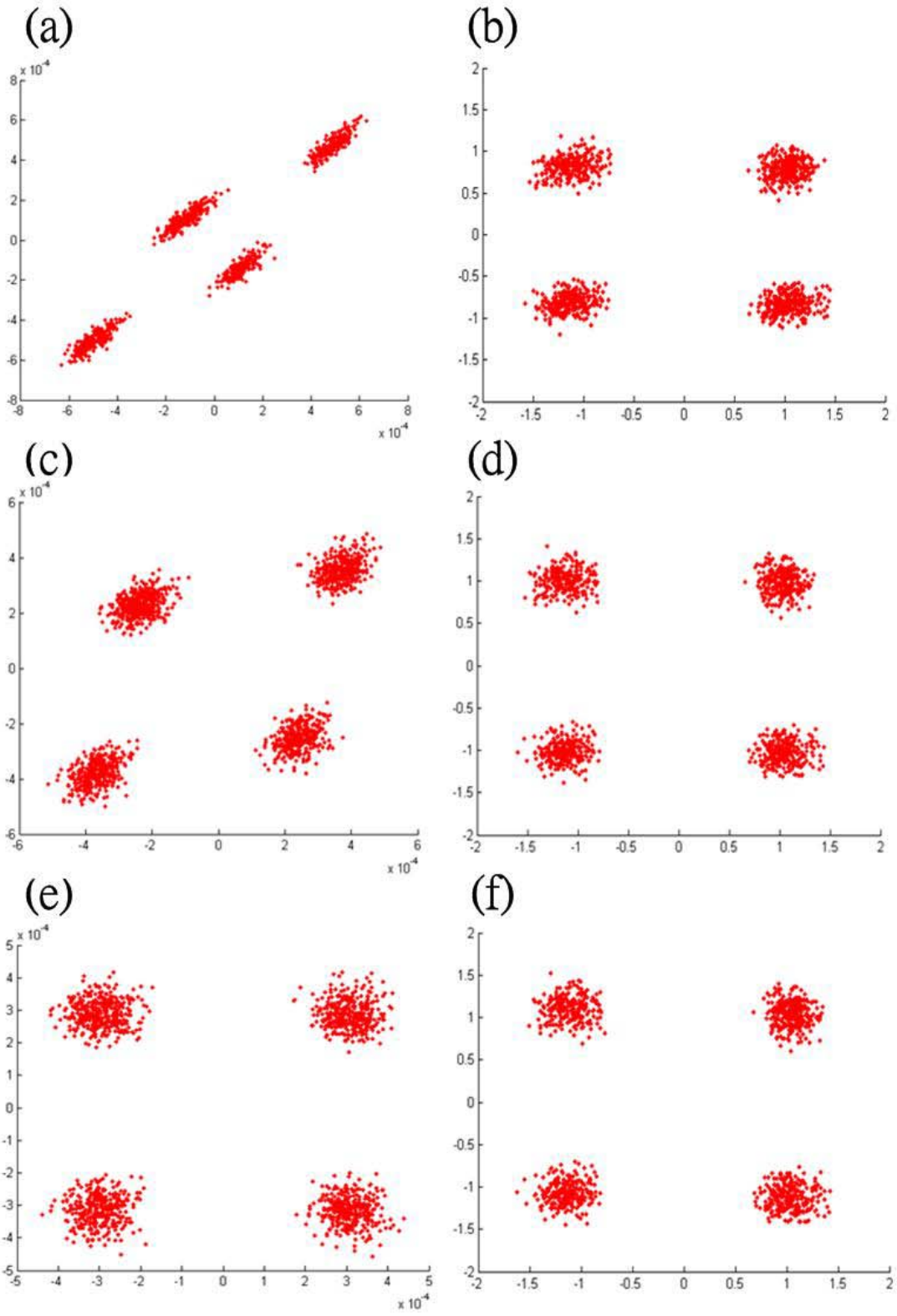

Figure 3-13 Constellations for simulation QPSK conjugate misalignment w/ and w/o GSOP. (a) 30° w/o GSOP (b) 30° w/ GSOP (c) 10° w/o GSOP (d)10° w/ GSOP (e) 0° w/o GSOP (f) 0° w/ GSOP

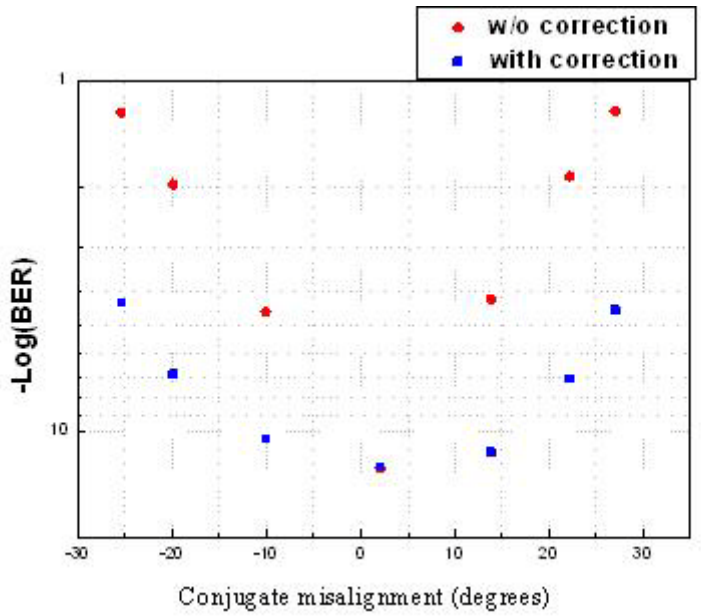

Figure 3-14 BER vs. conjugate misalignment for experimental single carrier QPSK.

Figure 3-13 and Figure 3-15 are the constellations for simulation and experimental 16-QAM conjugate misalignment with and without GSOP, respectively. Inset (a), (b), (c), (d), (e) and (f) of Figure3-13 and Figure3-15 illustrate 30° conjugate misalignment without GSOP, 30° conjugate misalignment with GSOP, 10° conjugate misalignment without GSOP, 10° conjugate misalignment with GSOP, 0° conjugate misalignment without GSOP and 0° conjugate misalignment with GSOP.

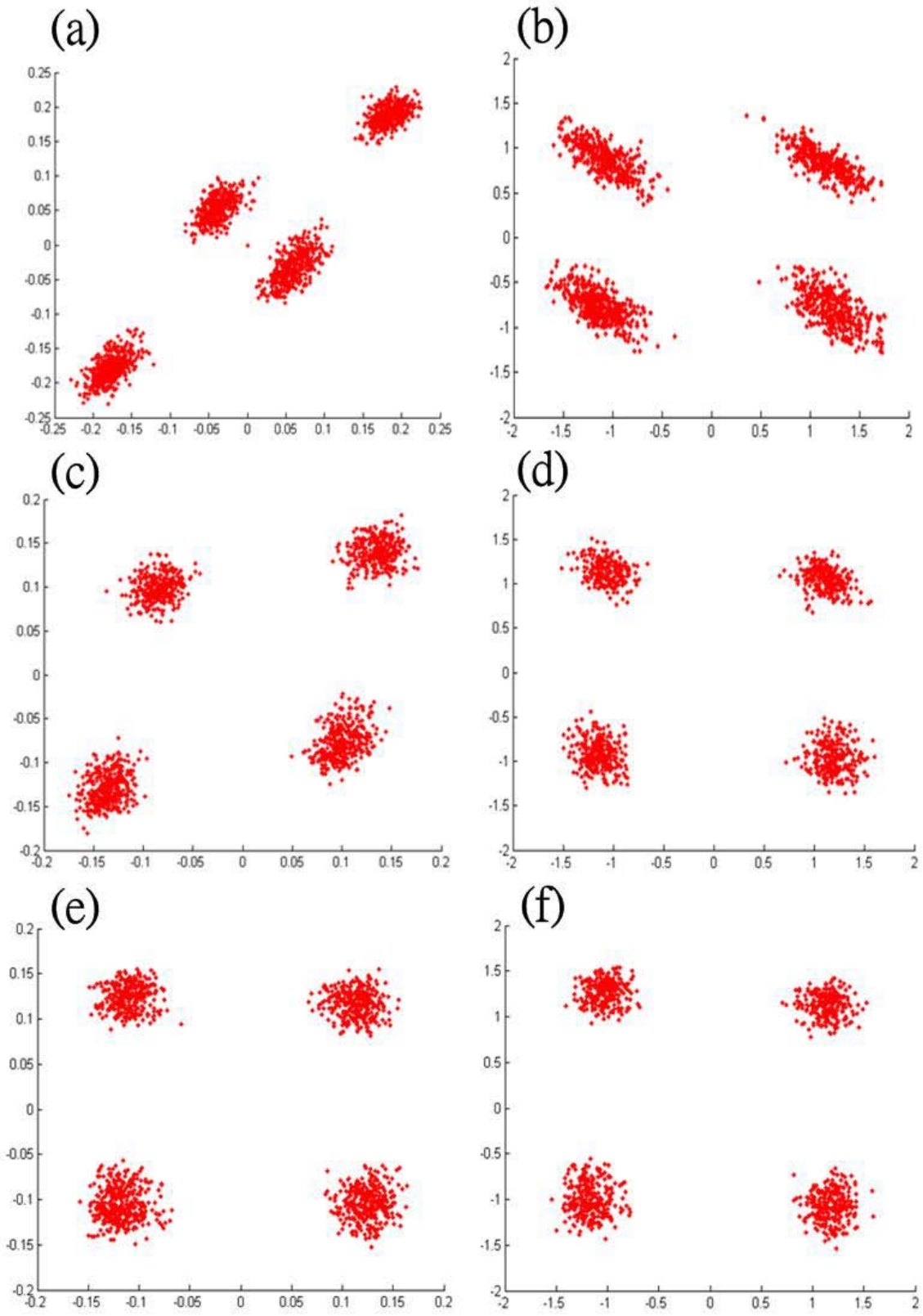

Figure 3-15 Constellations for experimental QPSK conjugate misalignment w/ and w/o GSOP. (a) 30° w/o GSOP (b) 30° w/ GSOP (c) 10° w/o GSOP (d)10° w/ GSOP (e) 0° w/o GSOP (f) 0° w/ GSOP

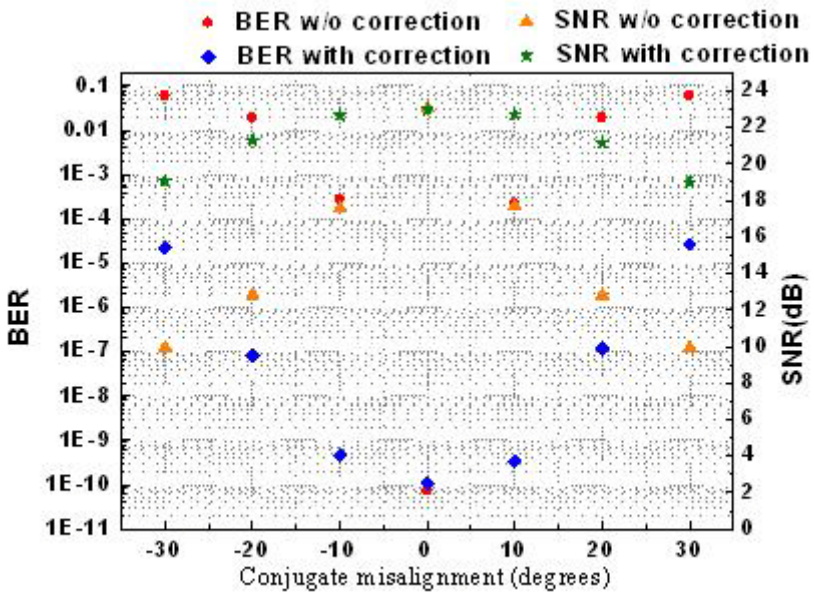

Figure 3-16 BER and SNR vs. conjugate misalignment for simulation single carrier 16-QAM.

Figure 3-16 is BER and SNR curves at different conjugate misalignment conditions for simulation 16-QAM and indicates that a 30° conjugate misalignment corresponding to about 12 dB SNR degradation. After employing the GSOP, only about 3 dB SNR degradation is observed.

Figure 3-17 shows the constellations for simulation 16-QAM conjugate misalignment with and without GSOP. Inset (a), (b), (c), (d), (e) and (f) of Figure3-17 illustrate 30° conjugate misalignment without GSOP, 30° conjugate misalignment with GSOP, 10° conjugate misalignment without GSOP, 10° conjugate misalignment with GSOP, 0° conjugate misalignment without GSOP and 0° conjugate misalignment with GSOP.

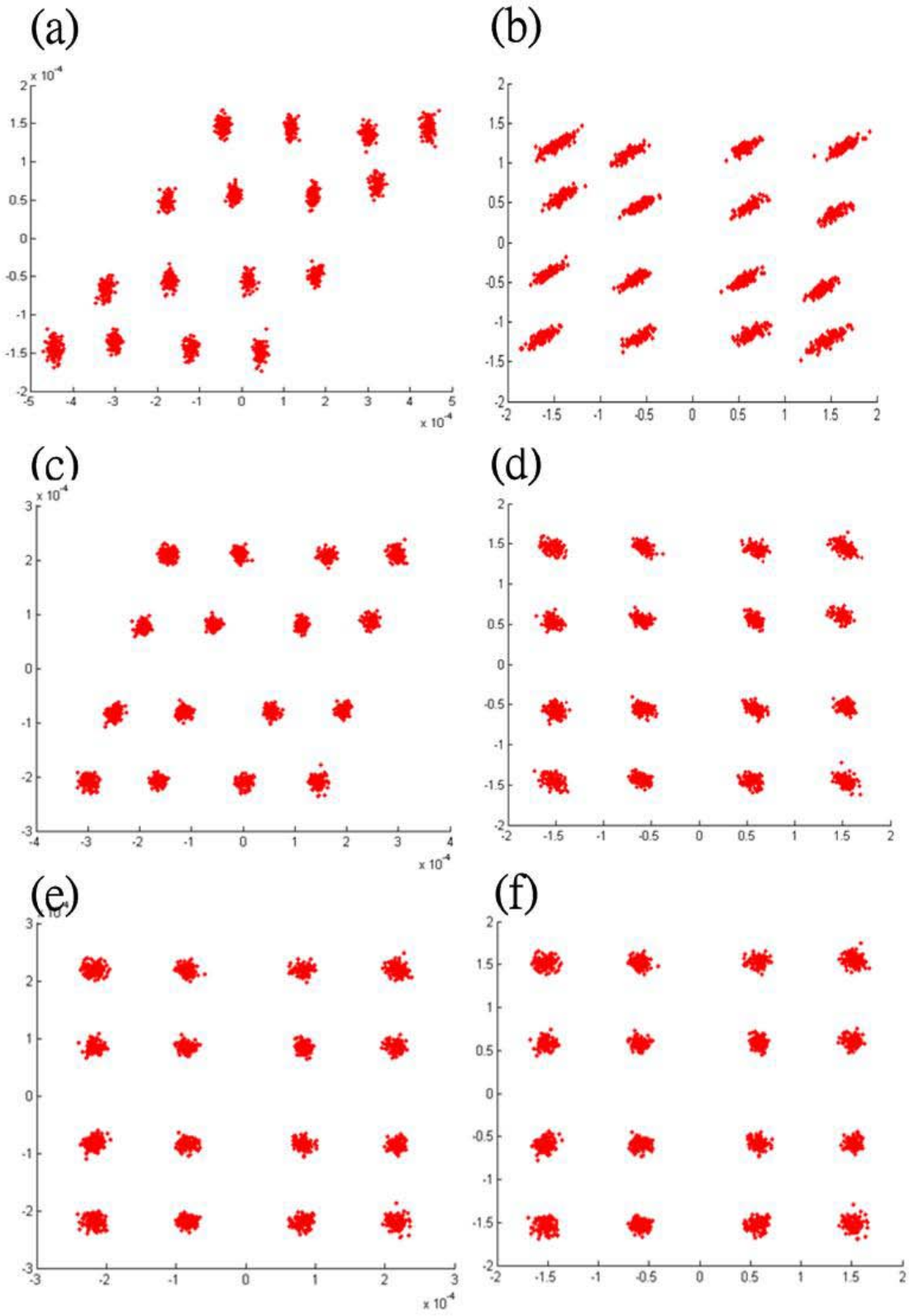

Figure 3-17Constellations for simulation 16-QAM conjugate misalignment w/ and w/o GSOP. (a) 30° w/o GSOP (b) 30° w/ GSOP (c) 10° w/o GSOP (d)10° w/ GSOP (e) 0° w/o GSOP(f) 0° w/ GSOP

In order to resolve I/Q imbalance, the GSOP scheme is unitized to compensate the amplitude mismatch and conjugate misalignment. After employing GSOP scheme, the imbalance effects can be solved.

3.4.5 Synchronization

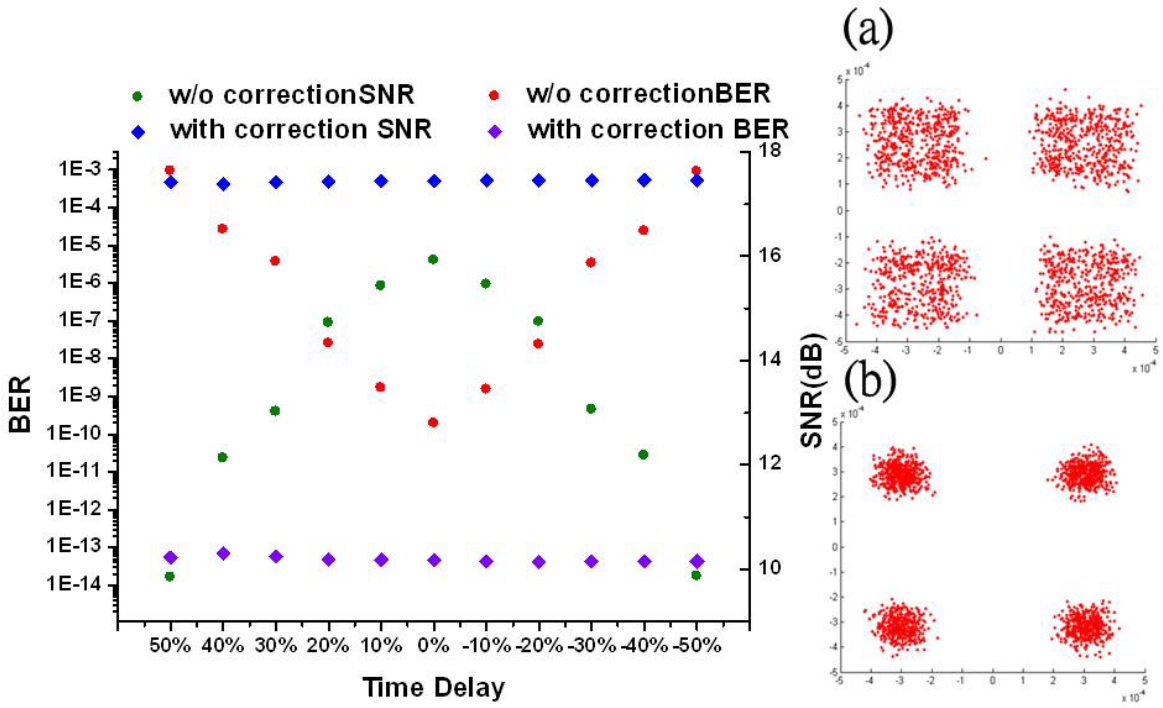

Figure 3-18 BER and SNR vs. Time Delay for simulation QPSK.
(a) Time delay 50% w/o correction.
(b) Time delay 50% with correction.

And now, I want to show you another imbalance factor - path length. If the lengths of data-I path and data-Q path are not exactly the same, the two data will not arrive at receiver at the same time. That may degrade the signal quality and distort signals.

We use VPI program and AWG to generate time delay effect. Figure3-18 and Figure 3-19 are BER and SNR curves at different time delay condition for simulation QPSK and experimental QPSK, respectively. Inset (a) and (b) of the two figures are

the constellations of time delay 50% without correction and with correction, respectively. In these figures, we can obtain as data-I and data-Q delay a half cycle, the performance is worst. That is due to the judging points are far away. The two figures show results with correction and without correction. We find out utilizing off-line software correction will compensate the factor effect. We use Matlab program to shift judging points to make them the same. Now the two data seems arrive at the same time.

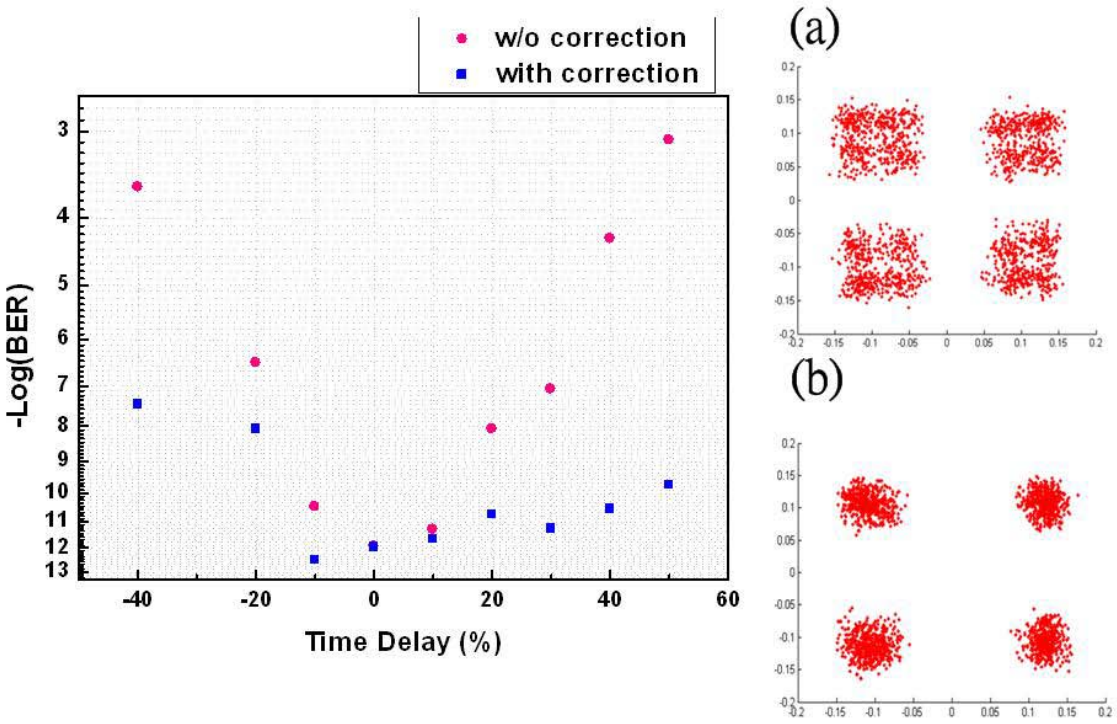

Figure 3-19 BER and SNR vs. Time Delay for experimental QPSK.
(a)Time delay 50% w/o correction.
(b)Time delay 50% with correction.

Figure 3-20 shows results of simulation 16-QAM signals. The worst condition is also time delay 50%. After using correction, the signals are improved, too. Inset (a) and (b) of this illustrate constellations of time delay 50% without correction and with correction. Inset (a) constellation size is large, and inset (b) constellation is clear.

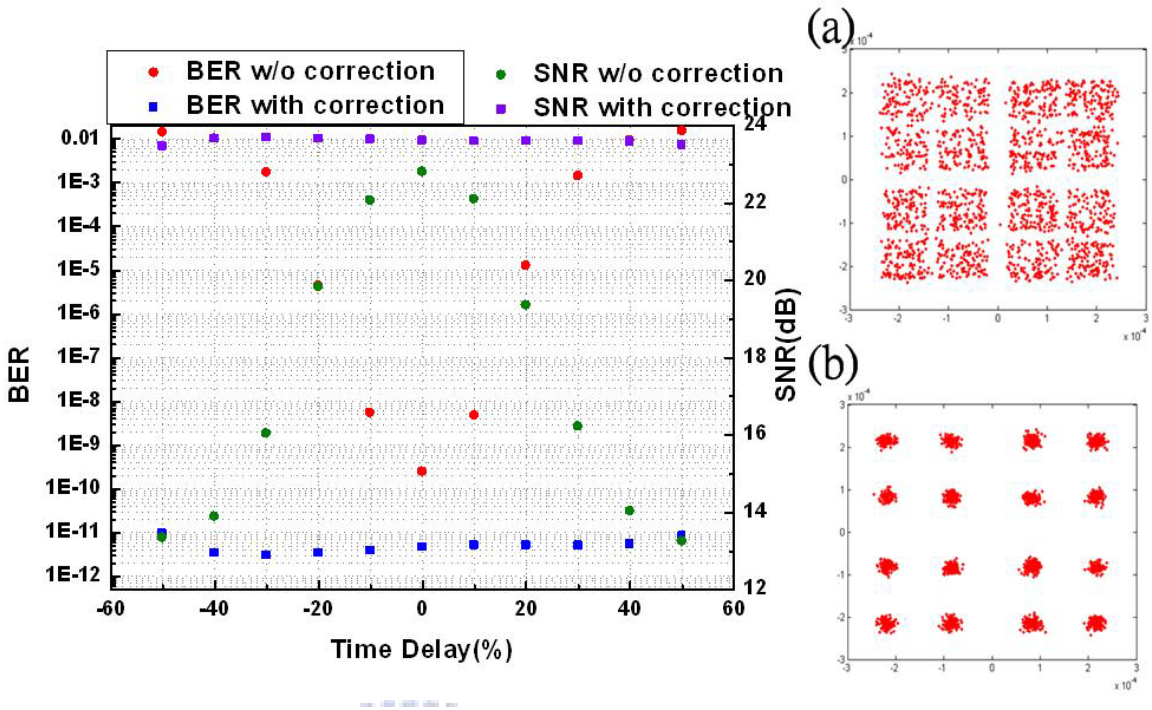

Figure 3-20 BER and SNR vs. Time Delay for simulation 16-QAM.

(c) Time delay 50% w/o correction.

(d) Time delay 50% with correction.

Chapter4 Experimental demonstration of proposed system

4.1 Preface

In chapter 3, we discuss the influence on the proposed setup due to the imbalance-effect. And now, I want to show you the detail about the novel proposed experimental setup and the experimental outcome. In this chapter, we will build up the experimental setup for the proposed system based on SSBCS modulation. Figure 4-1(a), (b) and (c) show the comparison of different DD-OFDM modulation scheme.

4.2 Comparison of different DD-OFDM modulation scheme

(a) Conventional SSB

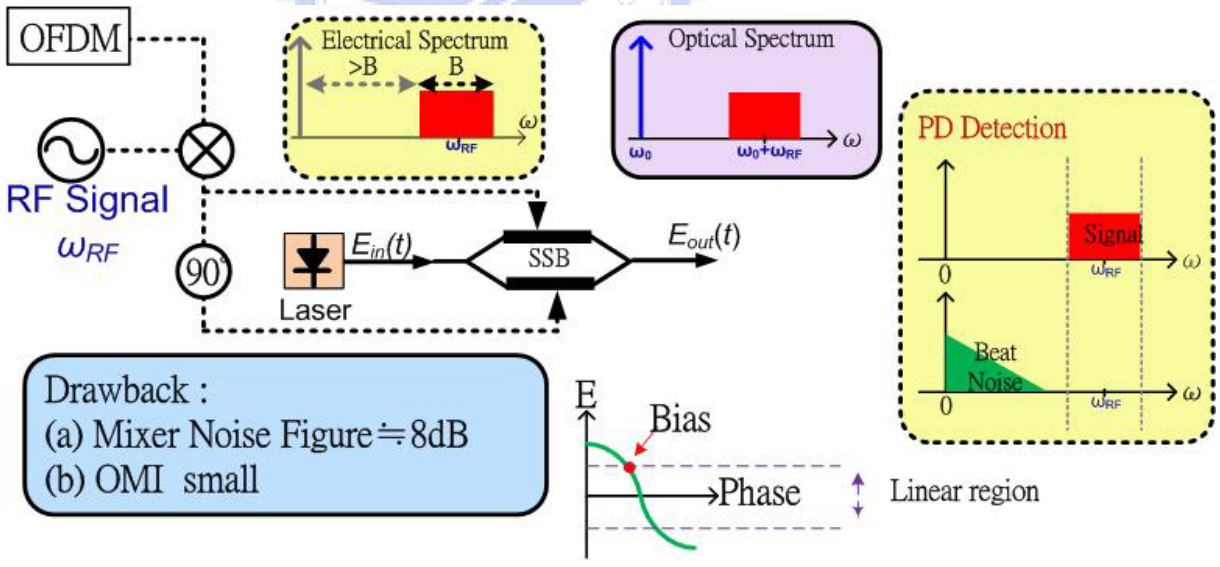

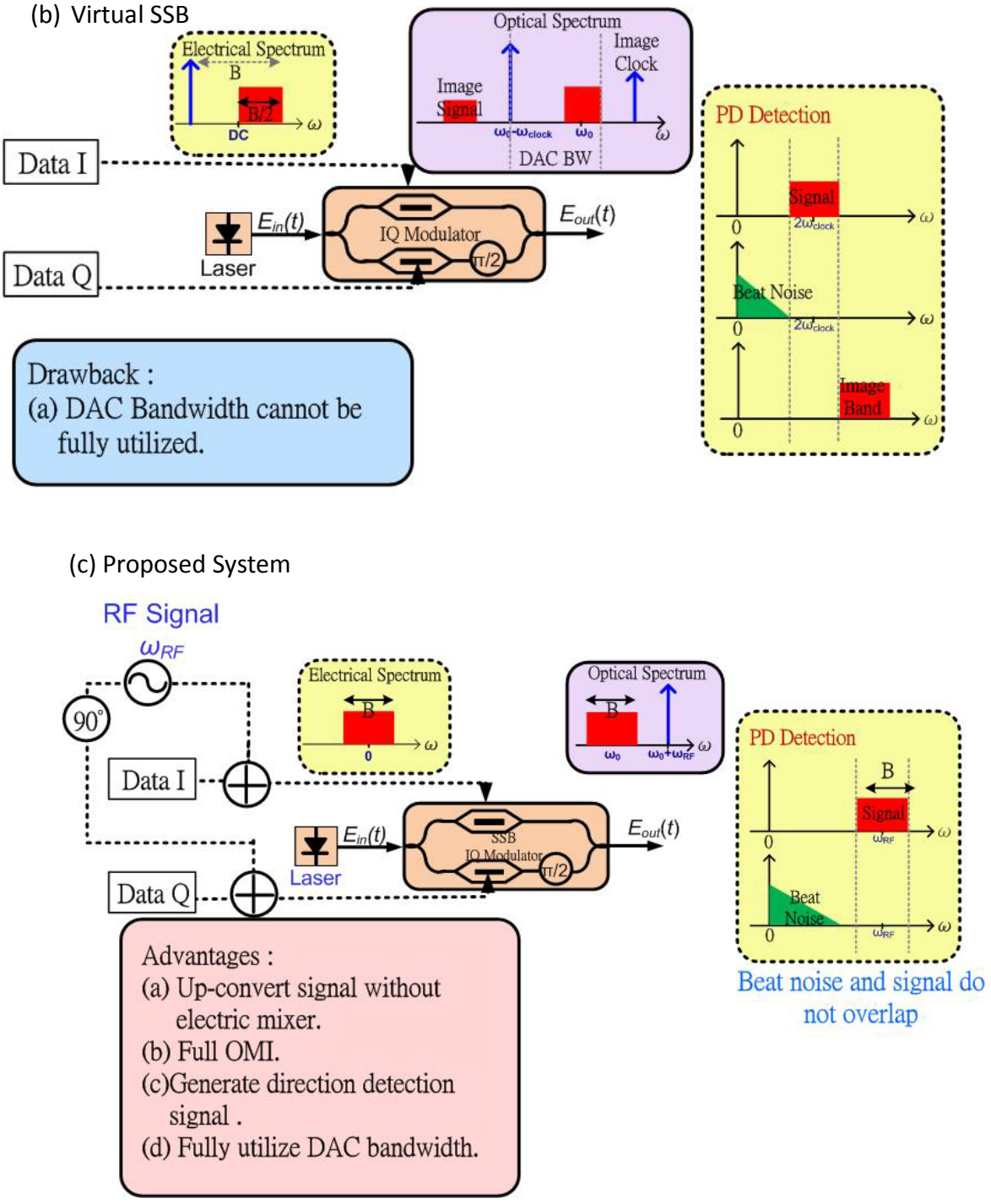

Figure 4-1 Comparison of different DD-OFDM modulation shceme.
(B: bandwidth of DAC, f_0: optical carrier frequency, f_0: intermedium frequency)

Before showing the concept of the proposed system, we see the comparison of different DD-OFDM modulation scheme shown as Fig4-1. Conventionally, optical direct-detection OFDM (DD-OFDM) signal is generated based on single-sideband

(SSB) modulation scheme via an external Mach-Zehnder modulator (MZM) as shown in inset (a) of Fig. 4-1. However, conventional SSB modulation approaches suffer from inferior sensitivities because the optical modulation index (OMI) is limited. Furthermore, to avoid beat noise after photo detection, an electrical I/Q mixer with a typical noise figure (NF) of more than 8 dB is needed to up-convert OFDM signal to intermedium frequency, which severely hinders implementation of highly spectral efficiency QAM OFDM signal for narrowband applications in the 10-Gb/s and above regimes. Recently, several modified SSB modulation schemes have been proposed to overcome this limitation. However, an electrical mixer is still needed to avoid the beat noise interference. Another DD-OFDM modulation scheme is virtual SSB modulation scheme without electrical I/Q mixer is proposed as shown in inset (b) of Fig. 4-1. The drawback is that half bandwidth of the DAC is wasted to avoid the beat noise interference.

This work presents an optical I/Q up-conversion for direct-detection OFDM signal generation as shown in inset (c) of Fig. 4-1. Since an electrical mixer is not needed to avoid the beat noise interference, the proposed system can support high level OFDM signal (i.e. 16 QAM or 64 QAM). Moreover, the bandwidth of digital-to-analog converter can be fully utilized.

4.3Concept of the proposed system

Figure 4-2 schematically depicts the principle of the proposed optical I/Q up-conversion for direct-detection signal generation. Inset (a) of Figure 4-2 shows how we generate optical subcarrier with carrier suppression. To realize direct-detection signals generation, we insert an optical subcarrier to induce remote beating by using

SSB modulation with carrier suppression . Except with a phase difference of 90°, the RF signals sent into the MZ-a and MZ-b are exactly the same. We bias MZ-a and MZ-b at the null point, the generated optical spectrum consists of an upper sideband (USB) and a lower sideband (LSB) with optical carrier suppression as shown in inset (a) of Fig. 4-2. When MZ-c is biased at the quadrature point, the polarity of LSB in lower arm opposes that in upper arm. The LSB will be eliminated whereas the USB is obtained.

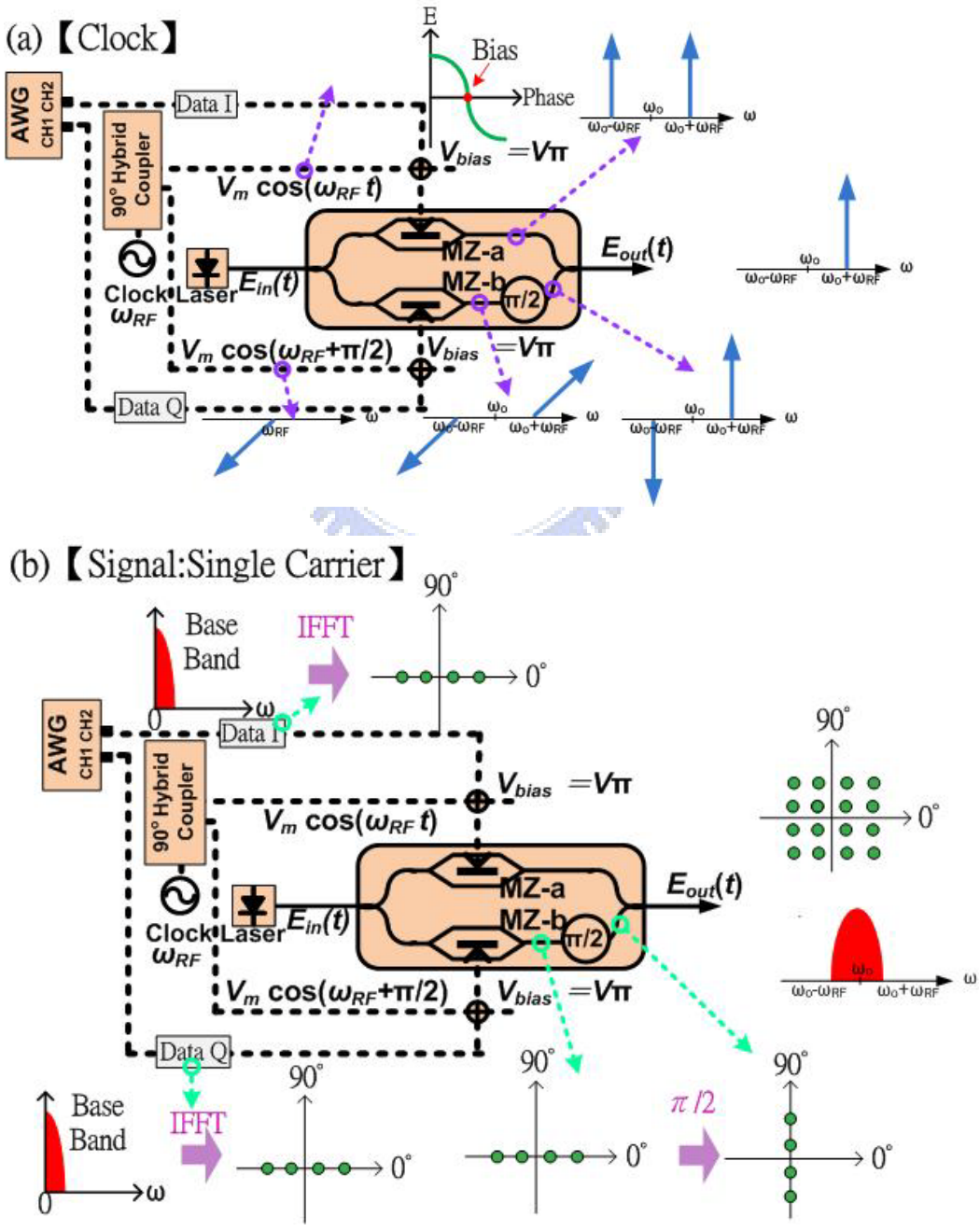

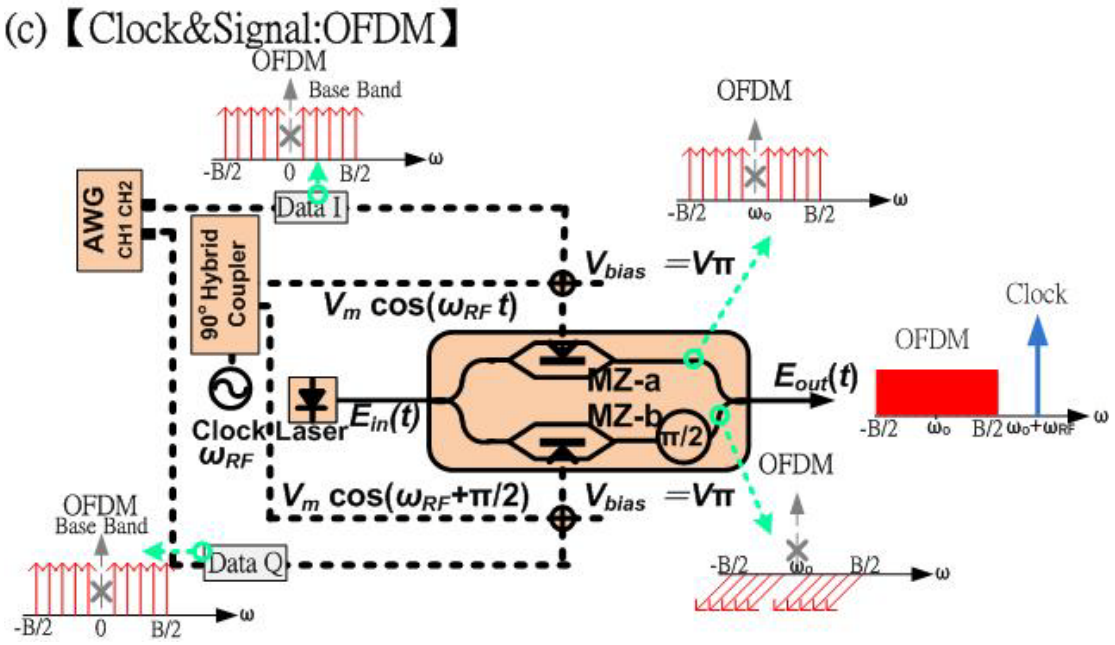

Figure 4-2 The Concept of All Optical IQ Up Conversion System.

And then, see inset (b) of Fig. 4-2. I want to use a single-carrier signal case to tell you how the I/Q modulation works. Data I and Q of single-carrier signal are sent to MZ-a and MZ-b of the optical I/Q modulator, respectively. To achieve high optical modulation depth and to operate in E-field linear region of the MZM, both MZ-a and MZ-b are biased at the null point. Therefore, optical single-carrier signal at the center frequency of optical carrier with carrier suppression is generated as shown in inset (b) of Fig. 4-2. And we utilize the $\pi/2$ phase delay modulation to rotate Data-Q to Q-axis (90°-axis) to forma m-QAM signal. Inset (c) of Fig. 4-2 is the case of OFDM signal.

Therefore, as both RF and OFDM signals are simultaneously sent to I/Q modulator, the generated optical DD-OFDM signal consisting of an un-modulated subcarrier and an OFDM-modulated carrier. After square-law photo-diode (PD) detection, electrical RF-OFDM signals are obtained. Note that the proposed OFDM transmitter does not need an electrical mixer with a typical NF of more than 8 dB to

avoid the beating noise interference, which is very important for highly spectral efficiency OFDM signals (i.e. 16-QAM or 64-QAM OFDM signal). Additionally, the relative intensity between the un-modulated and OFDM-modulated subcarriers can be easily tuned by adjusting the individual power of the electrical sinusoidal and OFDM signals to optimize the performance of the optical RF signal.

4.4 Experimental results for all optical IQ up conversion system

4.4.1 Experimental setup

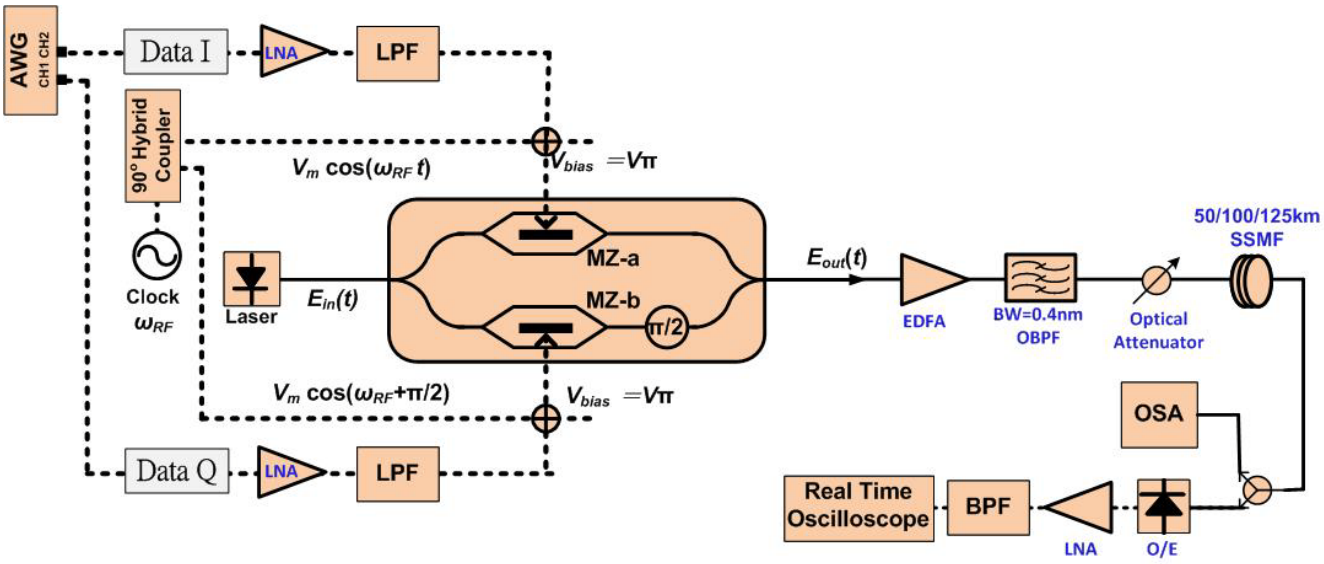

Figure 4-3 The Experimental Setup of All Optical IQ Up Conversion System.

Figure 4-3 depicts the experimental setup for all optical I/Q up conversion system via a I/Q modulator. We use a continue wave tunable laser (CW-TL) to generate light source about 1550nm. The light source is then passed through a polarization controller to achieve max optical power when the I/Q modulator is biased at full point. The signals (Data-I and Data-Q) are generated by a Tektronix® AWG7102 arbitrary waveform generator (AWG) using a Matlab® program. The sample rate and digital-to-analogue converter resolution of the AWG are 10 Gb/s and 10 bits, respectively. And then we use two the same type low noise amplifier (LNA) to amplify

Date I and Data Q to reach the best modulation index (MI) condition. Following, we use low pass filter to remove unwanted noise which is created by DSP signal generation method and AWG-machine. To realize optical direct-detection signal, a new optical subcarrier is generated at the LSB of the original carrier by 7.5 GHz. Generate sinusoidal wave as electrical driving signals that are used to generate an optical subcarrier. We use a 90°phase delay coupler to divide the sinusoidal wave into two parts. And then we bias both MZ-a and MZ-b at null point and set the phase modulator to delay $\pi/2$. To be able to transmit the signals, we utilize an EDFA to amplifier the optical power and an optical band pass filter to reduce ASE noise. Finally we use a Real Time Scope which is a Tektronix® DPO 71254 with a 50-Gb/s sample rate and a 3-dB bandwidth of 12.5 GHz. to capture the receiver-signals. We use off-line way to demodulate the signals.

4.4.2 Optimal condition for RF signals

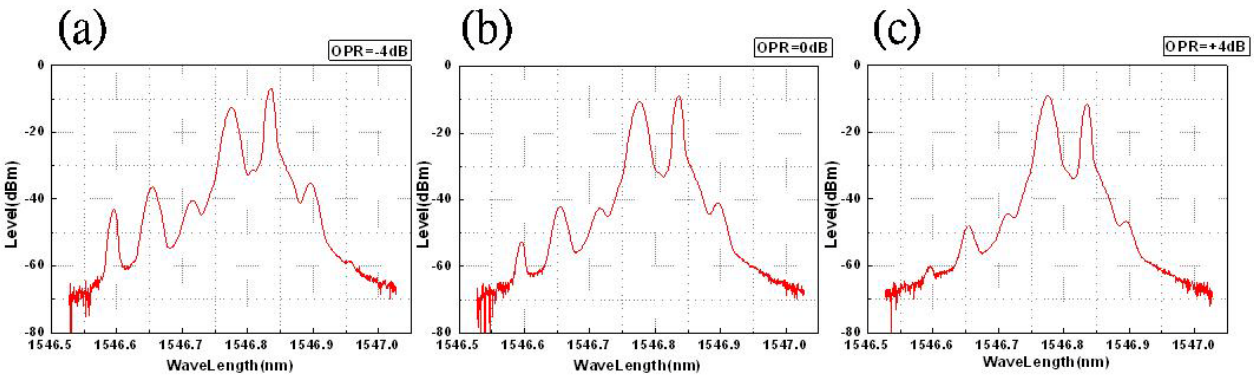

Figure 4-4 Optical Spectrum of single carrier QPSK signal.
OPR= Pd/Ps(dB), Pd: optical power of data-modulated optical carrier; Ps: optical power of 7.5GHz subcarrier.OPR=-4dB (b) OPR=0dB (c) OPR=4dB

Fig. 4-4 and Fig. 4-6 show the optical spectrums in different OPR (OPR= P_s/P_d, P_s and P_d are the optical power of the 7.5-GHz subcarrier and the 0-GHz data-modulated optical carrier, respectively.) for single carrier QPSK and OFDM 16QAM signals. The BER vs. OPR curves of single carrier QPSK and OFDM 16QAM signal are shown in Fig. 4-5 and Fig. 4-7. Single carrier QPSK signal best OPR condition is 0dB as shown in Fig 4-5. The blue star is the case without imbalance-correction and the red circle is the case with imbalance correction. OFDM 16QAM signal best OPR condition is 3dB as shown in Fig 4-7. The blue star case is captured at PD power equal to -14dBm and the other is at PD receiver power equal to -13dBm.

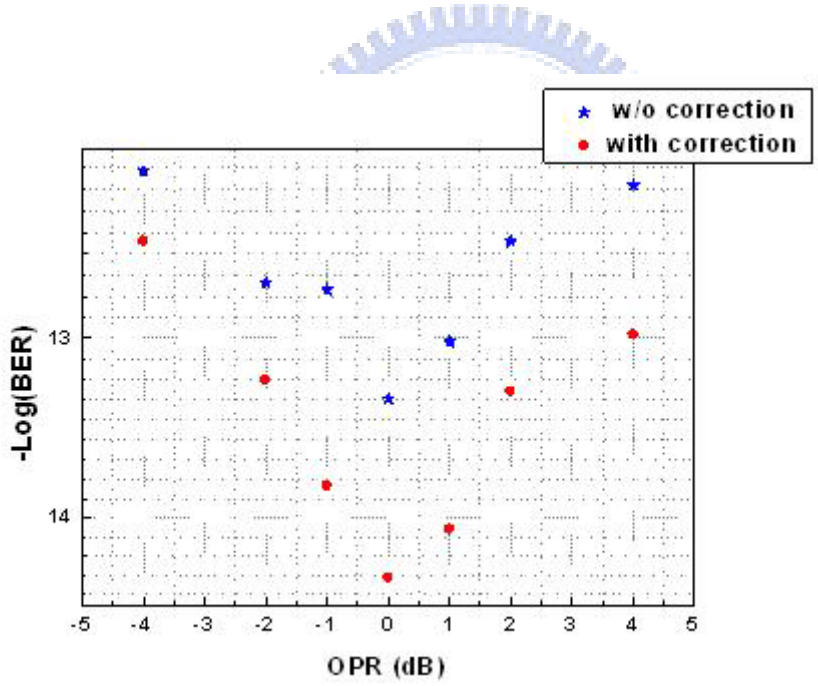

Figure 4-5 BER vs. OPR curve for single carrier QPSK signal.

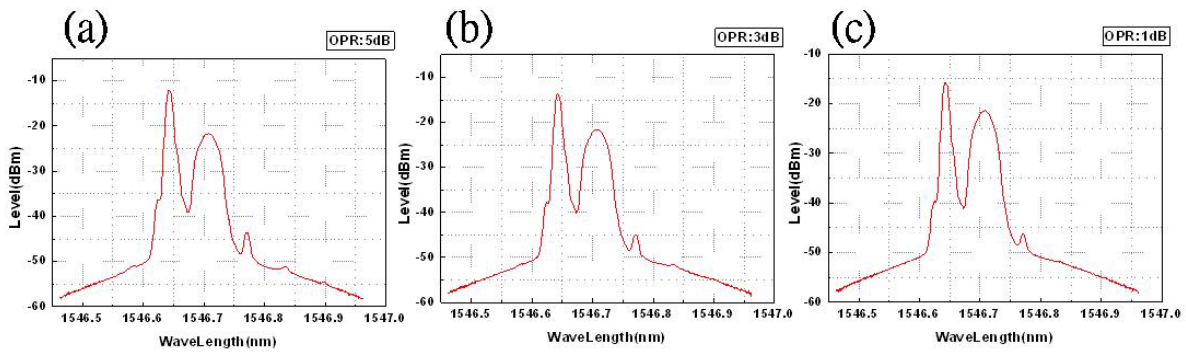

Figure 4-6 Optical Spectrum of OFDM 16QAM signal.
OPR= Pd/Ps(dB), Pd: optical power of data-modulated optical carrier; Ps: optical power of 7.5GHz subcarrier.OPR=5dB (b) OPR=3dB (c) OPR=1dB

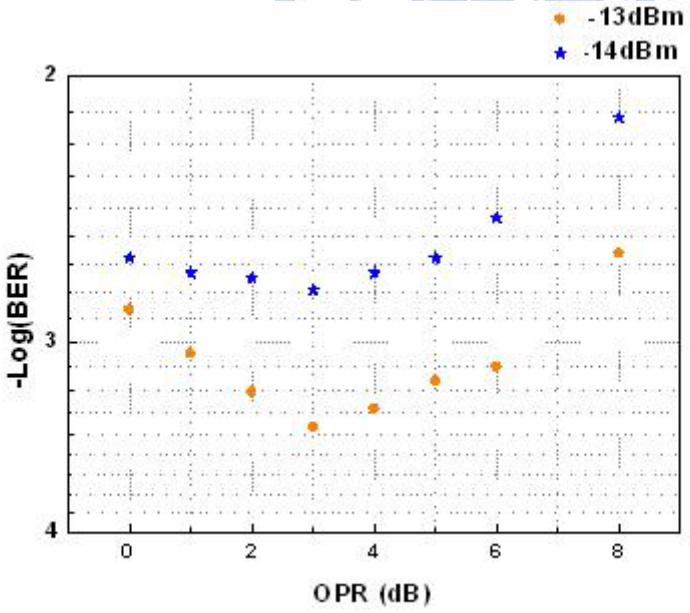

Figure 4-7 BER vs. OPR curve for OFDM 16QAM signal.

4.4.3 Transmission Results

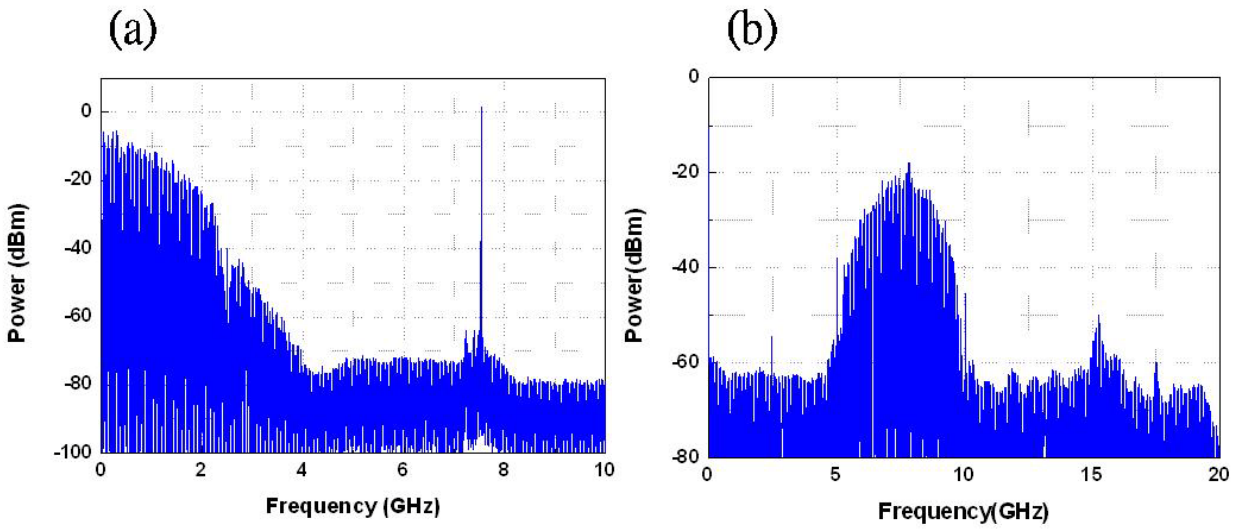

Figure 4-8 Electrical Spectrums for Single Carrier QPSK.
(a) Tx terminal Electrical Spectrum.
(b) Rx terminal Electrical Spectrum.

Figure 4-8 is the electrical spectrum for single carrier QPSK signal and a subcarrier. The single carrier QPSK signals are generated by a Tektronix® AWG7102 arbitrary waveform generator (AWG) using a Matlab® program. An optical 10-Gb/s single carrier QPSK signal that occupies a total bandwidth of 5 GHz can be generated, and its receiver signal electrical spectrum is shown as Figure 4-8 (b). We just need half bandwidth of receiver signal to generate Tx single carrier QPSK signal as shown Figure 4-8 (a), and a optical subcarrier is generated at the LSB of the original carrier by 7.5 GHz.

. The OFDM 16QAM signals are generated by a Tektronix® AWG7102 arbitrary waveform generator (AWG) using a Matlab® program, too. The IFFT length is 64. A 156.25-MSym/s 16-QAM symbol is encoded at 32 channels (i.e. channels 3-18 and 48-63) with the remaining 32 channels set to zero. Therefore, an optical 20-Gb/s 16-QAM OFDM signal that has 32 subcarriers and occupies a total bandwidth of 5 GHz can be generated, and its receiver signal spectrum as shown in Figure 4-9(b). The cyclic prefix is set to 1/256

symbol time. To realize optical direct-detection OFDM signal, a new optical subcarrier is generated at the LSB of the original carrier by 7.5 GHz, as shown in Fig. 4-9(a).

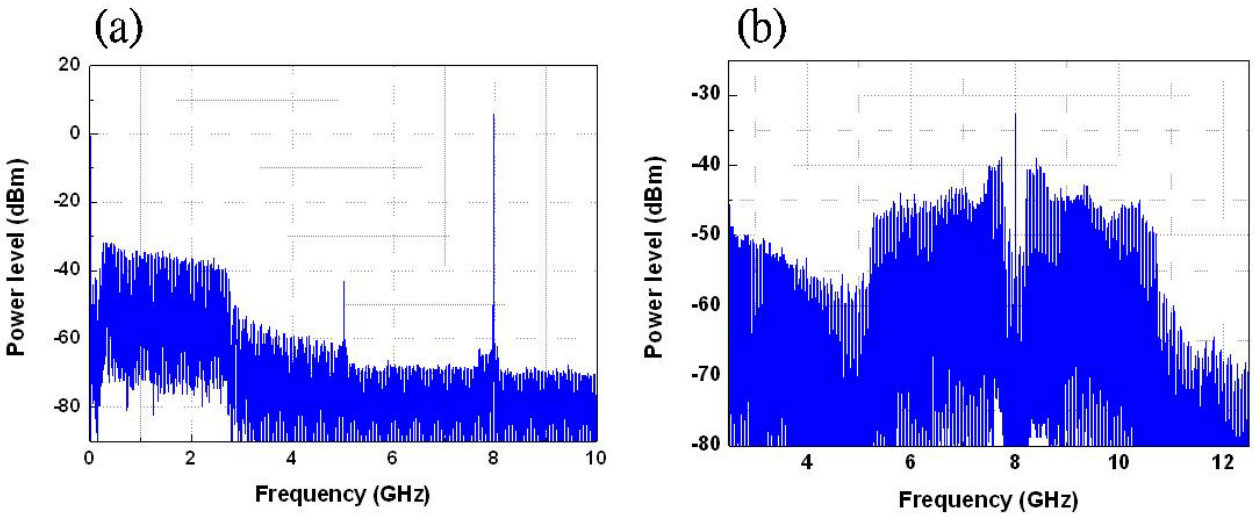

Figure 4-9 Electrical Spectrum for OFDM 16QAM.
(a) Tx terminal Electrical Spectrum.
(b) Rx terminal Electrical Spectrum.

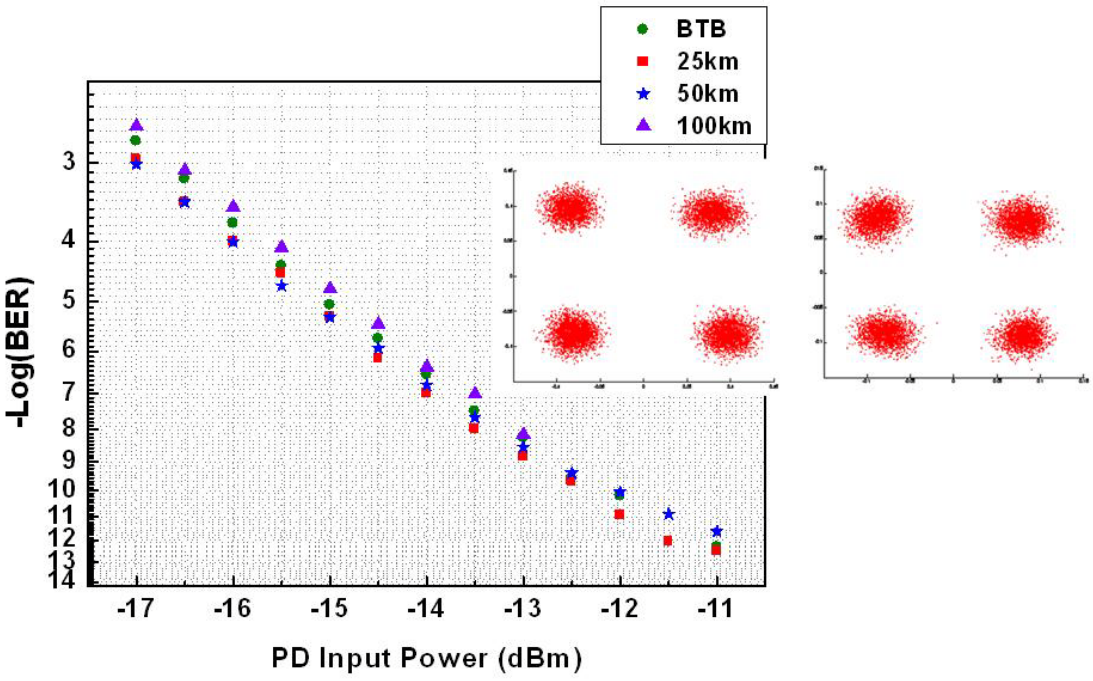

Figure 4-10 BER-Receiver Power curve for QPSK.

Figure 4-10 shows the BER performance of the single carrier QPSK signals, a receiver sensitivity of -13dBm is achieved at a BER of 10^{-9} in the BTB case. The penalty at a BER of 10^{-9} is negligible following 100-km SMF transmission. And left hand side constellation is the BTB case, right hand side is the after 100-km transmission case. The constellation size of each point of the two diagrams is almost the same. Figure 4-11 shows the constellations and eye diagrams of BTB, 25km, 50km, and 100km. And they are captured at PD input power equal to -12.5dBm.

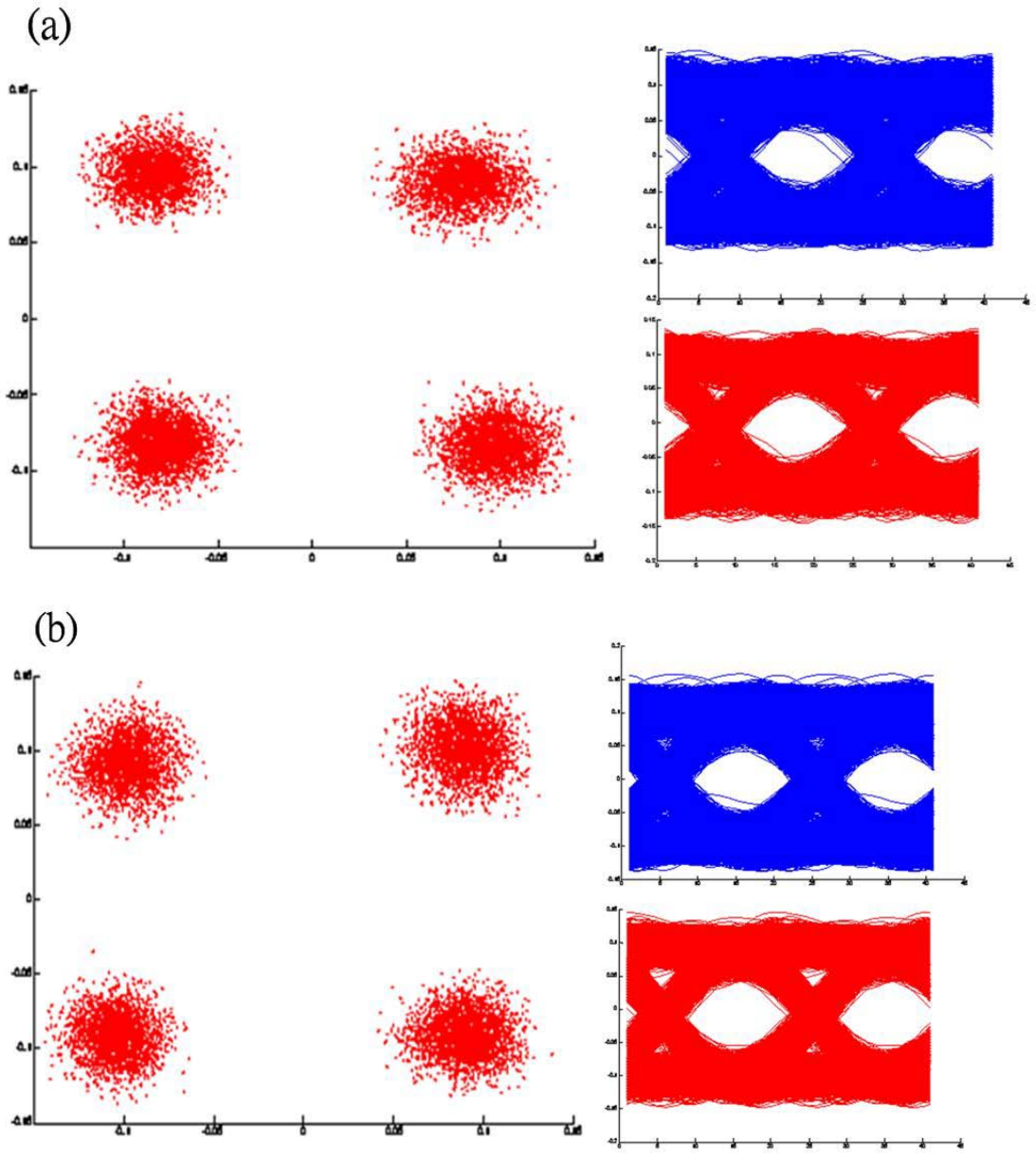

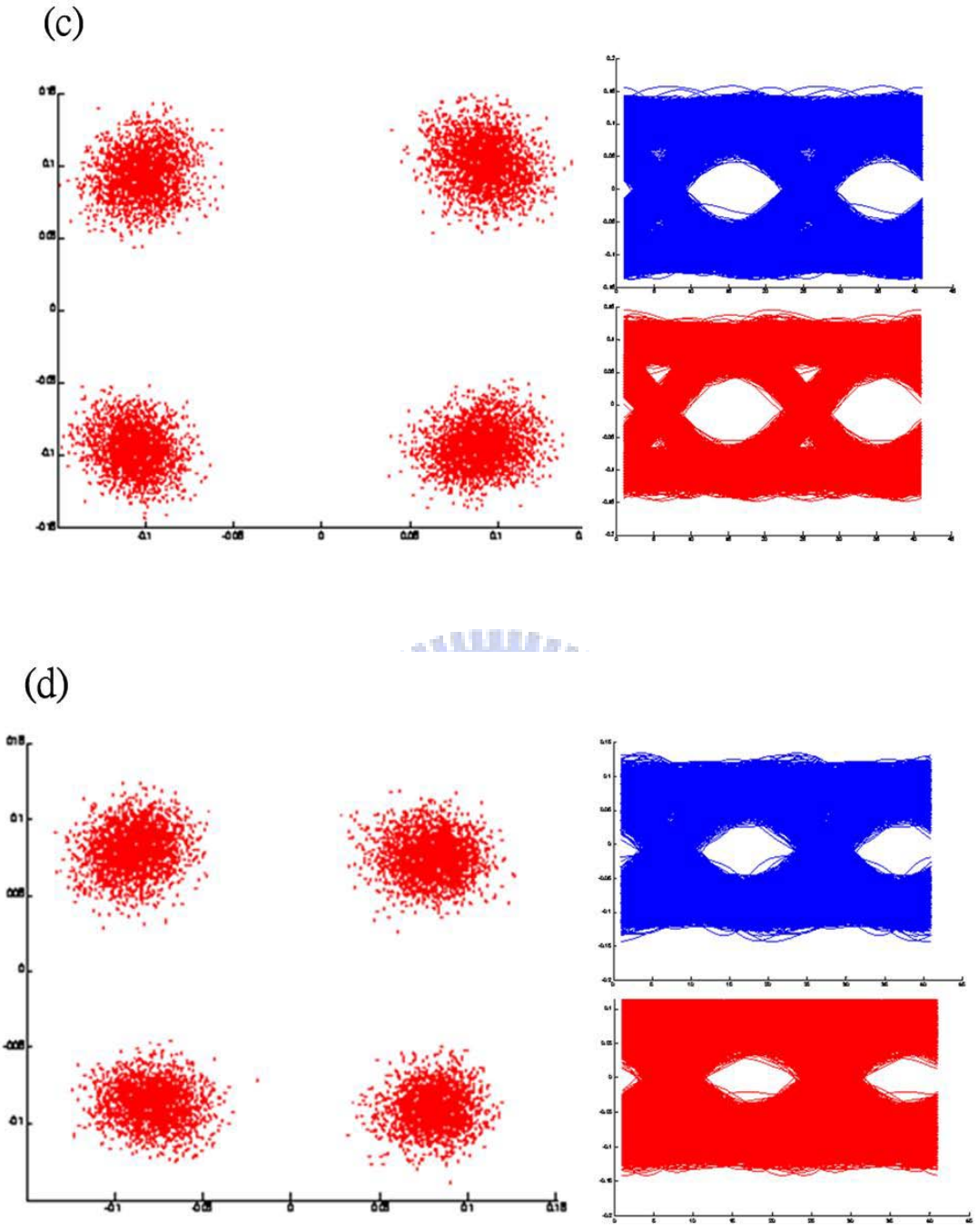

Figure 4-11 Constellations and eye diagrams for single carrier QPSK signals at PD Input Power=-12.5dBm. (a)BTB (b) 25km (c) 50km (d)100km

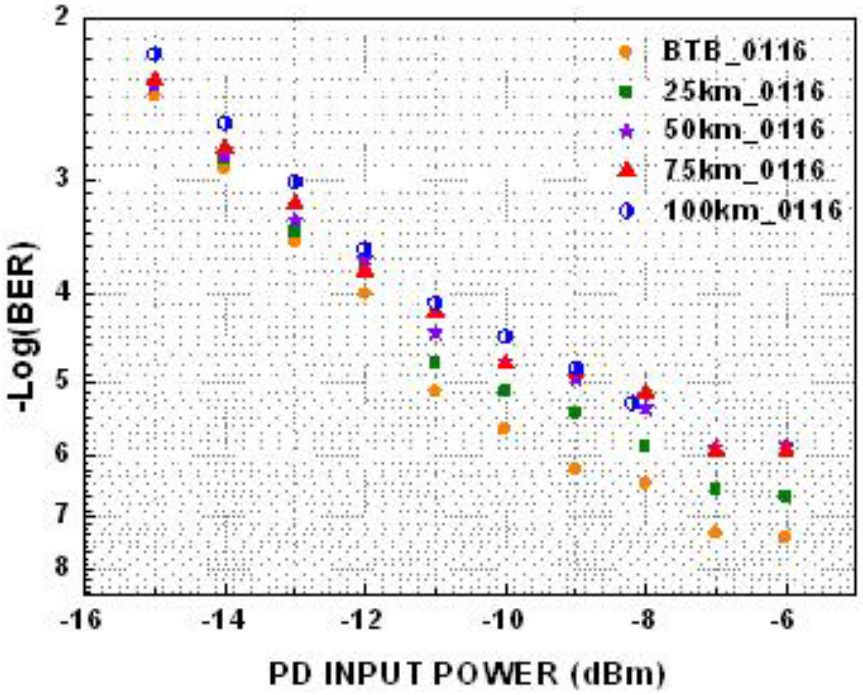

Figure 4-12 BER-Receiver Power curve for OFDM 16QAM.

Figure 4-12 shows the BER performance of the OFDM 16QAM signals, a receiver sensitivity of -14dBm is achieved at a BER of 10^{-3} in the BTB case. The penalty at a BER of 10^{-3} is about 1dB following 100-km SMF transmission. The constellation size of each point of Figure 4-13 constellations is almost the same. The inset (a), (b), (c), and (d) are BTB, 25km, 50km, and 100km, respectively. And they are captured at PD input power equal to -8dBm.

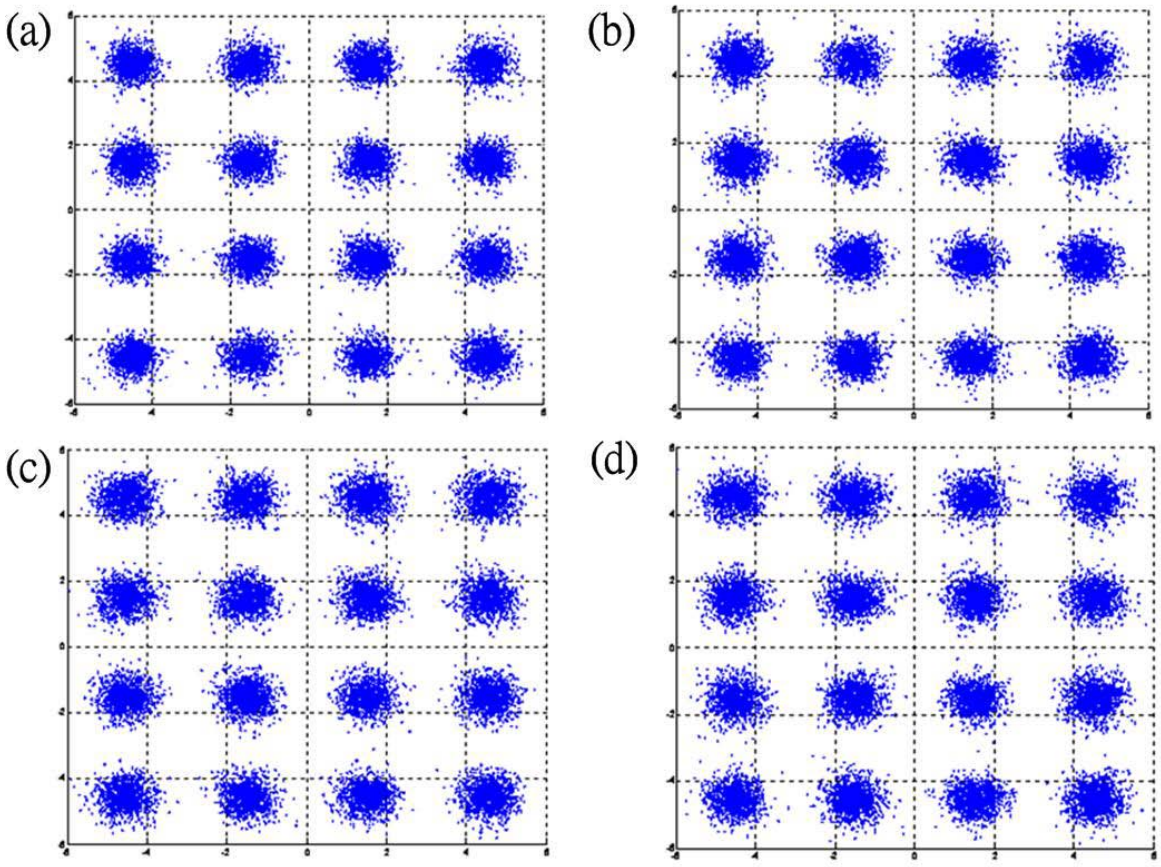

Figure 4-13 Constellations and eye diagrams for OFDM 16QAM signals at PD Input Power=-8dBm. (a)BTB (b) 25km (c) 50km (d)100km

4.5 The influence of phase noise

In this section, we investigate the laser linewidth impact on optical 60-GHz OFDM performance. With laser linewidth of 10MHz, BER of both 20-Gb/s 16-QAM and 14-Gb/s QPSK OFDM signals within 7-GHz license-free band is below the FEC limit following 100-km SMF transmission.

Figure 4-14 shows BER and SNR change with laser line-width of 28Gb/s OFDM 16-QAM for transmission 50-km and 100-km. We can find that when the laser line-width exceeds 100 KHz, the SNR drops quickly.

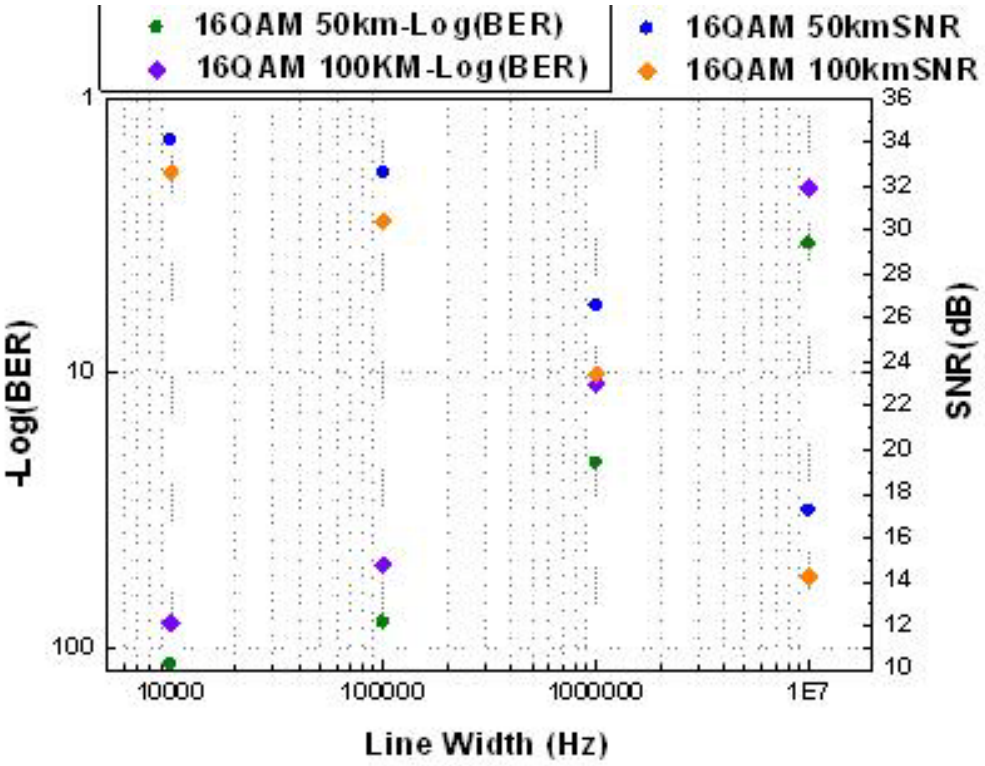

Figure 4-14 BER and SNR vs. Laser Line-Width for simulation 28Gb/s OFDM 16-QAM.

Figure 4-15 shows that the BER curves of 60-GHz 20-Gb/s 16-QAM OFDM signals using DFB laser. Note that the laser linewidth has more influence on 16-QAM signals than QPSK signals. As the transmission distance increases from 0 km to 100 km, the performance of 60-GHz 16-QAM OFDM signals gradually degrades due to de-coherence of optical un-modulated and OFDM-modulated sidebands. As transmission distance is 100 km, the BER of 60-GHz 20-Gb/s 16-QAM OFDM signals can be below the FEC limit with receiver power of more than -6dBm. If the ECL with linewidth of 10kHz is utilized, no significant receiver power penalty is observed after the transmission of 100-km SSMF as shown in Fig. 4-16.

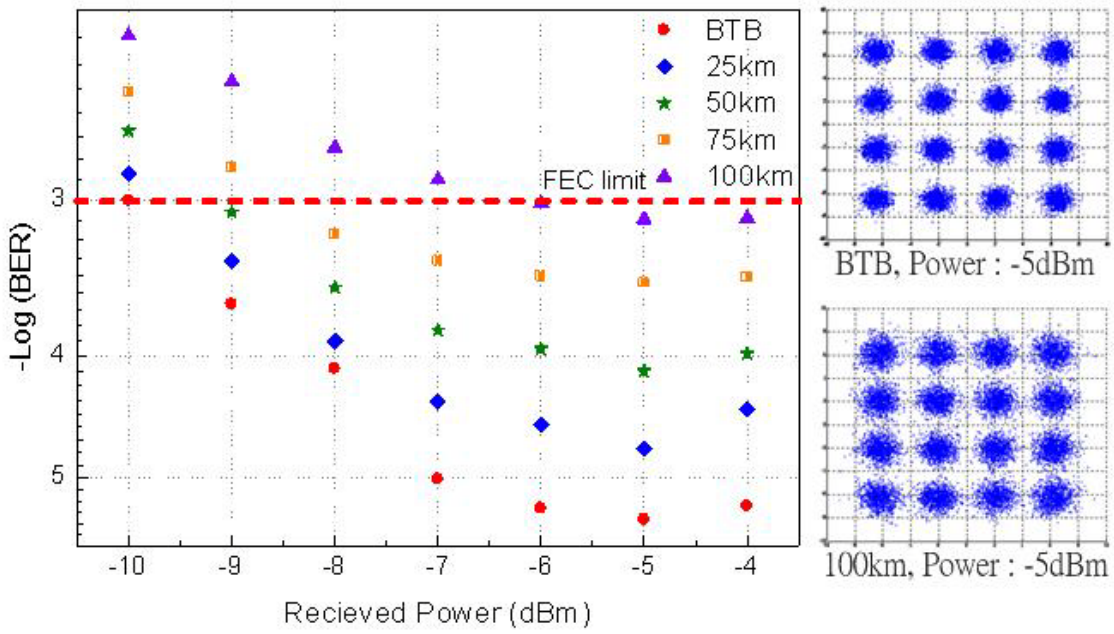

Figure 4-15 BER curves of 60-GHz 20-Gb/s 16-QM OFDM signals. The linewidth is 10 MHz.

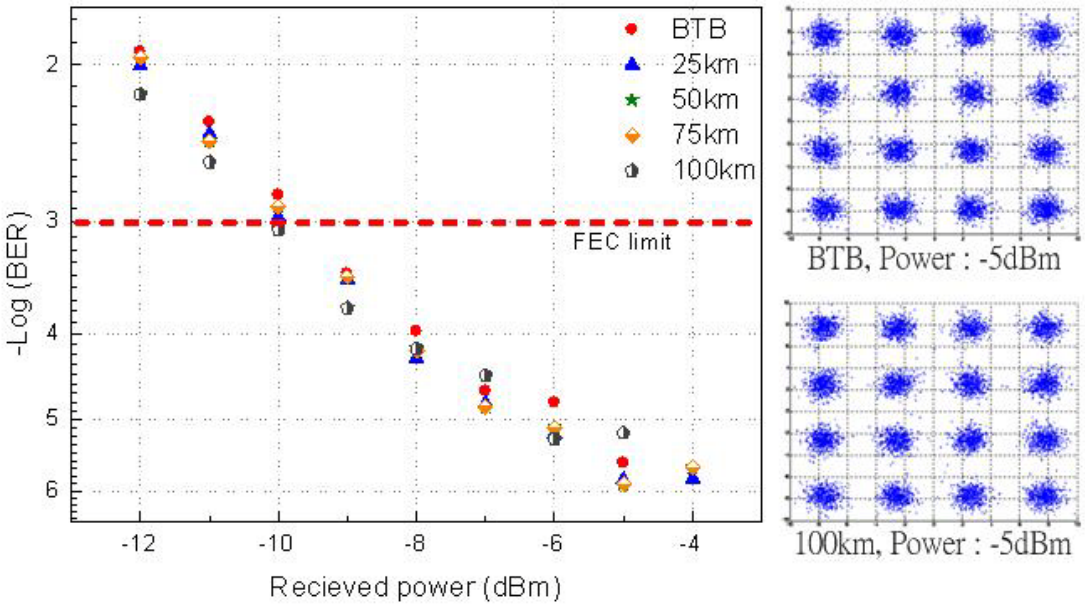

Figure 4-16 BER curves of 60-GHz 20-Gb/s 16-QM OFDM signals. The linewidth is 10 KHz.

To provide higher data rate within 7-GHz license-free band at 60 GHz, multi-level OFDM is utilized. As higher spectral efficiency modulation format is used, the laser linewidth will play more and more important due to de-coherence of optical un-modulated and OFDM-modulated sidebands caused by fiber chromatic dispersion. In this paper, we experimentally demonstrate that BERs of both 20-Gb/s 16-QAM and 14-Gb/s QPSK OFDM signals within 7-GHz license- free band are below the FEC limit following 100-km SMF transmission as DFB laser with the line-width of 10MHz is used.

Chapter5 60GHz system

5.1 Introduction of frequency quadrupling scheme

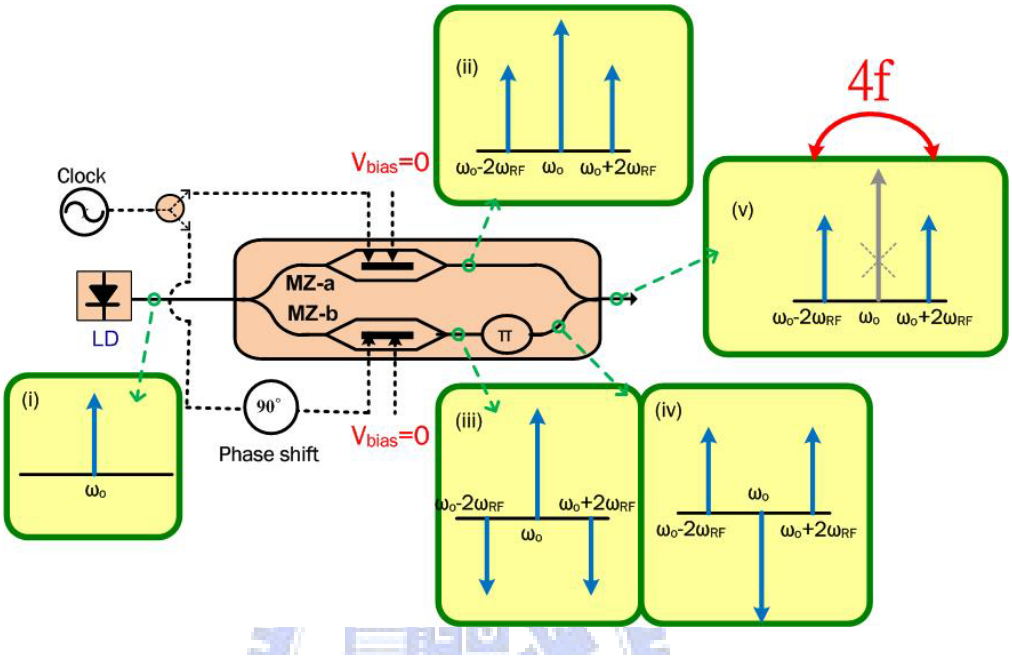

Figure 5-1 Frequency quadrupling scheme

In order to carry more and wider bandwidth signals, we have to utilize higher frequency system. And now I want to show you the concept of a frequency quadrupling 60GH system without using high speed components in transmitter terminal. It is used after I/Q modulator to up convert signals to 60GHz.

This part of the transmitter in the proposed system is frequency quadrupling, as shown in Figure 5-1. For simplicity, the figure shows only one optical input. Since MZ-a and MZ-b are biased at full point, the output spectrum are both double-sideband (DSB). The only difference between MZ-a and MZ-b is phase term. Compare to MZ-a, MZ-b has $+\pi$ phase shift at $+2\omega_{RF}$ term and $-\pi$ phase shift at $-2\omega_{RF}$ term. After that, a π phase shift is introduced at lower arm, And then combine the two arms. Finally, frequency quadrupling result is obtained.

5.2 Concept of the 60GHz system

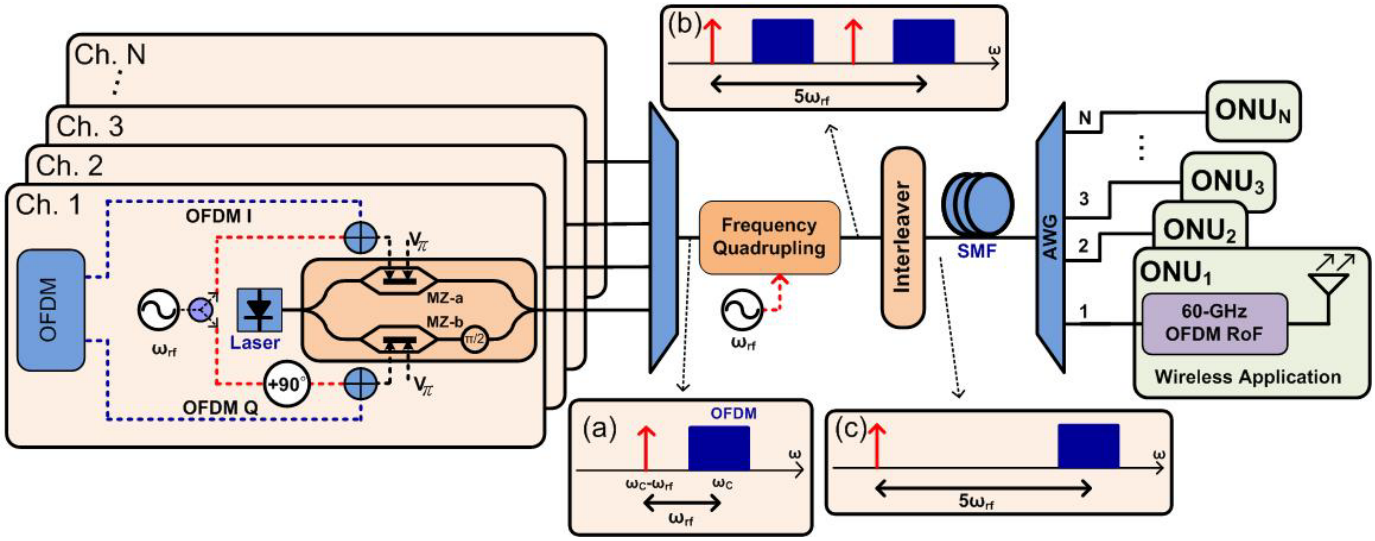

Figure.5-2 Conceptual diagram of the 60-GHz optical/wireless system using all-optical up-conversion.

Figure 5-2 schematically depicts the concept of the proposed 60-GHz OFDM RoF system employing all-optical up-conversion. The proposed 60-GHz OFDM transmitter consists of two dual-parallel modulators for photonic up-conversion and frequency quadrupling, respectively. For photonic up-conversion, OFDM I and Q signals are sent to MZ-a and MZ-b of the first dual-parallel modulator, respectively. To achieve high optical modulation depth and to operate in E-field linear region of the MZM, both MZ-a and MZ-b are biased at the null point. To realize direct-detection OFDM signals, we insert an optical subcarrier as a remote heterodyne scheme by using single side band (SSB) modulation with carrier suppression. Therefore, the generated optical OFDM signal consisting of an un-modulated subcarrier and an OFDM-modulated carrier, which can be converted into electrical RF OFDM signals by square-law photo-diode (PD) detection, can be produced as shown in inset (a) of Fig. 5-2. Then, the generated OFDM signal is up-converted by using the frequency

quadrupling technique as shown in inset (b) of Fig. 5-2. After an interleaver to filter out the unwanted sideband, frequency quintupling is achieved as shown in inset (c) of Fig. 5-2. Note that the proposed OFDM transmitter does not need any electrical mixer with a typical noise figure (NF) of more than 8 dB for up-conversion to 60 GHz. This is very important for highly spectral efficiency OFDM signals (i.e. 16-QAM and above) that requires higher signal-to-noise ratio (SNR). Additionally, the relative intensity between the un-modulated and OFDM-modulated subcarriers can be tuned by adjusting the individual power of the electrical sinusoidal and OFDM signals to optimize the performance of the optical RF signals.

5.3 Experimental setup

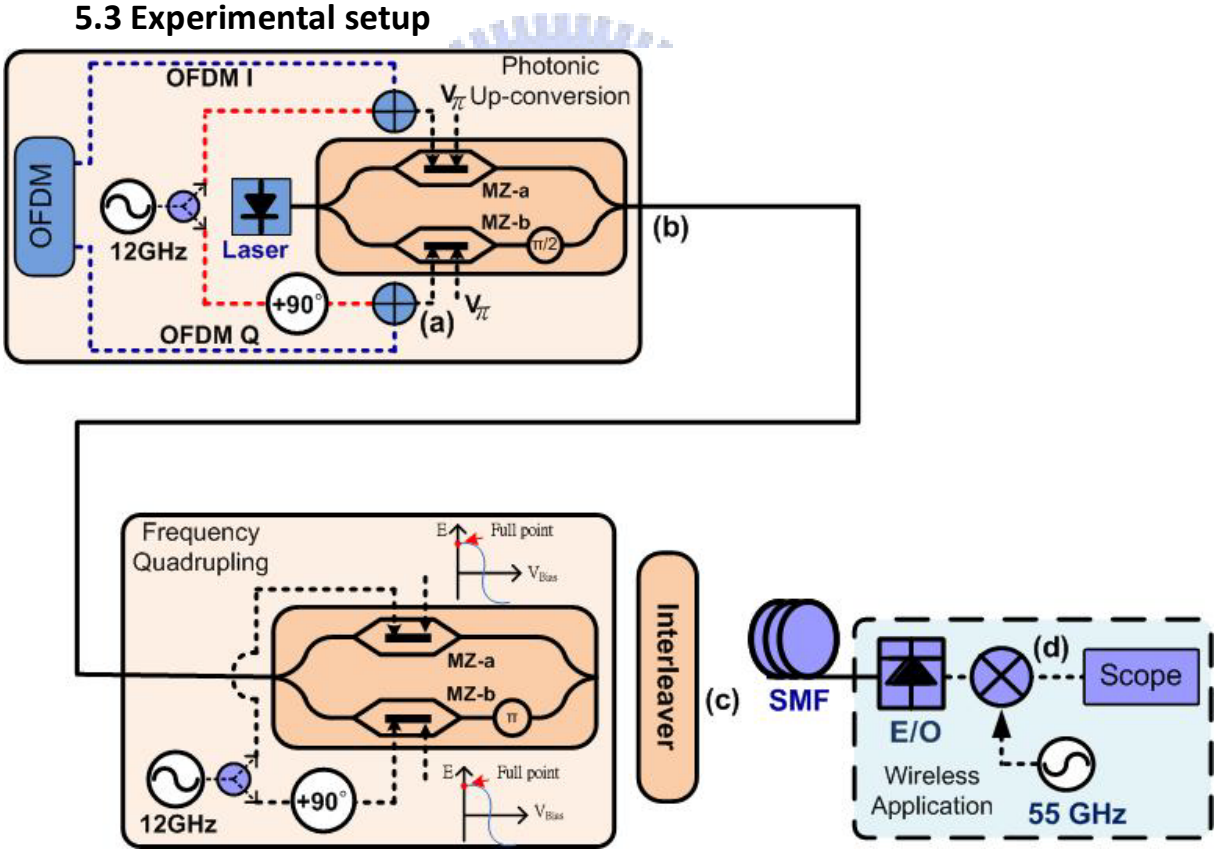

Figure.5-3 Experimental setup for proposed system.

Figure 5-3 depicts the experimental setup. The OFDM signals are generated by a Tektronix® AWG7102 arbitrary waveform generator (AWG) using a Matlab® program. The sample rate and digital-to-analog converter resolution of the AWG are 10 GHz and

8 bits, respectively. For 14Gb/s OFDM QPSK signals, the IFFT length is 64. A 156.25-MSym/s QPSK symbol is encoded at 45 channels (i.e. channels 3-25 and 42-63) with the remaining 9 channels set to zero. Therefore, an optical 14-Gb/s QPSK OFDM signal that has 45 subcarriers and occupies a total bandwidth of 7 GHz can be generated. For 20Gb/s OFDM 16QAM signals, the IFFT length is 64. A 156.25-MSym/s QPSK symbol is encoded at 32 channels (i.e. channels 3-18 and 48-63) with the remaining 32 channels set to zero. Therefore, an optical 20-Gb/s 16-QAM OFDM signal that has 32 subcarriers and occupies a total bandwidth of 5 GHz can be generated. For 28Gb/s OFDM QPSK signals, the IFFT length is 64. A 156.25-MSym/s QPSK symbol is encoded at 45 channels (i.e. channels 3-25 and 42-63) with the remaining 9 channels set to zero. Therefore, an optical 28-Gb/s QPSK OFDM signal that has 45 subcarriers and occupies a total bandwidth of 7 GHz can be generated. To realize optical direct-detection OFDM signal, a new optical subcarrier is generated at the lower sideband of the original carrier by 12 GHz. The generated OFDM signal is up-converted by using optical frequency quadrupling technique.

After a 50/100 GHz optical interleaver, OFDM signal at 60 GHz with frequency quintupling is generated at (c) of Fig. 5-3. A 100-km SMF is used to evaluate the transmission penalty of the system. After square-law PD detection, an electrical OFDM signal at 60 GHz is generated and down-converted to 5 GHz at (d) of Fig. 5-2. The down-converted OFDM signal is captured by a Tektronix® DPO 71254 with a 50-GHz sample rate and a 3-dB bandwidth of 12.5 GHz. An off-line DSP program is employed to demodulate the OFDM signal. The demodulation process includes synchronization, Fast Fourier Transform (FFT), one-tap equalization, and QAM symbol decoding. The bit error rate (BER) performance is calculated from the measured error vector magnitude (EVM).

5.3.1 Optimal condition for RF signals

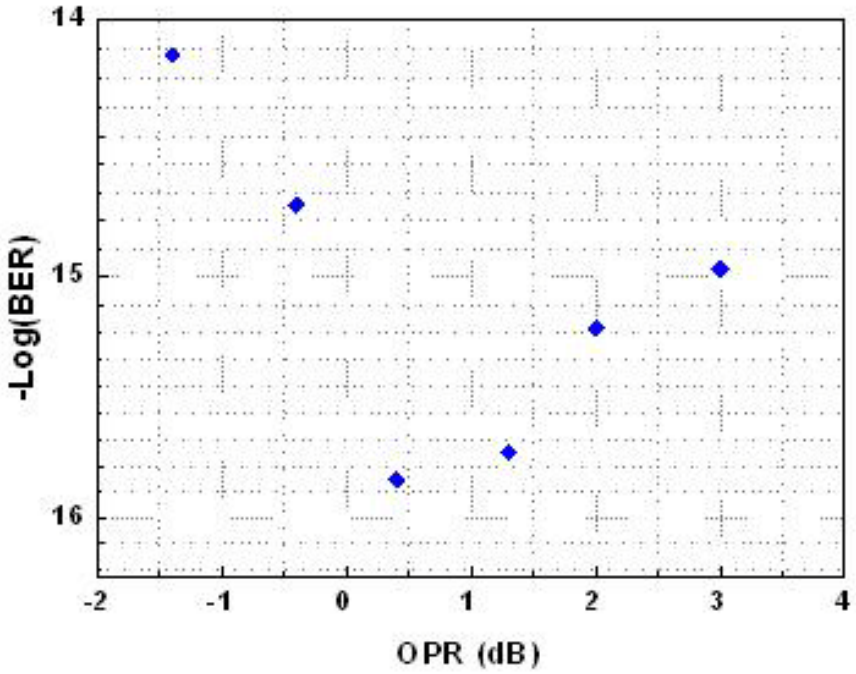

Figure 5-4.BER vs. OPR for OFDM QPSK.
OPR=Pd/Ps(dB). Pd: the optical power of data-modulated optical carrier.
Ps: the optical power of un-modulated subcarrier.

The relative intensity between optical un-modulated and data-modulated subcarriers strongly influences the performance of the optical OFDM signals. One of the advantages of the proposed OFDM transmitter is that the relative intensity between optical un-modulated and data-modulated subcarriers can be easily tuned by adjusting the individual amplitude of the driving sinusoidal and OFDM signals to optimize the performance of the direct-detection OFDM signals, respectively. Figure 5-4 illustrates the BER of the QPSK OFDM signals versus different optical power ratios (OPR) of the un-modulated subcarrier to the OFDM-encoded subcarrier as optical powers of 60-GHz OFDM signals are normalized before detection. The optimal OPR is 0.4 dB.

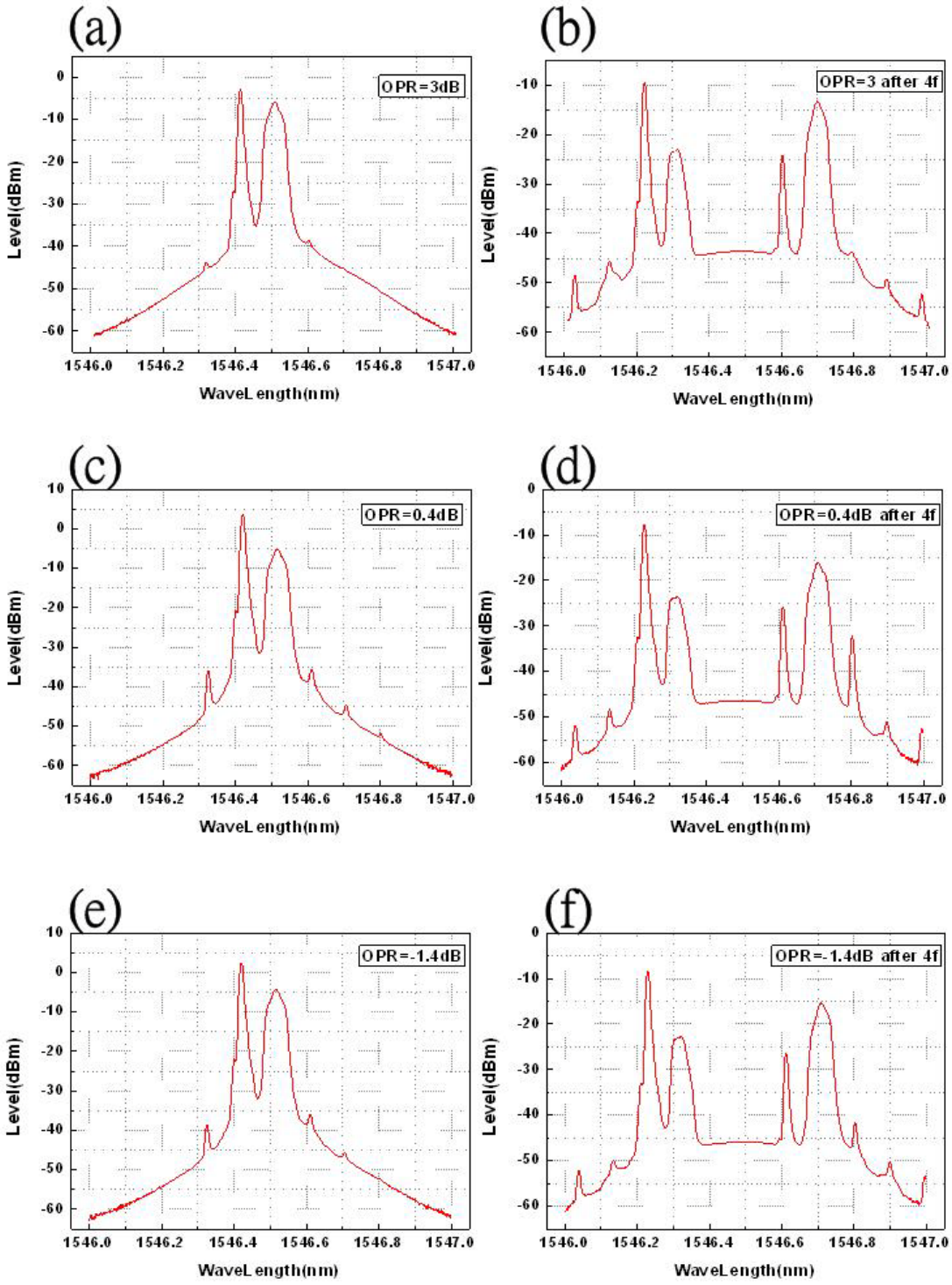

Figure 5-5.Optical Spectrums for OFDM QPSK.
(a)OPR=3dB (b) OPR=3dB after 4f-system (c) OPR=0.4dB (d) OPR=0.4dB after 4f-system(e) OPR=-1.4dB (f) OPR=-1.4dB after 4f-system

Figure 5-5 shows the optical spectrums of different OPRs. We define OPR is

optical power of un-modulated subcarrier over optical power of signals modulated optical carrier. And inset (a), (c), (e) of Figure 5-5 are OPR=3dB, OPR=0.4dB, OPR=-1.4dB before frequency quadrupling system, respectively. Inset (b), (d) and (f) illustrate OPR=3dB, OPR=0.4dB, OPR=-1.4dB after frequency quadrupling system and interleaver.

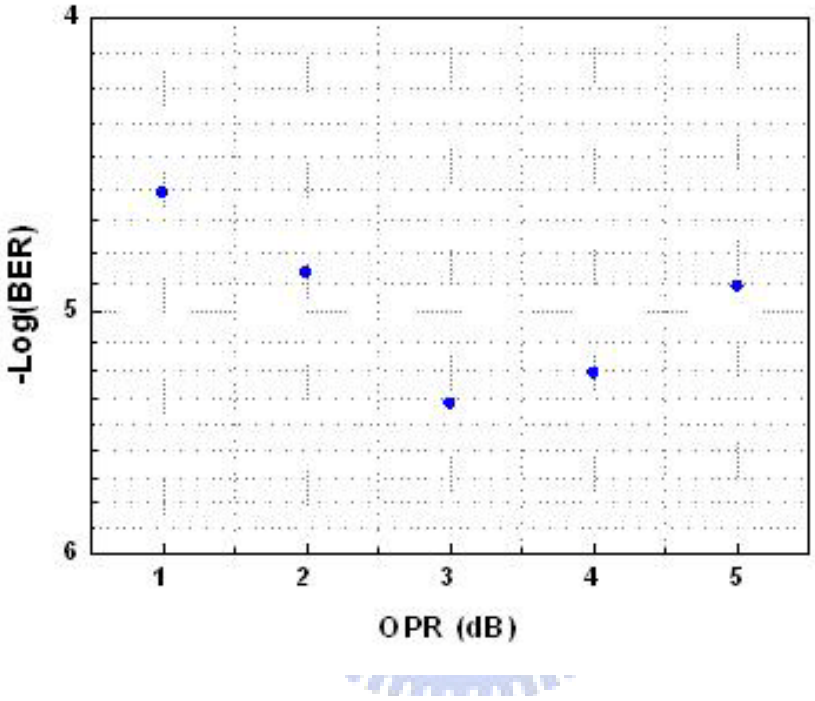

Figure 5-6.BER vs. OPR for 20Gb/s OFDM 16QAM.
OPR=Pd/Ps(dB). Pd: the optical power of data-modulated optical carrier.
Ps: the optical power of un-modulated subcarrier.

Figure 5-6 illustrates the BER of the 20Gb/s 16-QAM OFDM signals versus different optical power ratios (OPR) of the un-modulated subcarrier to the OFDM-encoded subcarrier as optical powers of 60-GHz OFDM signals are normalized before detection. The optimal OPR is 3 dB.

Figure 5-7shows the optical spectrums of different OPRs. And inset (a), (c), (e) of Figure 5-7 are OPR=1dB, OPR=3dB, OPR=5dB before frequency quadrupling system,

respectively. Inset (b), (d) and (f) illustrate OPR=1dB, OPR=3dB, OPR=5dB after frequency quadrupling system and interleaver. We find that when signals bandwidth wider, the optimal OPR seems to be larger.

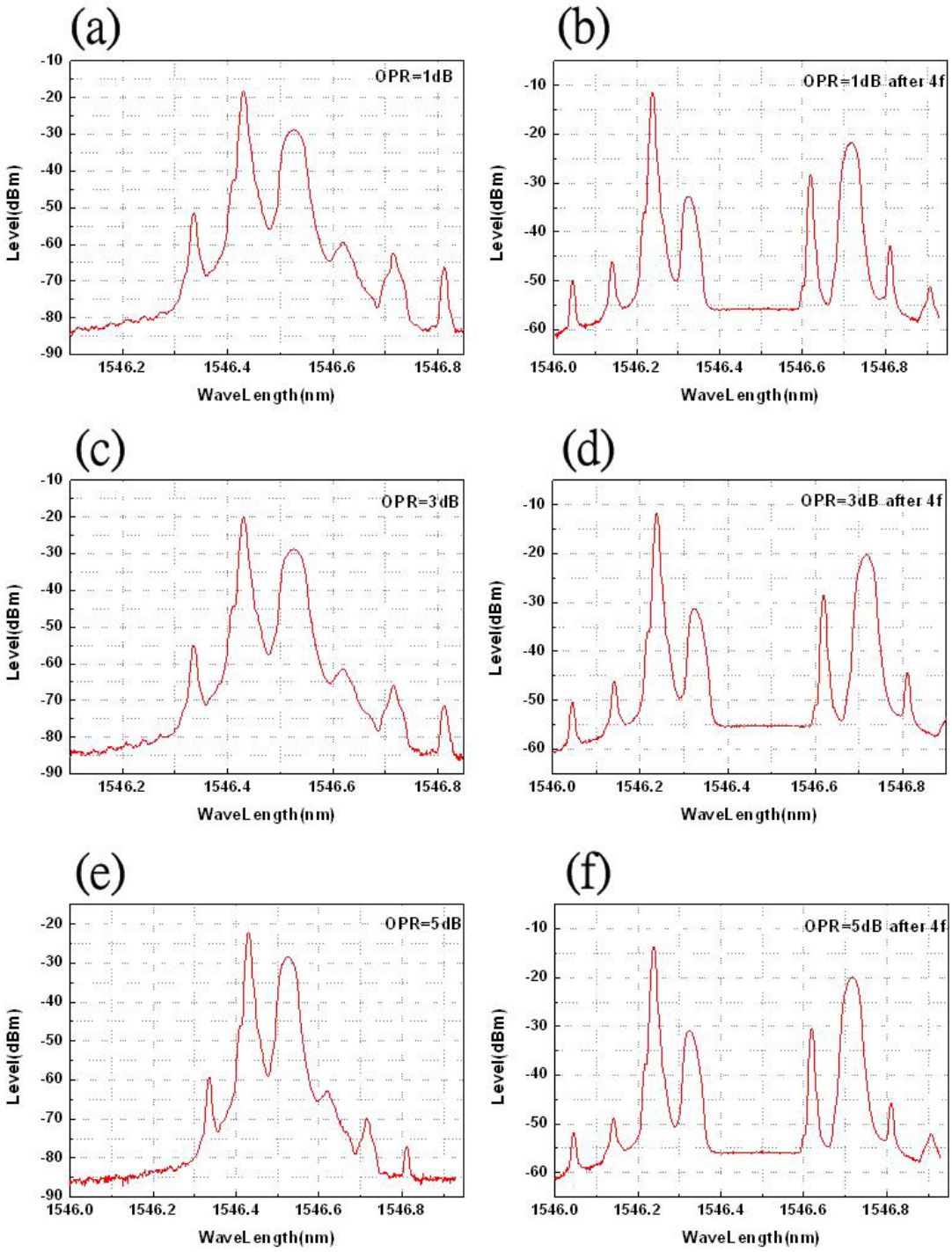

Figure 5-7.Optical Spectrums for 20Gb/s OFDM 16-QAM.
(a) OPR=1dB (b) OPR=1dB after 4f-system (c) OPR=3dB
(d) OPR=3dB after 4f-system(e) OPR=5dB (f) OPR=5dB after 4f-system

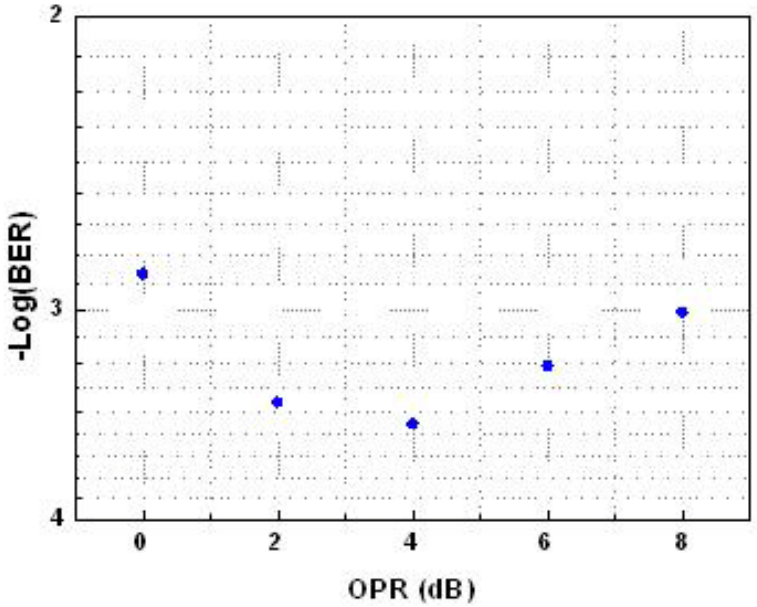

Figure 5-8.BER vs. OPR for 28Gb/s OFDM 16QAM.
OPR=Pd/Ps(dB). Pd: the optical power of data-modulated optical carrier.
Ps: the optical power of un-modulated subcarrier.

Figure 5-8 shows the BER of the 20Gb/s 16-QAM OFDM signals versus different optical power ratios (OPR) of the un-modulated subcarrier to the OFDM-encoded subcarrier as optical powers of 60-GHz OFDM signals are normalized before detection. The optimal OPR is 4 dB.

Figure 5-9 illustrates the optical spectrums of different OPRs. And inset (a), (c), (e) of Figure 5-7 are OPR=0dB, OPR=4dB, OPR=8dB before frequency quadrupling system, respectively. Inset (b), (d) and (f) illustrate OPR=0dB, OPR=4dB, OPR=8dB after frequency quadrupling system and interleaver. We also find that when signals bandwidth wider, the optimal OPR seems to be larger. The reason is as the data-rate becomes larger, it needs higher SNR.

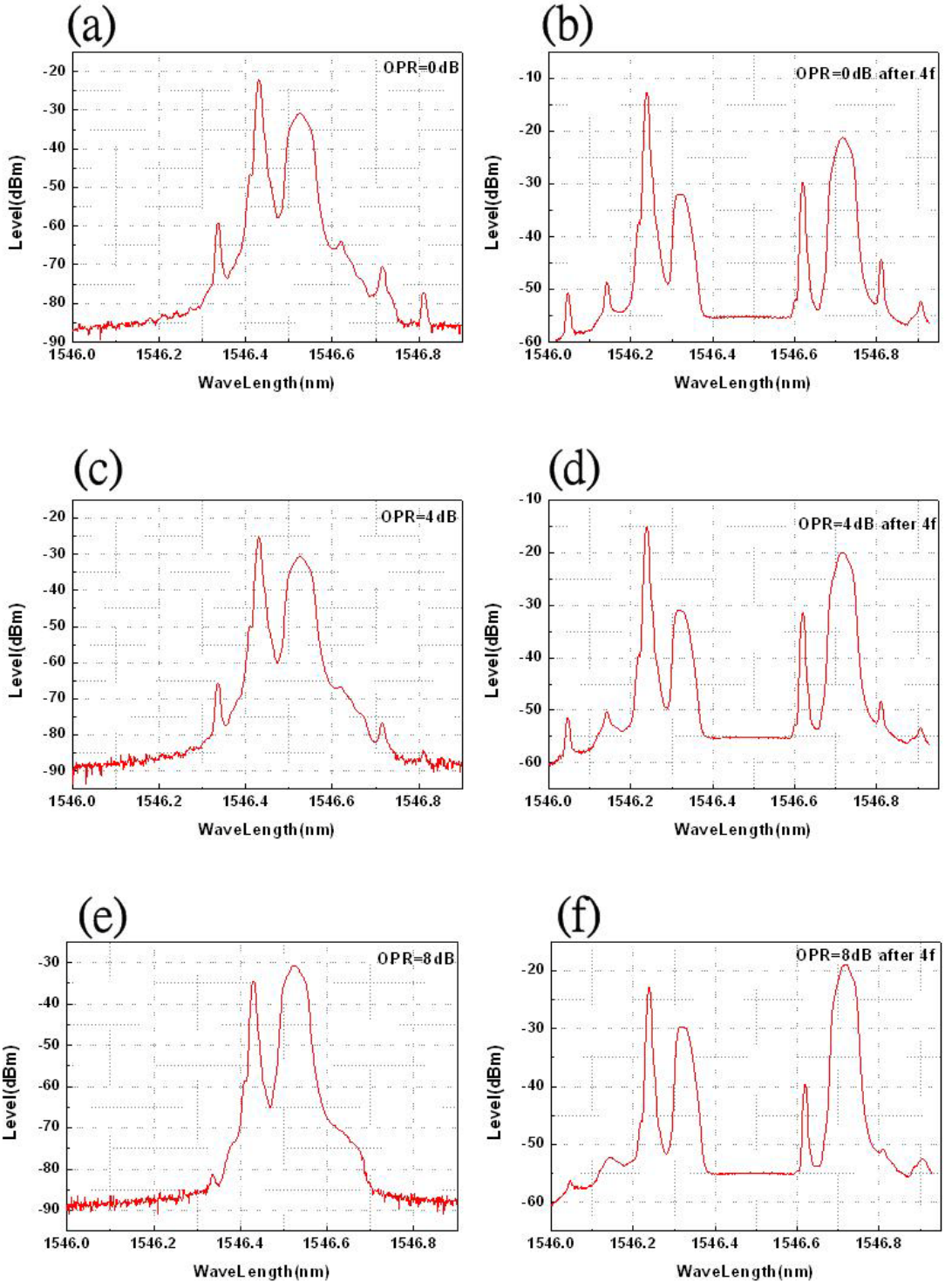

Figure 5-9.Optical Spectrums for 28Gb/s OFDM 16-QAM.
(a)OPR=0dB (b) OPR=0dB after 4f-system (c) OPR=4dB
(d) OPR=4dB after 4f-system(e) OPR=8dB (f) OPR=8dB after 4f-system

5.4 Experimental results and discussion

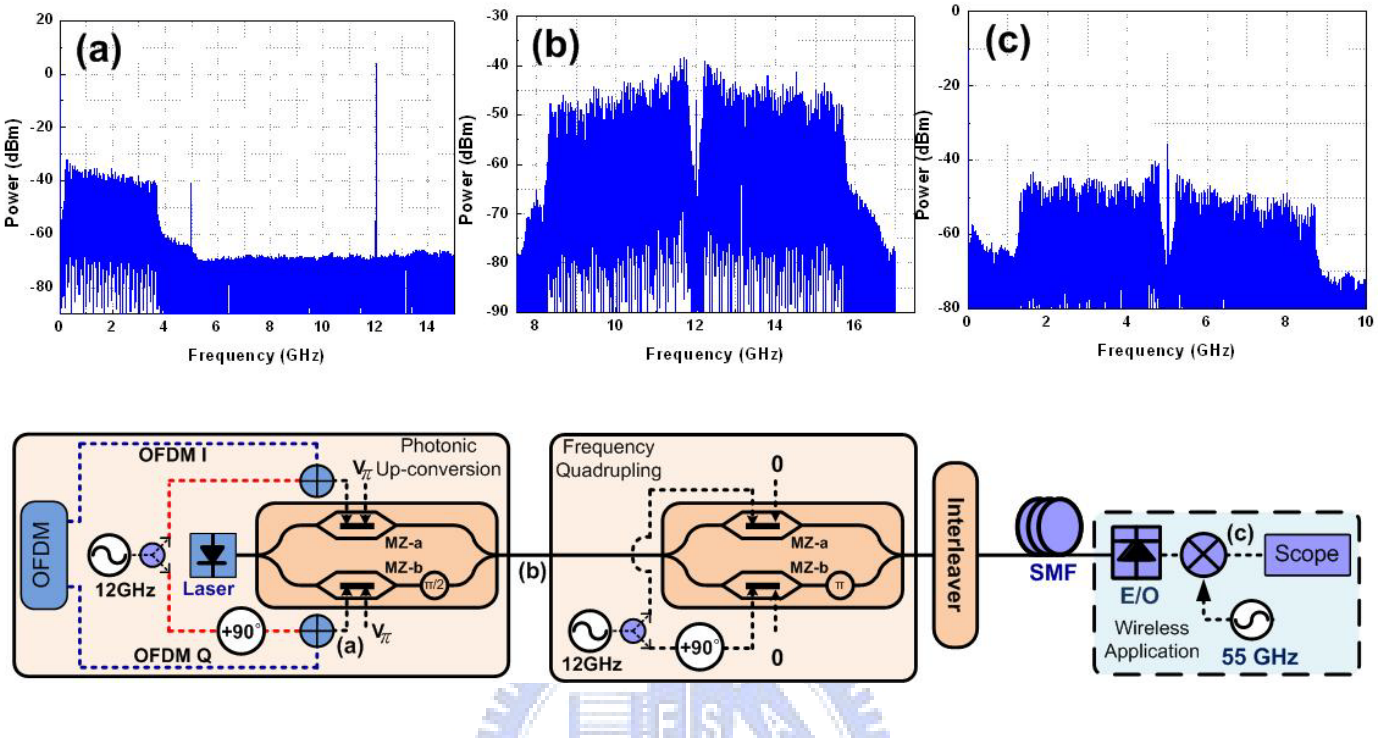

Figure 5-10. Electrical Spectrums of QPSK OFDM signals.
(a) Tx OFDM and subcarrier electrical spectrum.
(b) OFDM electrical spectrum after I/Q modulator.
(c) Rx OFDM electrical spectrum.

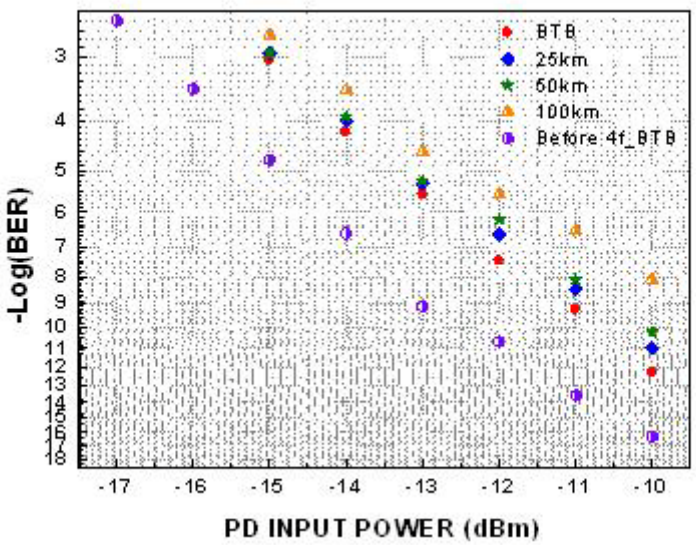

Figure 5-11. BER curves of the OFDM QPSK signals

Figure 5-10 illustrates the electrical spectrums for QPSK OFDM signals and

indicates where the spectrums belong to. Inset (a) of Figure 5-10 is the electrical spectrum of transmitter terminal OFDM signals and 12GHz-subcarrier. Inset (b) of Figure 5-10 is the one of OFDM signals after I/Q modulator. We can see the bandwidth is 7GHz. And Inset (c) of Figure 5-10 is the electrical spectrum of receiver QPSK OFDM signals. We down convert the signals to center frequency 5GHz.

Figure 5-12 shows QPSK constellation diagrams before and after the frequency quadrupling system in back-to-back (BTB) and following SMF transmission cases. The equalizer in OFDM transceiver is used to combat both frequency response of various millimeter-wave components at 60 GHz and fiber dispersion. Since the proposed OFDM transmitter can generate high-purity two-tone lightwave, the generated OFDM signals do not suffer from periodic fading issue due to fiber dispersion. Only in-band distortion of the OFDM-encoded subcarrier induced by fiber dispersion is considered. Since the symbol rate of each subcarrier is only 156.25 MSym/s, the fiber chromatic penalty can be ignored. Figure 5-11 shows the BER curves of the 14-Gb/s QPSK OFDM signals using optimal OPRs after transmission over 100-km SMF. After transmission 100-km, the sensitivity penalties is about 1dB. Compare purple circular symbols with red diamond symbols, the penalty of frequency quadrupling system is 2dB. Although it still worsens the performance a little, it does better than using electrical mixer with noise figure (NF) 8dB. Inset (a), (b), (c) and (d) of Figure 5-12 are BTB before frequency quadrupling, BTB, 50km and 100km, respectively. They are captured at PD input power equal to -11dBm.

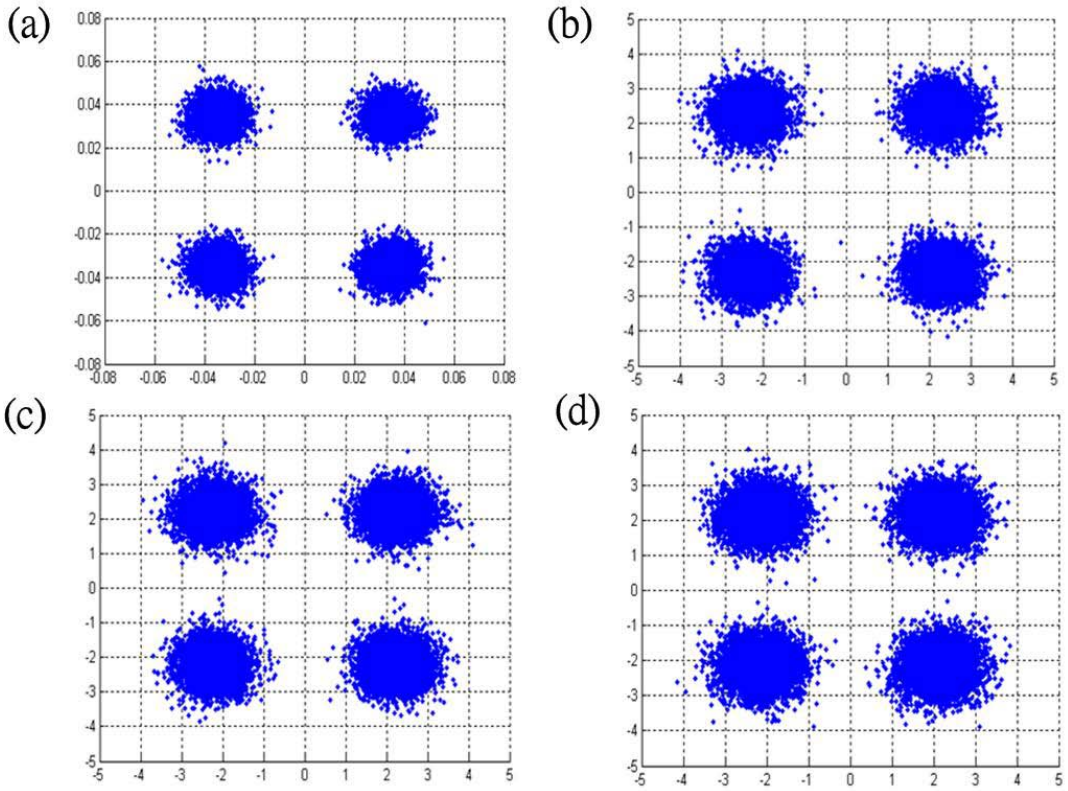

Figure 5-12. Constellations of QPSK OFDM signals (-11dBm).
(a) BTB before 4f (b) BTB (c) 50km (d) 100km

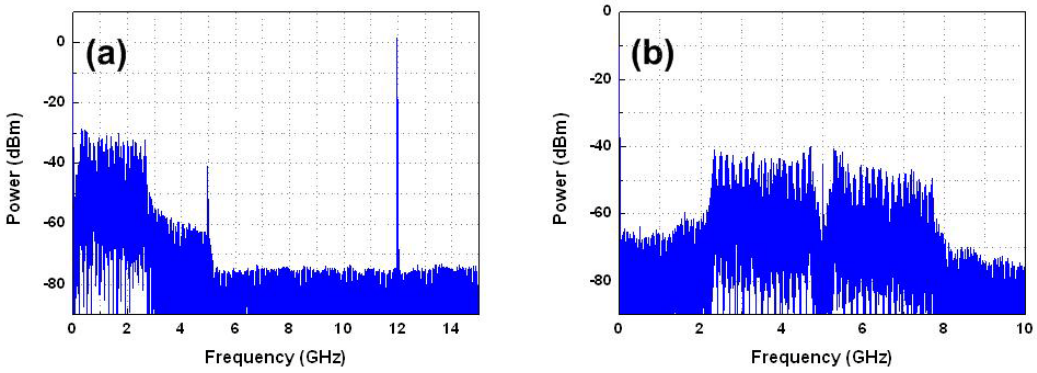

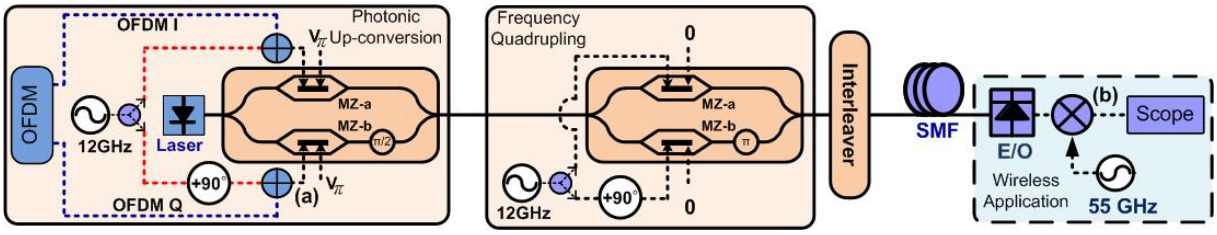

Figure 5-13. Electrical Spectrums of 20Gb/s 16-QAM OFDM signals.
(a) Tx OFDM and subcarrier electrical spectrum.
(b) Rx OFDM electrical spectrum.

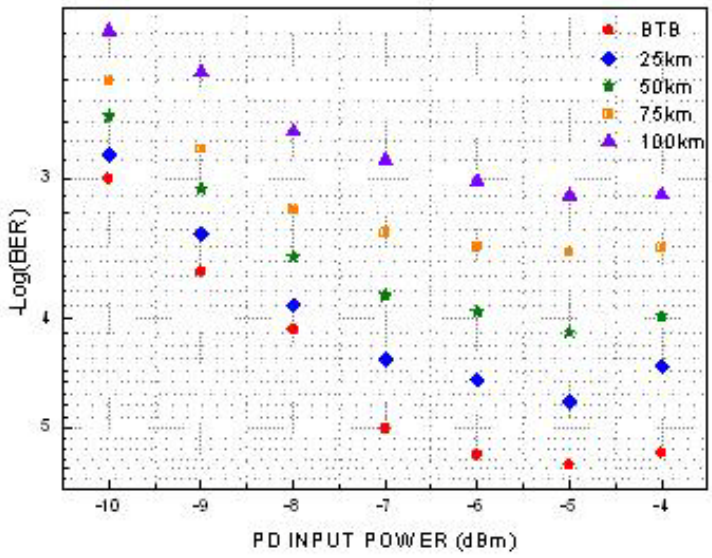

Figure 5-14. BER curves of the 20Gb/s OFDM 16-QAM signals using DFB Laser.

Figure 5-13 illustrates the electrical spectrums for 20Gb/s 16-QAM OFDM signals and indicates where the spectrums belong to. Inset (a) of Figure 5-13 is the electrical spectrum of transmitter terminal OFDM signals and 12GHz-subcarrier. Inset (b) of Figure 5-13 is the electrical spectrum of receiver 16-QAM OFDM signals. The bandwidth is 5GHz. We down convert the signals to center frequency 5GHz.

Figure 5-15 shows 16-QAM constellation diagrams after the frequency quadrupling system in back-to-back (BTB) and following SMF transmission cases. The equalizer in OFDM transceiver is used to combat both frequency response of various millimeter-wave components at 60 GHz and fiber dispersion. Since the proposed OFDM transmitter can generate high-purity two-tone lightwave, the generated OFDM signals do not suffer from periodic fading issue due to fiber dispersion. Only in-band distortion of the OFDM-encoded subcarrier induced by fiber dispersion is considered.

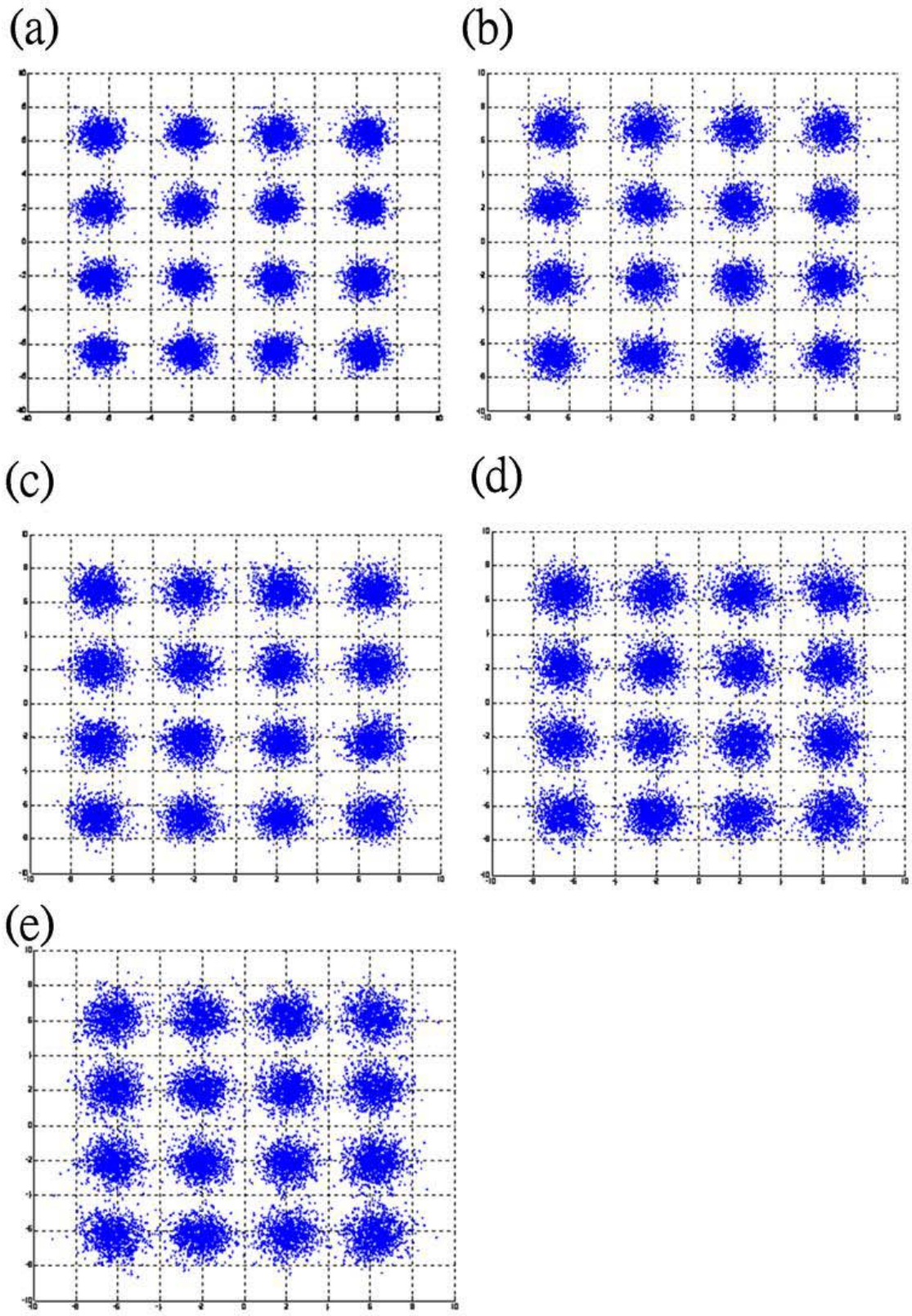

Figure 5-15. Constellations of 20Gb/s 16-QAM OFDM signals using DFB Laser (-5dBm). (a) BTB (b) 25km (c) 50km (d) 75km (e) 100km

Since the symbol rate of each subcarrier is only 156.25 MSym/s, the fiber chromatic penalty can be ignored. Figure 5-14 shows the BER curves of the 20-Gb/s 16-QAM OFDM signals using optimal OPRs and DFB Laser after transmission over 100-km SMF. After transmission 100-km, the sensitivity penalties is very large. The reason to explain large penalty is laser line-width. Following pages will show you a better result with smaller line-width light source. Inset (a), (b), (c), (d) and (d) of Figure 5-15 are BTB, 25km, 50km, 75km and 100km, respectively. They are captured at PD input power equal to -5dBm.

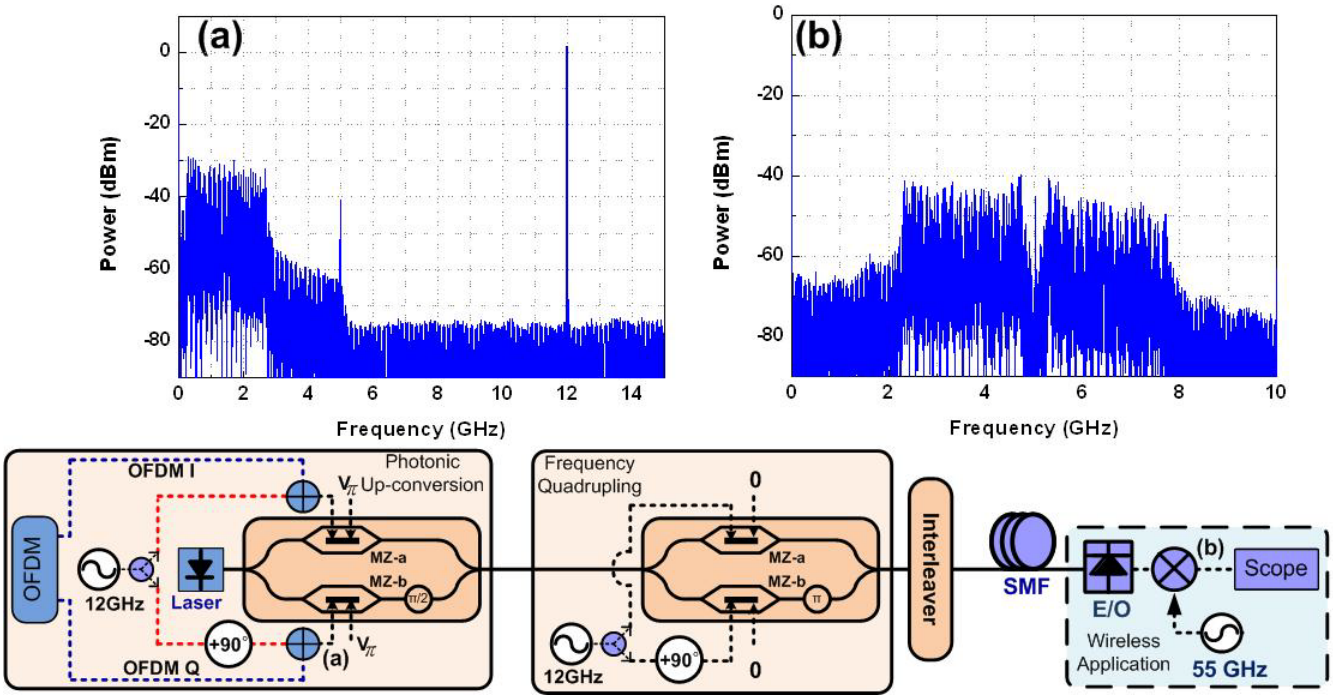

Figure 5-16. Electrical Spectrums of 20Gb/s 16-QAM OFDM signals with tunable laser (TL).
(a)Tx OFDM and subcarrier electrical spectrum.
(b)Rx OFDM electrical spectrum.

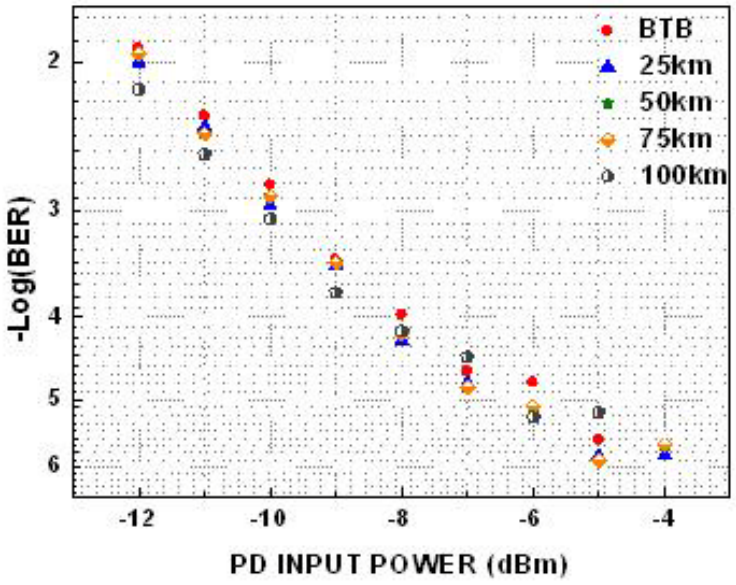

Figure 5-17. BER curves of the 20Gb/s OFDM 16-QAM signals using Tunable Laser.

Figure 5-16 illustrates the electrical spectrums for 20Gb/s 16-QAM OFDM signals with tunable laser and indicates where the spectrums belong to. Inset (a) of Figure 5-16 is the electrical spectrum of transmitter terminal OFDM signals and 12GHz-subcarrier. Inset (b) of Figure 5-16 is the electrical spectrum of receiver 16-QAM OFDM signals. The bandwidth is 5GHz. We down convert the signals to center frequency 5GHz.

Figure 5-18 shows 16-QAM constellation diagrams after the frequency quadrupling system in back-to-back (BTB) and following SMF transmission cases. The equalizer in OFDM transceiver is used to combat both frequency response of various millimeter-wave components at 60 GHz and fiber dispersion. Since the proposed OFDM transmitter can generate high-purity two-tone lightwave, the generated OFDM signals do not suffer from periodic fading issue due to fiber dispersion. Only in-band distortion of the OFDM-encoded subcarrier induced by fiber

dispersion is considered. Since the symbol rate of each subcarrier is only 156.25 MSym/s, the fiber chromatic penalty can be ignored. Figure 5-17 shows the BER curves of the 20-Gb/s 16-QAM OFDM signals using optimal OPRs and DFB Laser after transmission over 100-km SMF. After transmission 100-km, the sensitivity penalties is almost negligible. The two cases only have one difference, laser line-width. We replace DFB Laser with Tunable Laser to reduce light source line-width. Inset (a), (b), (c), (d) and (d) of Figure 5-18 are BTB, 25km, 50km, and 100km, respectively. They are captured at PD input power equal to -5dBm.

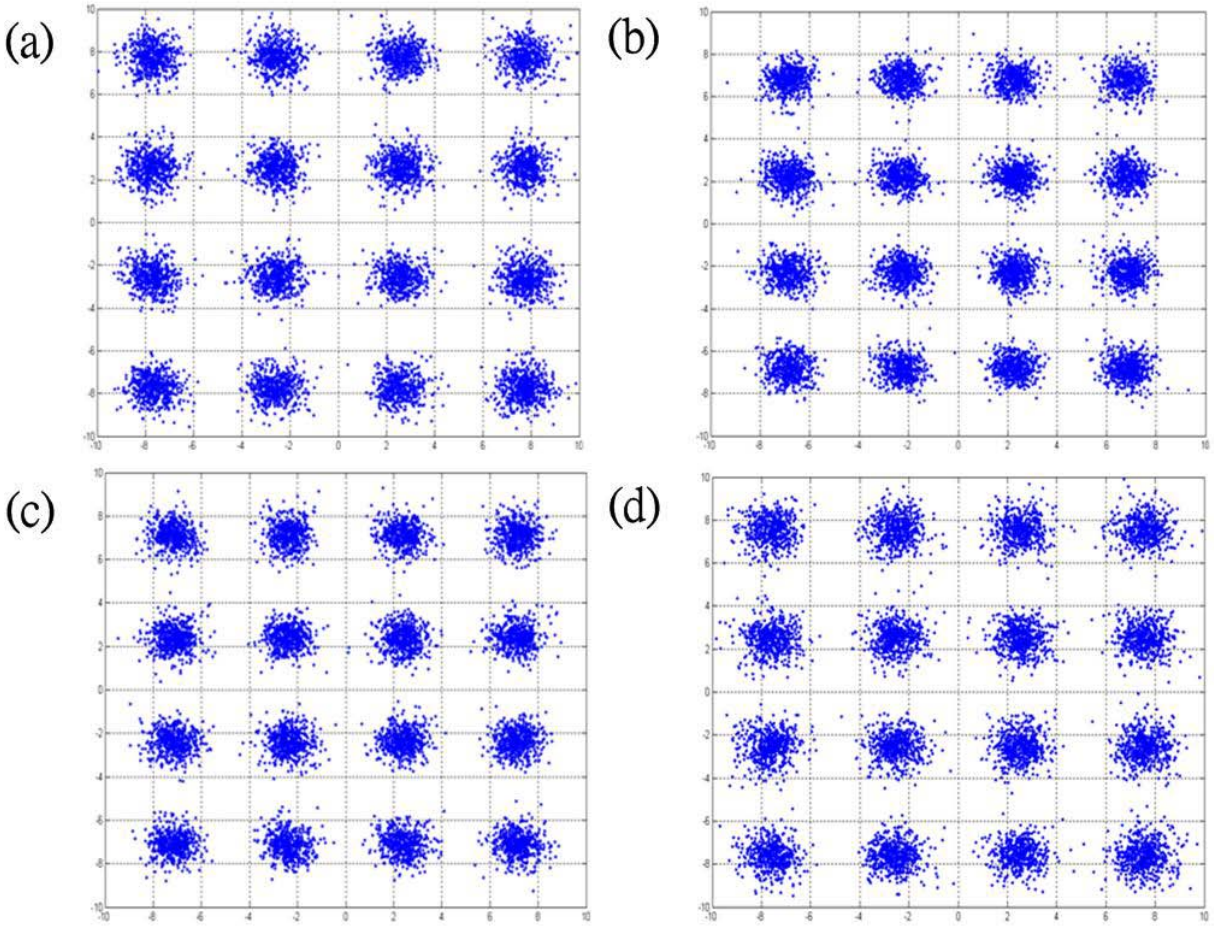

Figure 5-18. Constellations of 20Gb/s 16-QAM OFDM signals using Tunable Laser (-5dBm). (a) BTB (b) 25km (c) 50km (d) 100km

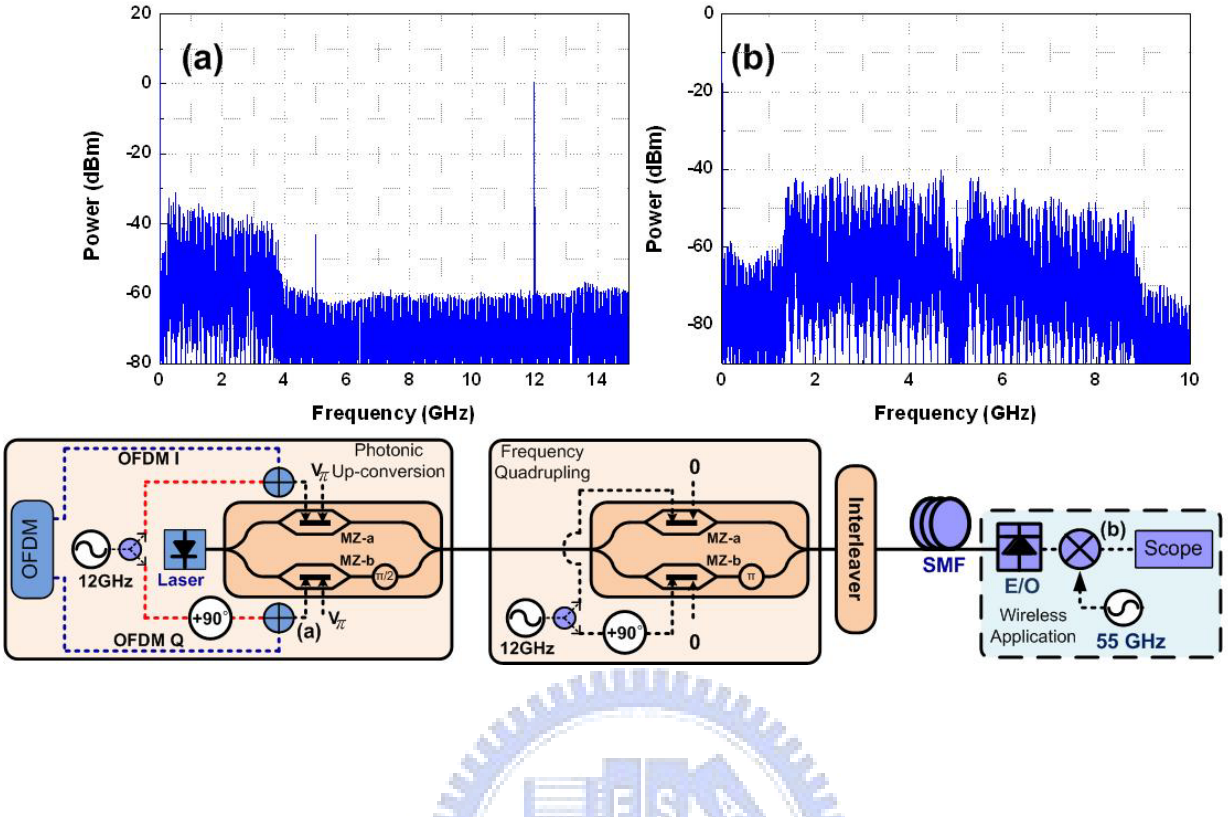

Figure 5-19. Electrical Spectrums of 28Gb/s 16-QAM OFDM signals with tunable laser (TL).
(a) Tx OFDM and subcarrier electrical spectrum.
(b) Rx OFDM electrical spectrum.

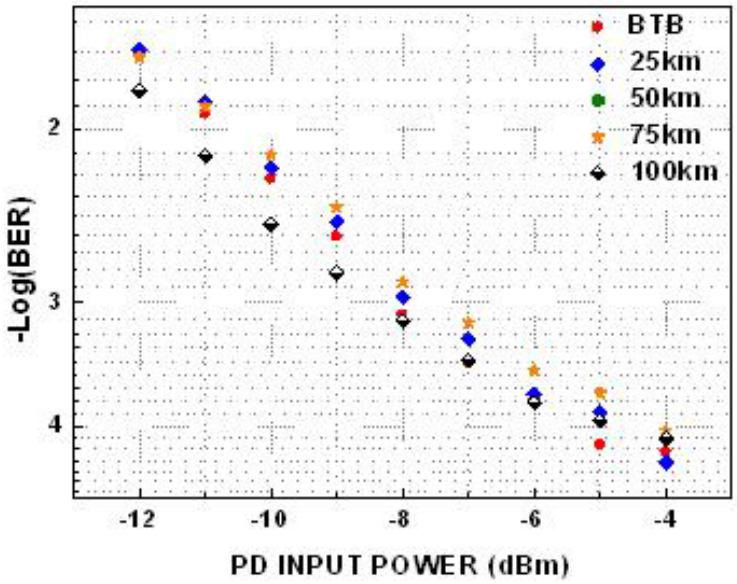

Figure 5-20. BER curves of the 28Gb/s OFDM 16-QAM signals using Tunable Laser.

Figure 5-19 illustrates the electrical spectrums for 28Gb/s 16-QAM OFDM

signals with tunable laser and indicates where the spectrums belong to. Inset (a) of Figure 5-19 is the electrical spectrum of transmitter terminal OFDM signals and 12GHz-subcarrier. Inset (b) of Figure 5-19 is the electrical spectrum of receiver 16-QAM OFDM signals. The bandwidth is 7GHz. We down convert the signals to center frequency 5GHz.

Figure 5-21 shows 16-QAM constellation diagrams before and after the one-tap equalizer in back-to-back (BTB) and following SMF transmission cases. The equalizer in OFDM transceiver is used to combat both frequency response of various millimeter-wave components at 60 GHz and fiber dispersion. Since the proposed OFDM transmitter can generate high-purity two-tone lightwave, the generated OFDM signals do not suffer from periodic fading issue due to fiber dispersion. Only in-band distortion of the OFDM-encoded subcarrier induced by fiber dispersion is considered. Since the symbol rate of each subcarrier is only 156.25 MSym/s, the fiber chromatic penalty can be ignored. Figure 5-20 shows the BER curves of the 28-Gb/s 16-QAM OFDM signals using optimal OPRs after transmission over 100-km SMF. The sensitivity penalties due to the fiber transmission are negligible. They are captured at PD input power equal to -4dBm.

By using all-optical up-conversion and frequency quintupling, we demonstrate 16-QAM OFDM signal generation and transmission with a record of 28 Gb/s within 7-GHz license-free spectrum at 60 GHz band. Transmission over 100-km SMF transmission with negligible penalty is achieved without any dispersion compensation.

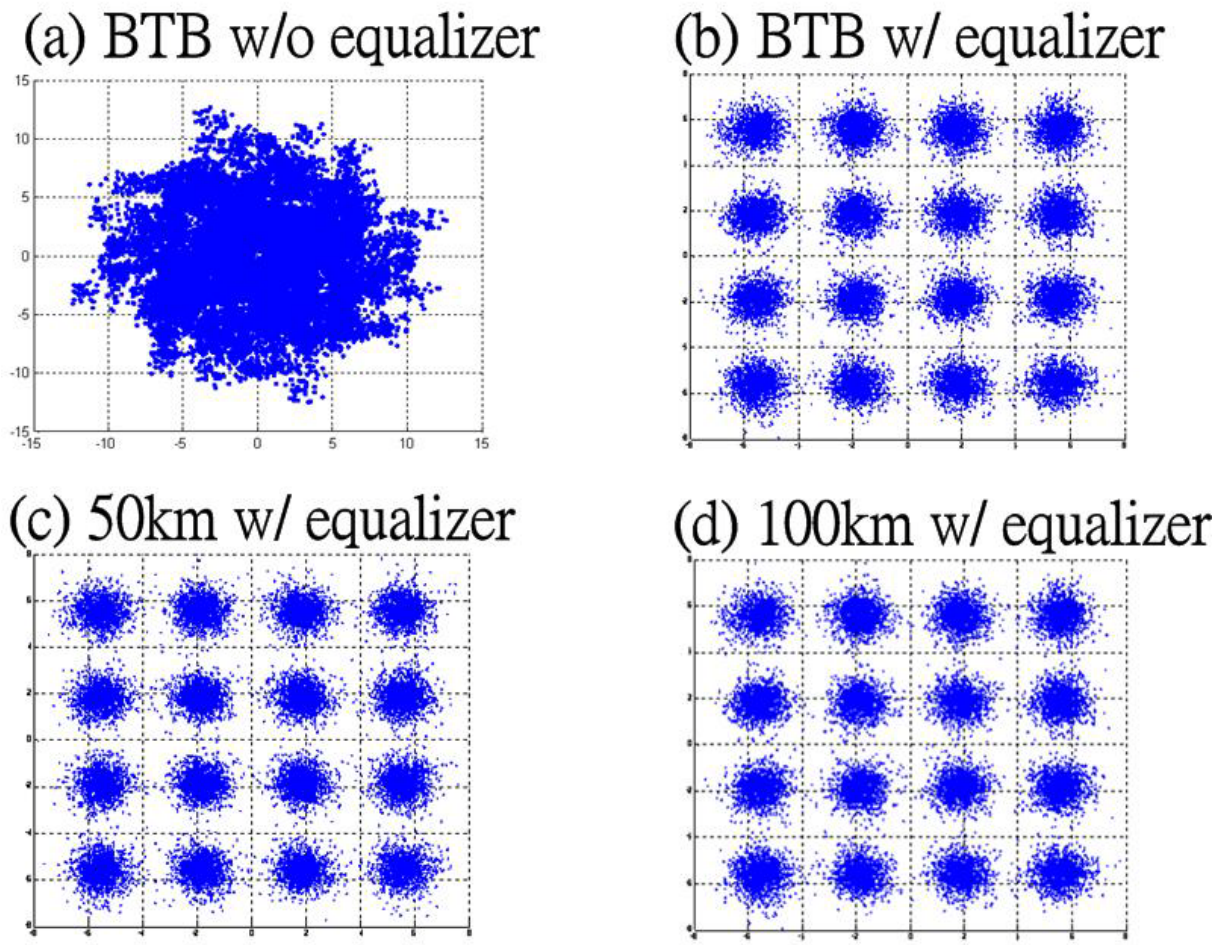

Figure 5-21. Constellations of 28Gb/s 16-QAM OFDM signals using Tunable Laser (-5dBm).

(a) BTB w/o E.Q. (b) BTB (c) 50km (d) 100km

Chapter 6

Conclusion

This work proposes a brand new modulation approach to generate optical vector signal by all optical up-conversion based on a modified SSB scheme. Since all optical up-conversion technique is used, the proposed system does not need high speed components at transmitter terminal compare with conventional modulation scheme using external modulator, and the system can generate direct detection vector signal. This system provides a solution that can satisfy the demand of 60GHz application within 7GHz license-free band.

Since the proposed DD-OFDM transmitter needs no mixer with a typical NF of more than 8 dB to avoid the beat noise interference after detection, it has a great potential to support multi-level format (i.e. 16 QAM or 64 QAM) OFDM signal for narrow applications beyond 10 Gb/s. Error free (10^{-9}) of 10-Gb/s 16-QAM OFDM signal is demonstrated and negligible penalty is observed after 125-km SMF transmission. We also demonstrate 16-QAM OFDM signal generation and transmission with a record of 28 Gb/s within 7-GHz license-free spectrum at 60 GHz band. Transmission over 100-km SMF transmission with negligible penalty is achieved without any dispersion compensation.

REFERENCES

[1] A. J. Lowery and J. Armstrong, “Orthogonal-frequency-division multiplexing for dispersion compensation of long-haul optical systems,” Opt. Express 14, 2079-2084 (2006).

[2] I. B. Djordjevic and B. Vasic, “Orthogonal frequency division multiplexing for high-speed optical transmission,” Opt. Express 14, 3767-3775 (2006).

[3] H. Bao and W. Shieh, “Transmission simulation of coherent optical OFDM signals in WDM systems,” Opt. Express 15, 4410-4418 (2007).

[4] W. H. Chen, and W. I. Way, “Multichannel Single-Sideband SCM/DWDM Transmission System,” J. Lightwave Technol 22, 1697-1693 (2004).

[5] C. Wu, and X. Zhang, “Impact of Nonlinear Distortion in Radio Over Fiber Systems with Single-Sideband and Tandem Single-Sideband Subcarrier Modulations,” J. Lightwave Technol. 24, 2076-2090 (2006).

[6] J. Yu, Z. Jia, L. Yi, G. K. Chang, and T. Wang, “Optical millimeter wave generation or up-conversion using external modulators,” IEEE Photon. Technol. Lett. 18, 265–267 (2006).

[7] J. J. O’Reilly, P. M. Lane, R. Heidemann, and R. Hofstetter, “Optical generation of very narrow linewidth millimeter wave signals,” Electron. Lett. 28, 2309–2311 (1992).

[8] M. Weiß, A. Stöhr, M. Huchard, S. Fedderwitz, B. Charbonnier, V. Rymanov, S. Babiel, and D. Jäger, “60GHz Radio-over-Fibre Wireless System for Bridging 10Gb/s Ethernet Links,” ECOC2008, Tu.3.F.6 (2008).

[9] Z. Jia, J. Yu, Y. T. Hsueh, H. C. Chien, and G. K. Chang, “Demonstration of a Symmetric Bidirectional 60-GHz Radio-over-Fiber Transport System at 2.5-Gb/s over a Single 25-km SMF-28,” ECOC2008, Tu.3.F.5 (2008).

[10] J. J. Vegas Olmos, K. Kitayama, and T. Kuri, “Time-Slotted Full-Duplex Access Network for Baseband and 60-GHz Millimeter-Wave-Band Radio-over-Fiber,” OFC2008, OThP5 (2008).

[11] C. T. Lin, Y. M. Lin, J. Chen, S. P. Dai, P. T. Shih, P. C. Peng, and S. Chi, “Optical

direct-detection OFDM signal generation for radio-over-fiber link using frequency doubling scheme with carrier suppression," Opt. Express 16, 6056-6063 (2008).

[12] P. T. Shih, C. T. Lin, W. J. Jiang, J. Chen, H. S. Huang, Y. H. Chen, P. C. Peng, and S. Chi, "WDM up-conversion employing frequency quadrupling in optical modulator," Opt. Express 17, 1726-1733 (2009).

[13] C. Lim, M. Attygalle, A. Nirmalathas, D. Novak, and R. Waterhouse, "Analysis of optical carrier-to-sideband ratio for improving transmission performance in fiber-radio links," IEEE Trans. Microw. Theory Tech. 54, 2181–2187 (2006).

[14] V. J. Urick, J. X. Qiu, and F. Bucholtz, "Wide-band QAM-over-fiber using phase modulation and interferometric demodulation," IEEE Photon. Technol. Lett. 16, 2374-2376 (2004).

[15] B. J. C. Schmidt et al, OFC 2007, PDP 18.

[16] W. R. Peng et al., ECOC'08 paper Mo.3.E.6.

[17] E.Z. Wong et al., Proc. OPT'08, Sat-S29-04

[18] I. Fatadin et al., Photon. Technol. Lett. 20, 1733 (2008).

Appendix

Publication

International Journals and Conferences:

1. Chun-Ting Lin, Po-Tsung Shih, Wen-Jr Jiang, ***Er-Zih Wong***, Jason(Jyehong) Chen, and Sien Chi, "Vector Signal Generation at Microwave/Millimeter-wave Bands Employing Optical Frequency Quadrupling Scheme," to be published Optics Lett..
2. J.-W. Shi, F.-M. Kuo, Y.-S. Wu, Nan-Wei Chen, Po-Tsung Shih, Chun-Ting Lin, Wen-Jr Jiang, ***Er-Zih Wong***, Jason (Jyehong) Chen, and Sien Chi, "A W-Band Photonic Transmitter-Mixer Based on High-Power Near-Ballistic Uni-Traveling-Carrier Photodiodes for BPSK and QPSK Data Transmission under Bias Modulation," to be published at *IEEE Photon. Technol. Lett.*
3. Chun-Ting Lin, Wen- Jr Jiang, Jason (Jyehong) Chen, Po Tsung Shih, Peng-Chun Peng, ***Er-Zih Wong***, and Sien Chi, "Novel Optical Vector Signal Generation with Carrier Suppression and Frequency Multiplication Based on a Single-Electrode Mach-Zehnder Modulator," IEEE Photon. Technol. Lett., Vol. 20, No. 24, pp. 2060-2062, Dec. 2008.
4. Wen-Jr Jiang, Chun-Ting Lin, ***Er-Zih Wong***, Po-Tsung Shih, Jason(Jyehong) Chen, and Sien Chi, "A Novel Optical Direct-Detection I/Q Up-Conversion with I/Q Imbalance Compensation via Gram-Schmidt Orthogonalization Procedure", European Conference and Exhibition on Optical Communication (ECOC 2009).
5. Chun-Ting Lin, ***Er-Zih Wong***, Wen-Jr Jiang, Po-Tsung Shih, Jason(Jyehong) Chen, and Sien Chi, "28-Gb/s 16-QAM OFDM Radio-over-Fiber System Within 7-GHz License-Free Band at 60 GHz Employing All-Optical Up-conversion," Conference on Lasers and Electro-Optics (CLEO), 2009, post deadline paper CPDA8, Baltimore U.S.A.
6. Po-Tsung Shih, Chun-Ting Lin, Wen-Jr Jiang, ***Er-Zih Wong***, Jason (Jyehong) Chen1, Sien Chi, Y.-S. Wu, F.-M. Kuo, Nan-Wei Chen, Jin-Wei Shi, "W-Band Vector Signal Generation via Optical Millimeter-Wave Generation and Direct Modulation of

NBUTC-PD," OFC 2009, paper OWP4, San Diego, U.S.A.

7. Chun-Ting Lin, Wen- Jr Jiang, ***Er-Zih Wong***, Sheng-Peng Dai, Jason(Jyehong) Chen, Yu-Min, Lin, Po Tsung Shih, Peng-Chun Peng, and Sien Chi, "Experimental Demonstration of Optical 5-Gb/s 16-QAM OFDM Signal Generation and Wavelength Reuse for 1.25-Gbit/s Uplink Signal" ECOC 2008, Brussels Expo., Belgium.
8. C. T. Lin, W. J. Jiang, ***E. Z. Wong***, J. Chen, P. T. Shih, P. C. Peng, S. Chi, "Optical Vector Signal Generation Using Double Sideband with Carrier Suppression and Frequency Multiplication", CLEO/QELS 2008, paper CThR5, San Jose, U.S.A.

Vita

Er-Zih Wong

Contact Information:

Phone: 0916916107

Address: No.14, Ren-ai St., Fongyuan City,

Taichung County 42044, Taiwan (R.O.C.)

E-mail: shoko369896@hotmail.com

Education:

• M.S: Electro-Optical Engineering, National Chiao Tung University, Taiwan. (Sept. 2007 ~ present, Degree Expected: July 2009)

Advisors: Associate Prof. Jason (Jyehong) Chen; Prof. Sien Chi;

• B.S., Department of Electrophysics, National Chiao Tung University, Taiwan. (Sept. 2003 ~ Jun. 2007);

Professional Skills and Contributions:

• **Design and implementation of highest capacity hybrid access network:**
  28-Gb/s 16-QAM OFDM Radio-over-Fiber System Within 7-GHz License-Free Band at 60 GHz Employing All-Optical Up-conversion (CLEO post-deadline paper *CPDA8*)

• **Optical millimeter-wave (60 GHz ~ 130 GHz) signal generation.**
  Vector Signal Generation at Microwave/Millimeter-wave Bands Employing Optical Frequency Quadrupling Scheme (*Optics Lett., OFC, ECOC*)

• **High spectrum efficiency modulation format (OFDM, QAM ect.).**
  Experimental Demonstration of Optical 5-Gb/s 16-QAM OFDM Signal Generation and Wavelength Reuse for 1.25-Gbit/s Uplink Signal (*OFC*)

• **W-band (100 GHz) hybrid access network design**
  W-Band Vector Signal Generation via Optical Millimeter-Wave Generation and Direct Modulation of NBUTC-PD (*OFC, submitted to PTL*)